On the Modelling and Optimisation of Urban Energy Fluxes

PAR

Jérôme Henri KÄMPF

ÉCOLE POLYTECHNIQUE
FÉDÉRALE DE LAUSANNE

Suisse
2009

ii

Abstract

Around 3/4 of global resources are currently consumed in urban settlements, with corresponding adverse environmental consequences. According to population forecasts this situation will worsen in the coming years. It is therefore imperative that we understand how to design less resource intensive urban settlements.

Software for the modelling and optimisation of resource flows are of interest to support urban designers in achieving this objective. To this end we have, in the first instance, tackled the problem of optimising the layout and form of buildings for the utilisation of solar radiation by using a multi-objective evolutionary algorithm. This new methodology facilitates a considerably more exhaustive search of the parameter space than manual trial and error which has been favoured in past studies. However, multi-objective optimisers involve many redundant evaluations when only one objective (the energy consumption) and analytical constraints (the volume of the urban form has to remain within bounds) are taken into account. To resolve this, we developed a new evolutionary algorithm that avoids evaluations of potential solutions that violate constraints. This is a hybrid based of the CMA-ES and HDE evolutionary algorithms. This hybrid algorithm achieves 100% convergence to the global minimum relating to two highly multi-modal benchmark functions and good results compared to the multi-objective evolutionary algorithm previously used and to a hybrid of heuristic and direct search methods (PSO/HJ) for real-world problems.

Key contributions have also been made to the development of a new urban energy modelling tool: CitySim. These contributions include a mono and multi-zone thermal model, which is linked to an HVAC model that takes into account the increased energy demands due to the use of air as medium for heating, cooling and fresh air supply. In order to complete the provision of heating/cooling as well as electricity, the most commonly used energy conversion systems are modelled. Outputs from these systems may also be coupled with a model of sensible/latent heat storage.

Finally the new hybrid evolutionary algorithm was used to optimise the energy performance of a case study of 26 buildings in the Matthäus district (Basel) using CitySim as the energy modelling tool. The results indicated that air conditioning plant should not be necessary in Switzerland if occupants behave appropriately. Concrete strategies for minimising the primary energy demand for the case study were also identified subject to constrained investment capital. This demonstrated that optimally (environmentally) sustainable solutions can be found at the urban scale, to help guide urban designers' decisions.

Keywords

iv

Résumé

Environ 3/4 des ressources globales sont actuellement consommées dans les régions urbanisées, avec leur pendant de conséquences environnementales négatives. D'après les prédictions de l'évolution de la population, cette situation va s'aggraver dans les prochaines années. Il est donc impératif de comprendre comment planifier des habitats urbains moins gourmands en ressources.

Un logiciel de modélisation et d'optimisation des flux de ressources est donc intéressant pour aider les planificateurs urbains à réaliser cet objectif. Pour ce faire, nous avons commencé par appréhender le problème de l'optimisation du placement et de la forme des bâtiments pour une meilleure utilisation de la radiation solaire en utilisant un algorithme évolutionnaire multi-objectif. Cette nouvelle méthodologie permet une recherche de l'espace des paramètres plus exhaustive que les essais et erreurs utilisés de préférence par le passé dans les études. Toutefois, l'utilisation d'un optimiseur multi-objectif implique des évaluations inutiles quand on a un seul objectif (la consommation d'énergie) et des contraintes analytiques (le volume de la forme urbaine doit rester compris dans un certain intervalle). Pour améliorer la situation, un nouvel algorithme évolutionnaire qui évite l'évaluation des solutions violant les contraintes a été développé. Il s'agit d'un hybride basé sur les algorithmes évolutionnaires CMA-ES et HDE. Celui-ci a montré 100% de convergence au minimum global sur deux fonctions de test hautement multimodales et de bons résultats en comparaison à l'algorithme évolutionnaire multi-objectif utilisé précédemment et à un hybride de méthodes directes et heuristiques (PSO/HJ) pour des problèmes du monde réel.

Des contributions clés ont été apportées au développement d'un outil de modélisation énergétique en milieu urbain: CitySim. Ces contributions comprennent un modèle thermique mono et multizone lié à un modèle CVC (chauffage, ventilation et climatisation) qui prend en compte l'utilisation de l'air comme moyen de transport de l'énergie pour le chauffage/climatisation et le renouvellement d'air. Afin de répondre aux demandes de chauffage/refroidissement et électriques, les systèmes de conversion d'énergie les plus utilisés sont modélisés. Ceux-ci peuvent être liés à une modèle de stockage d'énergie sensible et latente.

Finalement le nouvel algorithme évolutionnaire hybride a été utilisé pour optimiser la performance énergétique d'un un cas d'étude de 26 bâtiments au coeur du district de Matthäus (Bâle) en employant CitySim comme outil de modélisation énergétique. Les résultats nous ont indiqués que la mise en place de climatisations n'est pas nécessaire en Suisse si les occupants se comportent de façon adaptée. De plus, des stratégies concrètes pour la min-

imisation de la consommation d'énergie primaire de notre cas d'étude ont été identifiées dans une limite d'investissement fixée. Nous avons démontré que des solutions (environnementalement) optimales ont été trouvées à l'échelle urbaine, permettant d'apporter une aide à la prise de décision des planificateurs urbains.

Mots-clés

Simulation énergétique urbaine; Optimisation; Algorithmes évolutionnaires; CitySim; Modèle thermique; Transformation d'énergie; CVC; Modélisation de l'irradiation

Remerciements

Je tiens particulièrement à remercier le *Professeur Jean-Louis Scartezzini* qui m'a encouragé à faire une thèse de doctorat dans son laboratoire (Energie Solaire et Physique du Bâtiment). Après quelques hésitations, dont un passage dans le monde de l'enseignement secondaire, j'ai finalement suivi son conseil et plongé dans le bain de la recherche.

Je remercie le *Professeur Darren Robinson* qui a été mon guide tout au long de ce travail. Ses idées d'avant-garde ont fait de mon labeur un passionnant voyage au coeur de l'optimisation et de la modélisation physique. Nous avons su au fil de ces quatre années tisser des liens qui nous ont rapprochés.

Many thanks to *Doctor Michael Wetter* from the Lawrence Berkeley National Laboratory with whom I learned a lot during my two stays in California. His precise and sharp way of thinking brought rigor to my dissertation.

Un grand merci au *Docteur François Maréchal* du Laboratoire d'Energétique Industrielle qui n'a pas hésité à partager ses ressources afin de m'aider dans mon travail. Je pense que notre collaboration a été fructueuse. Dans la foulée, un énorme merci à *Raffaele Bolliger* du même laboratoire sans qui le Chaptre 2 n'aurait surement pas existé. Ses compétences avec MOO et OSMOSE, nos discussions intéressantes et son expertise dans l'utilisation du cluster Pleiades ont contribué significativement à l'avancement de ma thèse.

Many thanks to *Professor Jonathan Wright* who came over from the United Kingdom to be part of my thesis jury. His interesting remarks improved the overall quality of the thesis.

Merci infiniment au *Professeur Alain Clappier* qui travaillait au Laboratoire de Pollution des Airs et des Sols du temps de mon doctorat. Son expertise dans la résolution d'équations différentielles et nos discussions interminables sur les qualités humaines des scientifiques m'ont apporté une vision plus critique du monde académique. Sa disponibilité n'avait d'égal que sa capacité à dénicher les erreurs dans mon code.

Mes remerciements au *Professeur Marco Tomassini* de l'Université de Lausanne qui m'a donné un grand coup de main pour les corrections de l'article sur l'algorithme évolutionnaire hybride et dont les cours ont toujours été source d'enrichissement pour moi.

Merci au *Docteur Julien Nembrini* du Laboratoire de Design et Media qui m'a procuré le cas d'étude "Photovoltaic extension of a Mansion". Son enthousiame et sa motivation pour la recherche ont été un exemple à suivre tout au long de ma thèse.

Je tiens encore à remercier le *Docteur Nicolas Morel* et le *Professeur Claude-Alain Roulet* pour les discussions très enrichissantes que j'ai eues avec eux, ainsi que tous les doctorants du LESO-PB (et d'autres laboratoires) qui sont

Contents

List of Figures

Chapter 1

Introduction

Urban areas contain around half of the global population on earth and their population is forecasted to increase to 70% of the earth during the next forty-three years (see Table 1.1). In the more developed regions, this proportion will even grow to 86%. Moreover, nowadays some 75% of global resource

| | Population in billion | | | | | |
| | 2007 | | 2025 | | 2050 | |
Country or area	Urban	Rural	Urban	Rural	Urban	Rural
World	3.294 (49%)	3.377	4.584 (57%)	3.426	6.398 (70%)	2.793
More developed regions[a]	0.910	0.313	0.995	0.264	1.071	0.174
Less developed regions[b]	2.384	3.064	3.590	3.162	5.327	2.619
Least developed countries[c]	0.225	0.580	0.452	0.734	0.967	0.775
Other less developed countries[d]	2.159	2.485	3.137	2.428	4.360	1.844
Less developed regions, excluding China	1.815	2.297	2.758	2.538	4.290	2.238
Sub-Saharan Africa[e]	0.290	0.517	0.539	0.654	1.065	0.696

[a]More developed regions comprise Europe, Northern America, Australia/New Zealand and Japan
[b]Less developed regions comprise all regions of Africa, Asia (excluding Japan), Latin America and the Caribbean plus Melanesia, Micronesia and Polynesia
[c]The least developed countries are 50 countries, 34 in Africa, 10 in Asia, 5 in Oceania plus one in Latin America and the Caribbean
[d]Other less developed countries comprise the less developed regions excluding the least developed countries
[e]Sub-Saharan Africa refers to all of Africa except Northern Africa, with the Sudan included in sub-Saharan Africa

Table 1.1: Urban and rural areas in 2007 and a perspective for 2025 and 2050 [United Nations, 2007]

consumption takes place within urban settlements, which cover only 2% of the earth's surface [Girardet, 1999]. It is therefore imperative that we understand how to minimise resource consumption in the urban environment, as it is widely accepted that combustion of non-renewable fossil fuels leads to

1

climatic disorders. This risk can be addressed on two fronts in urban sites: energy can be better conserved and fossil fuels can be displaced by renewable energy. To quantify the potential for these two strategies, some form of mathematical model is necessary. With that objective in mind, the present thesis aims at developing new software for modelling the energy performance of urban districts. This would enable us to examine detailed scenarios for improving the energy performance of specific buildings or ensembles of them; likewise systems for energy conversion and storage. Furthermore, we introduce to this software computational optimisation algorithms to enable us to efficiently explore the infinite parameter space which is defined by the myriad urban design variables. In this the objective function to minimise is net urban energy consumption. The final objective is to acquire the data required by these models to analyse the City of Basel and to test concrete strategies for improving its net primary energy consumption.

1.1   State of the art

Models of the energy demands of individual buildings are very well developed. Indeed these have evolved from basic core dynamic thermal models developed during the 1970s and 80s (e.g. Clarke [1977], Gough [1982]) to integrated design tools boasting simultaneous solution of building, plant, mass flow, embedded CFD and electrical power flow equation sets [Clarke, 2001]. They have also now been extensively validated [Lomas et al., 1997]. It was only during the late 1990s that research in simulating the environmental performance of the built environment started to shift from individual buildings to the urban scale.

1.1.1   Renewable energy potential of urban sites

Good progress has been made in refining the prediction of the potential to utilise solar radiation in the urban context. Compagnon and Raydan [2000] have developed a computer method for producing irradiation histograms identifying the proportion of the urban surface (building facades and roofs) for which photovoltaic solar systems may be viable. Montavon et al. [2004] and Robinson [2006] applied this approach to target specific urban surfaces for which both passive and active systems are viable, as well as daylighting technologies. Similar techniques have also been developed by Mardaljevic and Rylatt [2000] and Robinson and Stone [2004b]. Figure 1.1 shows an irradiation image produced using the latter technique.
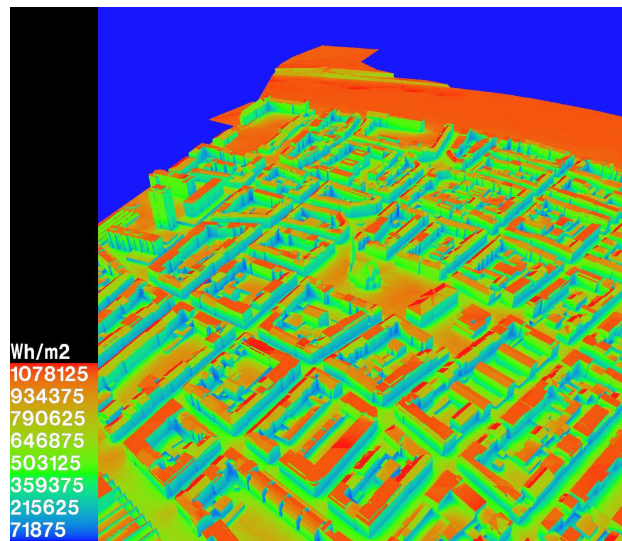
Figure 1.1: An annual irradiation image for the Matthäus district in Basel, Switzerland. It was chosen for the "Image of the month of February 2008" by the Swiss National Science Foundation.

1.1.2 Urban-scale energy models

Several urban-scale energy models have been developed in recent years. The majority of these models concentrate exclusively upon domestic energy consumption, such as BREHOMES [Shorrock and Dunster, 1997] and EEP [Jones et al., 1998], although SEP [Gadsden et al., 2003] also evaluates the integration of solar water heating and photovoltaics into domestic buildings. The first model to deal with non-domestic buildings was LT-Urban [Robinson and Baker, 2000], but this crudely represents occupancy characteristics using fixed schedules and assumes a facade design and internal zoning schema in its prediction of energy consumption due to heating, lighting, ventilating and cooling. Neither the domestic or non-domestic models support predictions of energy supply from the range of renewable energy technologies whilst representing all principal energy consumption end uses. Only DREAM-City [Titheridge and Boyle, 1995] takes a more holistic view of urban energy demands, but this has crude temporal resolution and does not explicitly represent the physicality of the urban environment. Resolving this was the objective in developing SUNtool [Robinson et al., 2006], s software tool for predicting energy demands for the range of building types in a way that is sensitive to the urban context and also consider intrinsic differences between similar buildings owing to occupant behaviour influences, e.g. due to interactions with lights, blinds, window openings and HVAC controls. It includes a

suite of energy supply models as well as models to predict water and waste flows, so that urban designers may optimise sustainability of masterplanning proposals. SUNtool was designed to model the resource flows of projects involving tens of buildings and in this it represented a considerable step forward from one building simulation to many buildings simulation. SUNtool is physically rigorous in many of its integrated models (for the neighbourhood scale).

1.1.3   Optimisation of a building's energy performance

Detailed simulation programs are increasingly used to asses the energy performance of individual buildings. In Switzerland, the law requires every new construction or refurbishment to meet energy consumption standards such as SIA 380.1, or soon to be standards such as the Minergie and Minergie P labels. In Europe, the European Directive on Energy Performance of Buildings (EPBD) lays down minimum requirements of the energy performance of buildings. These performance standards along with raising energy costs increase the demand for development and usage of building simulations programs such as ESP-r [Clarke, 2001], TRNSYS [Bradley and Kummert, 2005] and EnergyPlus [U.S. Department of Energy, April 2009]. When it comes to the energy performance optimisation of buildings, the end-users of the simulation programs may test different scenarios in search of the best performing one. However, when the possible changes are numerous, comparing all combinations manually becomes impracticable. Computerised algorithms were developed to overcome that problem, such as this very simple one: definition of parameters, discretisation of those, exhaustive evaluation of all combinations and selection of the best performing one. But when the exhaustive evaluation is computationally not feasible, optimisation algorithms that searches in a clever way the parameter space were developed.

Caldas and Norford [2002] have used Genetic Algorithms (GAs) to optimise design solutions in terms of building thermal and lighting performance. This study addressed the placing and sizing of windows in a simple office building. The evaluation criteria (or fitness function) was chosen to be related to the energy consumed for heating, cooling and lighting on an annual basis. The authors outlined that different runs of the optimisation tool may lead to different solutions with similar performance, and this might be an advantage for the designer in choosing between available alternatives. Wright et al. [2002] applied multi-objective optimisation using GAs (MOGA) for the identification of the trade-off characteristic between the energy cost of a building and the occupant thermal discomfort. Wetter and Wright [2004] compared the performance of different algorithms in minimizing a building's energy

consumption for lighting, ventilating, cooling and heating. The range of algorithms tested include both direct and heuristic (probabilistic) search. The authors concluded that the smoothness of the function to optimise may favour one algorithm over another.

Heuristics were mainly used in the past to solve optimisation problems at the building scale.

1.2 Hypothesis

Intelligent urban planning can help reduce the energy demand of cities to obtain a 2000 watts per capita society [Jochem, 2004]. Moreover, it is increasingly likely that urban scale predictions will be required. Indeed, for example, the London Energy Plan wants to limit further climate change by reducing London's carbon dioxide emissions. Likewise, the new BRE Environmental Assessment Method (BREEAM) for Communities will assist planners to independently measure and certify the overall potential sustainability of a masterplan proposal during the planning stage of the development control process. An urban scale prediction tool should be able to evaluate the building performance depending on the urban geometry [Baker and Hoch, 1988], building design, systems efficiency and occupant behaviour. Such a tool is referred to as *holistic*.

The hypothesis that we wish to test in this thesis may be summarised as follows:

> Computational methods, in conjunction with an holistic urban simulation tool, can be used to identify optimal solutions for urban environmental sustainability.

In this work we address environmental sustainability. In particular, we will focus on minimising the net energy consumption, which remains the dominant determinant of the urban environmental sustainability. In this we seek to identify an optimal solution by minimising the energy (consumption) function.

1.2.1 Computational methods

The optimisation algorithms can be of different types: direct search (technique that do not explicitly use derivatives, Kolda et al. [2003]), indirect search of the optimal solution using a mathematical criteria (steepest descent for example) and heuristic search that use stochastic operators (such as Genetic Algorithms).

In all generality, the optimisation algorithms search for a minimum[1] of a function f that depends on n independent decision variables. In formal terms, we are looking for the infimum and the corresponding set of variables that minimises the function as in Equation 1.1.

$$inf \quad \{f(\vec{x}) \mid \vec{x} \in M \subseteq \mathbb{R}^n\} \tag{1.1}$$

where

$$
\begin{array}{ll}
n \in \mathbb{N} & \text{dimension of the problem} \\
f : M \to \mathbb{R} & \text{objective function} \\
M = \{\vec{x} \in \mathbb{R}^n \mid g_j(\vec{x}) \geq 0, \forall j \in \{1, ..., m\}\}, M \neq \emptyset & \text{feasible region} \\
m \in \mathbb{N} & \text{number of constraints}
\end{array}
$$

The set of inequality constraints $g_j : \mathbb{R}^n \to \mathbb{R}, \quad \forall j \in \{1, ..., m\}$ includes a special case of constraints due to the domain boundaries $l_i \leq x_i \leq h_i$, where $l_i, h_i \in \mathbb{R}$ and $i = 1..n$. The symbol l_i refers to the lower bound and h_i to the upper or higher bound of the domain.

The function f is found to be non-linear, multi-modal, discontinuous and hence non-differentiable in simulation-based building energy optimisation [Wetter and Polak, 2004]. We have therefore excluded indirect search algorithms, as they rely on the function's derivatives and selected heuristics, as they do not require smoothness of the objective function but instead use probabilistic operators to search for an improvement in the objective function. We are mindful however that for such problems, one cannot guarantee that the global optimum will be found with a finite number of simulations. Such algorithms are nevertheless able to find a good solution in a computationally tractable way.

1.2.2 Holistic simulation tool

A new holistic simulation tool based on the ideas behind SUNtool was developed from scratch. SUNtool was conceived to support the environmental design of urban masterplans accommodating both domestic and non-domestic buildings, the solver has a reduced dynamic thermal model at its core. This takes inputs from a detailed shortwave and longwave radiation model which considers obstructions to both sun and sky as well as reflections from adjacent obstructions [Robinson and Stone, 2004a]. Predictions of internal illumination from the same model [Robinson and Stone, 2005, 2006] and indoor temperature are input to a family of stochastic models [Page et al., 2005], which simulate occupants' presence [Page et al., 2008] and their interactions

---

[1]A maximisation may also be performed by reversing the sign of the objective function

with lights and shading devices; windows; water and electrical appliances; refuse production [Page et al., 2007]. The thermal and electrical demands are linked with an energy centre model, which may be building-embedded, centralised or both [Robinson et al., 2007]. Based on a predictor-corrector approach, if energy supply is insufficient to meet the demand, new internal conditions are calculated in the thermal case or uses are prioritised in the electrical case. SUNtool is comprised of a graphical user interface (GUI) with which the geometry of buildings within a neighbourhood may be defined and attributed according to their constructional and operational characteristics. This information is then parsed to a solver, that does computations for energy, water and waste fluxes. Figure 1.2 shows the communications between the interface and the solver. The new holistic tool *CitySim* is designed for
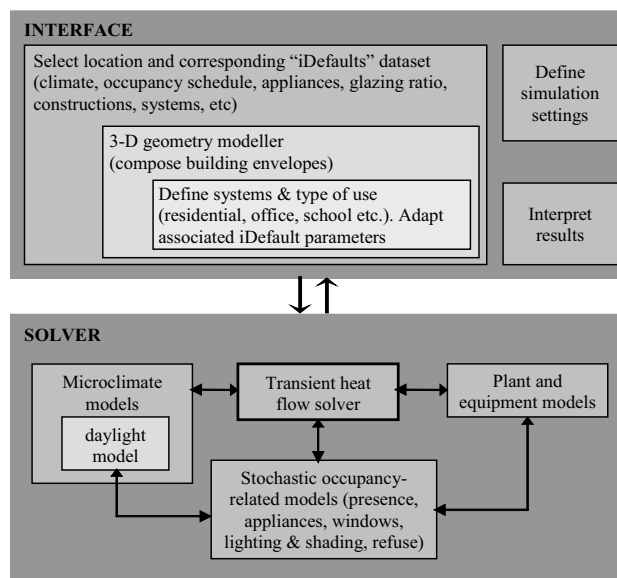
Figure 1.2: A sketch of the SUNtool principles.

a scaleless application, from the single building to the entire city, based on more rigorous physical and statistical models. CitySim has in common with SUNtool the simplified radiosity algorithm for the determination of the short-wave and longwave radiation. New models for Thermal, HVAC and Energy Conversion Systems are key developments provided in this thesis that are needed to demonstrate the hypothesis.

1.2.3   Demonstration methodology

The testing of our central hypothesis is organised in the present thesis as follows: we start by defining the methodology to optimise a first approximation of the energy performance at the urban scale, the total shortwave irradiation incident on building envelopes, we then propose a new evolutionary algorithm that can handle constraints in an efficient way. We describe some core models that have been contributed in the present work to the development of CitySim. We finally optimise the energy performance of a group of buildings, simulated using CitySim, in combination with the new EA.

Chapter 2

First order approximation of urban energy performance

Work related to this chapter was presented at the CISBAT Conference held in Lausanne (CH) in September 2007 [Kämpf et al., 2007] and published in the Special Issue of the journal Solar Energy [Kämpf et al., 2009].

According to Robinson and Baker [2000], adjacent urban structures can exert a significant influence on a building's energy consumption. In particular available passive solar gains and daylight can offset demands for heating and artificial lighting, and these depend on the geometry of both the building and its urban context. Moreover with the appropriate technologies, solar radiation can also contribute to the provision of hot water and electricity. An interesting issue in city planning is the placement of this solar energy conversion technology. For this, Mardaljevic and Rylatt [2000] have computed irradiation images of complex urban environments (where shading is an inevitable consequence of buildings' form) using the popular ray tracing program RADIANCE [Larson and Shakespeare, 1998]. The output images identified which are the most profitable surfaces on which to install energy conversion systems. Montavon et al. [2004] and Scartezzini et al. [2002] have used the same ray tracing program, but with a technique of computing a seasonal (annual or winter) solar irradiation distribution. Their procedure, named PPF [Compagnon, 2000], outputs values that can be used to produce histograms of irradiation as a function of built area. Using a similar approach Cheng et al. [2006] have proposed a parametric study of 18 different models, each representing a particular combination of built form and density, comparing their solar irradiation potential. Their attempt to test alternatives geometrical shapes for urban areas is valuable, but the trial and

error method they used is unlikely to identify the an optimal geometric form in terms of maximising the solar irradiation potential, given the very small number of cases tested.

The purpose of this chapter was to test the principle of optimisation processes using as parameters the geometric factors defining a collection of buildings in an urban scene, and minimising their energy consumption. As a first approximation we take minimising the energy consumption as being equivalent to maximising the solar energy flux incident on buildings' envelopes, taking into account geometrical constraints regarding the layout and form of these buildings due to urban planning regulations.

2.1 Solar irradiation potential determination

In order to predict as precisely as possible the irradiation on hypothetical buildings, we have chosen to use the well-known ray-tracing program RADI-ANCE [Larson and Shakespeare, 1998]. This backward ray-tracing tool can simulate radiant energy exchanges throughout a scene of arbitrary geometric complexity, considering obstructions both to the sun and the sky due to the surrounding (urban) landscape, as well as reflected energy from this landscape. We employ RADIANCE in a similar fashion to PPF [Compagnon, 2004], by supplying a virtual geometric model along with grid-points and normal vectors on each surface with which a program called rtrace can calculate the incident irradiance (W/m^2) given a sky radiance distribution and sun position and radiance. The virtual geometrical model is in a RADI-ANCE specific text file format [Larson, 1992] and contains the surfaces of elements in the scene and (optionally) one or more light sources. In order to compute the irradiation (Wh/m^2) as opposed to irradiance (W/m^2), we define a cumulative sky, as in Robinson and Stone [2004b], for the period of interest. The sky defines 145 Tregenza patches with corresponding cumulative radiance ($Wh \cdot m^{-2} \cdot sr^{-1}$) in three channels (red, green and blue) for the corresponding shortwave part of the electro-magnetic spectrum. This procedure allows us to simulate the irradiation throughout a given period using just a single RADIANCE simulation. The product of this irradiation (Wh/m^2) and the surface area covered by the grid point (m^2), for the whole set of grid points, gives the total irradiation received by a building (Wh). This irradiation calculation is summarised in Figure 2.1.

Each measuring point corresponds to a sub-surface on which the irradiation is supposed to be uniform. The distribution of the grid-points on the building surfaces should be as uniform as possible and their number should be adapted to the precision we desire in the prediction of the total irradiation.

annual irradiation I_i on n sampling points, relating to a region of known surface area A_i

cumulative sky over a year (hemispherical view)

RADIANCE

$$\sum_{i=1}^{n} I_i \cdot A_i \cdot 10^{-9}$$

total annual irradiation on building (GWh)

building surfaces decomposed into sampling points with normal vector
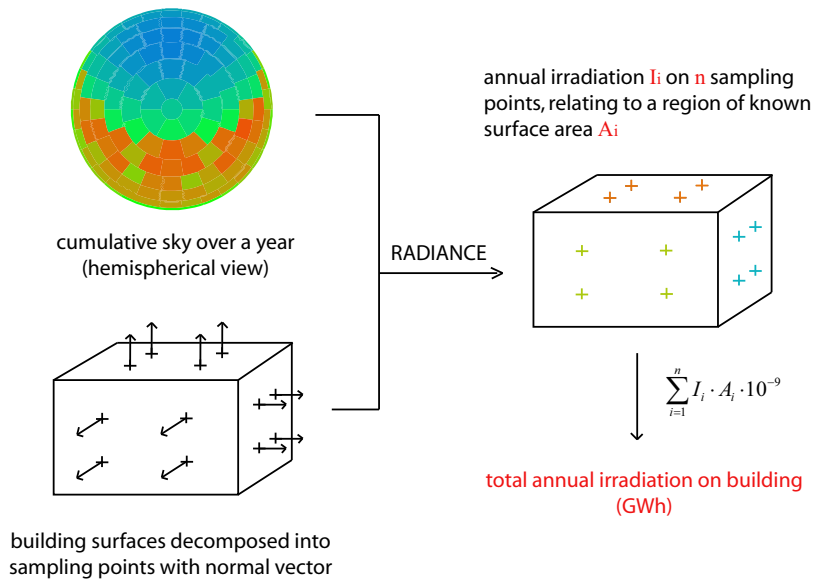
Figure 2.1: Principle of irradiation calculation using Radiance

We therefore devised a method to decompose the buildings' surfaces into four smaller surfaces that can in turn also be subdivided. Figure 2.2 shows the procedure for triangular and quadrilateral decomposition, depending if the original surface is triangular or quadrilateral. The criteria to stop this
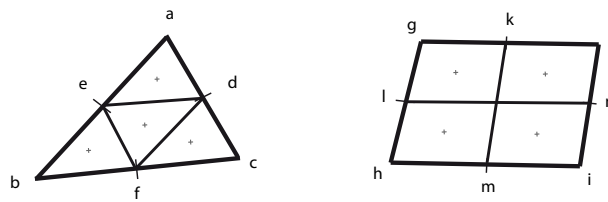
Figure 2.2: The building's surface decomposition

subdivision is a maximum allowable surface area, which is adapted according to our desired precision. Due to the large number of sampling points for each of a potentially large number of simulations, it is desirable to find a compromise between accuracy and computing time. To this end a sensitivity analysis was carried out to determine both the maximum allowed surface area and the RADIANCE simulation parameters.

2.2   Multi-objective optimiser

The irradiation $I_\Omega(P, \vec{dS})$ (Wh/m^2) at point P over the hemisphere Ω pointed by the direction $\vec{dS}$ can be defined as:

$$I_\Omega(P, \vec{dS}) = \int_\Omega R(P, \vec{d\Omega})\vec{dS} \cdot \vec{d\Omega}, \qquad (2.1)$$

where $R(P, \vec{d\Omega})$ is the cumulative radiance (Wh/(m^{2}sr)) at point P received from the infinitesimal directional solid angle $\vec{d\Omega}$. This integral is subdivided in three contributions in RADIANCE: the direct component from the light sources, the corresponding specular component and the diffuse component which contains the rest of the hemisphere [Larson and Shakespeare, 1998, p.496]. In our case, the cumulative sky being defined as a "glow" material, it is not considered as a light source. The irradiation integral therefore simplifies to the diffuse component, which is approximated using Monte-Carlo sampling and refined where strong radiation gradients appear. This results in the irradiation calculation being dependent of the random number generator.

Moreover, the decomposition of surfaces provides a number of sampling points, for which the irradiation calculation takes place, that varies according to the dimensions of the surfaces. This results in a total irradiation over all surfaces to be a noisy non-linear function of the shape parameters. To address such problems, we selected heuristics and more precisely an Evolutionary Algorithm.

As a first test of principle we collaborated with the Industrial Energy Systems Laboratory at EPFL, who made available their multi-objective optimiser MOO [Molyneaux, 2002, Leyland, 2002] and its interface OSMOSE [Bolliger et al., 2005, Gassner and Maréchal, 2009, Maréchal et al., 2005] which can be coupled with a third party objective calculation. MOO is an advanced Evolutionary Algorithm that goes through the phases of recombination, mutation and selection of potential solutions. It has a collection of recombination and mutation operators, and the advantage to store and possibly use the selected parents' recombination and mutation methods to produce children. OSMOSE is an interface used to connect MOO in Matlab with any model that is not Matlab based. As shown in Figure 2.3, OSMOSE receives the value of the parameters of interest from MOO and parses them to the model. After the evaluation of this model, the objective function values are recovered and returned to MOO.

The best compromise between objective functions is represented by a Pareto front, which contains only undominated solutions. The Pareto dominance is
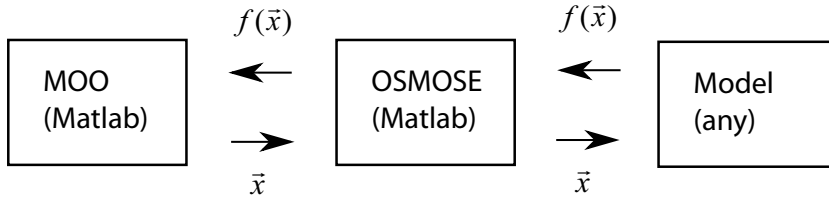
Figure 2.3: The optimisation principle with MOO and OSMOSE

defined by $\vec{x_1}$ strictly dominates $\vec{x_2}$ if $f_k(\vec{x_1}) \leq f_k(\vec{x_2})$ for all objectives k, but with at least one strict equality. For a two-objective optimisation problem, if one fixes the value of one objective, the corresponding point on the Pareto front indicates the best value that can be obtained for the other objective. The number of evaluations of the model to obtain a sufficiently complete Pareto front is not known a priori, and should be large enough to avoid, as much as possible, sub-optimal solutions.

2.3 Application to the Matthäus district

The Land Register and Surveying Office of Canton Basel-Stadt (Grundbuch und Vermessungsamt) has a numerical 3D model of the entire Canton at its disposal. The reference database of this 3D digital model stems from different sources, in particular from the Cadastral Survey of Switzerland (including building footprints and elevations, vegetation footprints, urban networks, . . .). This data was combined to prepare a 3D model of the Matthäus District in Basel as part of the SOLURBAN project [Scartezzini et al., 2002, Montavon et al., 2004].
In this application, the shape of three different urban forms (based on Martin and March [1972] and environmentally reviewed by Steemers et al. [1997]) is optimised. The built forms studied are presented in Figure 2.4. These three urban shapes have been placed with a hypothetical site in the centre of the Matthäus district, so that sky obstructions and reflections due to the surrounding buildings are also considered. For each case, the buildings have been designed with standard dimensions of 10-14m depth and 11-13m width, following local regulations.

2.3.1 Parameterisation

Each family of built form is parameterised to allow its representation by a vector of real numbers. The "Terraces Flat Roofs" scenario is represented by
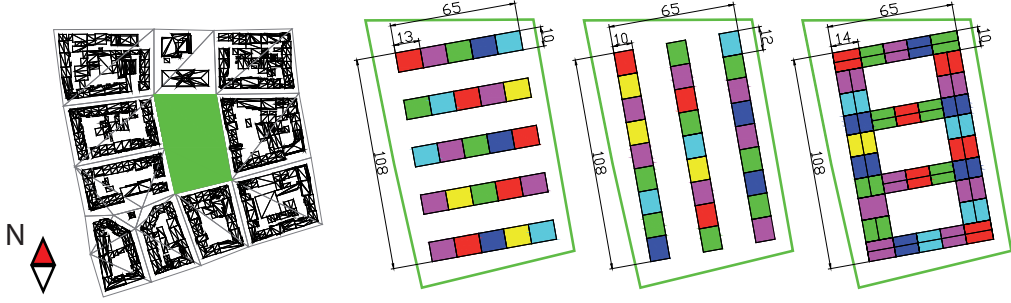
Figure 2.4: Surroundings in the Matthäus district of the supposed constructible zone and three typical urban built forms (Terraces Flat Roofs, Slabs Sloped Roofs and Terrace Courts)

a vector of 25 components representing the heights of the terrace buildings:

$$\vec{x_1} = (h_1, .., h_{25}) , h_i \in [0, 14[, i = 1..25 \qquad (2.2)$$

The "Slabs Sloped Roofs" scenario uses a vector containing the heights of the buildings and a parameter that encodes the orientation of the roof and its height:

$$\vec{x_2} = (h_1, p_1, .., h_{27}, p_{27}) , h_i \in [0, 14[, p_i \in [0, 1[, i = 1..27 \qquad (2.3)$$

The "Terrace Courts" scenario is represented by a vector containing the heights of the facades and the heights of the roofs:

$$\vec{x_3} = (h_1, hr_1, .., h_{32}, hr_{32}) , h_i \in [0, 14[, hr_i \in [0, 4[, i = 1..32 \qquad (2.4)$$

Regulations for the Matthaeus district in Basel require that the maximum height of facades is 14 meters, and that the maximum height of roofs is 4 meters from the uppermost part of the facade.

2.3.2 Objective functions

The period of interest (POI) in this application was taken to be the heating period, assumed to be six months from November to April. In order to minimise buildings' energy demands, in this first approximation, we *maximise* the incident irradiation during the heating period I_{tot} offset by the corresponding thermal losses Q_{th}:

$$f_1(\vec{x}) = I_{tot}(\vec{x}) - Q_{th}(\vec{x}) \qquad (2.5)$$

We also make the hypothesis that buildings can be fitted with active shading devices to avoid the risk of overheating. For this we consider that the solar energy that is absorbed by blinds may be converted into electricity; for example using flexible photovoltaic cells. The steady-state thermal losses Q_{th} (in Wh) are calculated as follows:

$$Q_{th}(\vec{x}) = \sum_{i=1}^{p} U_{building} \cdot A_{building}(\vec{x}) \cdot \Delta T_i = U_{building} \cdot A_{building}(\vec{x}) \cdot \overline{\Delta T} \cdot p, \quad (2.6)$$

where $U_{building}$ is the average building U-Value (W/(m^{2}K)), $A_{building}$ is the total exposed surface area of the building (m^2), ΔT_i is the heating degree-hour (Kh) relating to an internal building's temperature of 20°C at hour i, p is the number of hours of the period of interest and $\overline{\Delta T} = \frac{1}{p} \sum_{i=1}^{p} \Delta T_i = \frac{1}{p} \sum_{i=1}^{p} \max((20°C - T_{ext,i}) \cdot 1\text{h}, 0)$ is the time-averaged positive temperature difference (K) between inside at 20°C and outside during the period. This crude approximation of the thermal losses ignores the solar and casual gains in the building and gives the total energy that has to be provided by any means to the building in order to maintain at least 20°C. It represents a pessimistic (or upper) value for the thermal needs.

A compiled model was written in C++ in order to read a text file containing the optimisation parameters and write in another file the corresponding objective function values. The model creates the 3D geometry, computes its volume, its external surface area and associated thermal losses and finally calls RADIANCE for the calculation of the solar irradiation potential, as shown schematically in Figure 2.5.
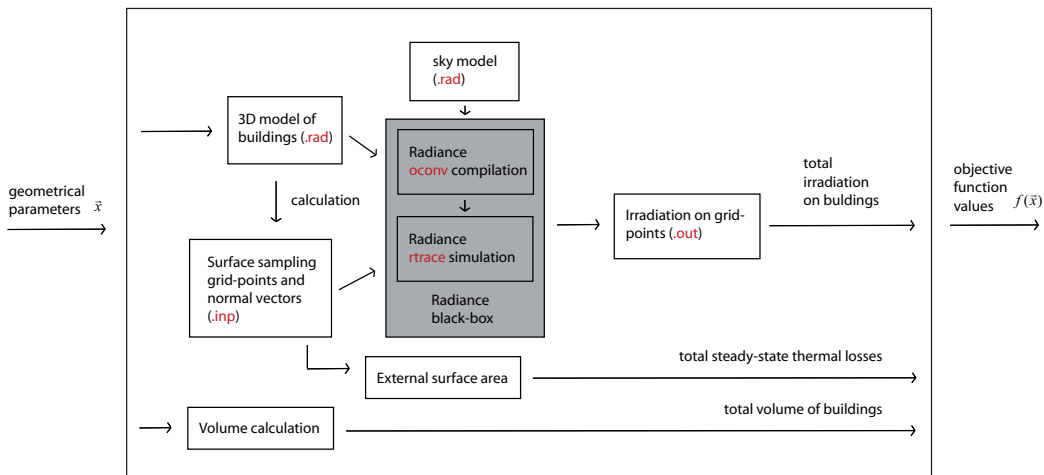
Figure 2.5: The compiled model that calculates the objective function values

For this application, we want to find how to place a given number of lodging units corresponding to a volume by identifying the best buildings' shape for that volume. *We have therefore set two competing objectives: the first one maximises the irradiation offset by the thermal losses (Equation 2.5) and the second one minimises the volume.* For the calculation of the first objective, the irradiation corresponds to the energy absorbed by the exposed envelopes. In our case with surfaces having a 20% lambertian reflectance for each channel (red, green and blue), this equates to 80% of the incident irradiation due to the sun, sky and two inter-reflections from other surfaces. For the calculation of the second objective, the time-averaged positive temperature difference was 15 K, calculated from a Meteonorm climate file. The building U-Value was taken to be 0.38 W/(m²K), following the SIA 380/1 (2009) standard (based on a 20% glazing ratio and a glazing U-value of 1.1 W/(m²K) and 80% opaque material having a U-value of 0.2 W/(m²K)).

2.3.3 Results

Computations were run in parallel on EPFL's 128 CPU core pleiades2 cluster. RADIANCE version 4.0a was used for the irradiation calculation. For each urban built form studied a Pareto frontier, defined as the best individuals that are not strictly dominated, was formed after 18000 evaluations. By "not strictly dominated" we mean that we cannot find any other individual in the algorithm search history that is better for all objectives at the same time. Moving along the Pareto frontier, we experience a trade-off between the objectives.

Terraces Flat Roof

In Figure 2.6 we present results for the first case: "Terraces Flat Roofs". We have superimposed on the Figure three optimal cases corresponding to 40%, 60% and 80% of the total allowed volume. These optimal cases are false-coloured between blue and red to represent the heating-period irradiation on the buildings calculated by RADIANCE. The irradiation is a part of the first objective represented in Figure 2.6 by the x-axis. For visualisation reasons, we only show the parameterised buildings on the Figure and not the surrounding buildings, but the latter were included in the simulations.
We can also see in Figure 2.6 where the algorithm reduces the total volume by diminishing the height of buildings. It seems to have conserved the symmetry of the sky, resulting in symmetrical building placement along the North-South axis. At 40% of the total allowed volume, we notice an arena shaped urban form with a hole in the southern direction to admit solar en-
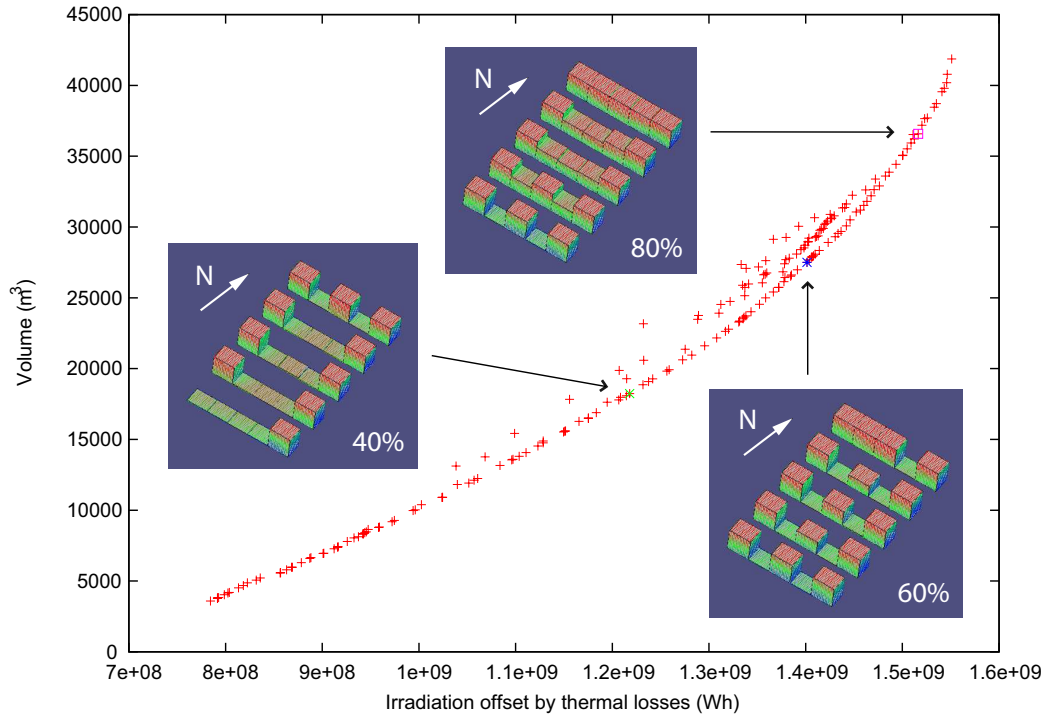
Figure 2.6: Pareto fronts of clusters of solutions for the "Terraces Flat Roof" scenario: the irradiation offset by the thermal losses on the x-axis and the volume on the y-axis.

ergy. At 60%, the interior blocks in the South-North direction start to grow, leaving holes on theirs sides for solar penetration. Finally at 80%, the urban form is filled further preferentially towards the North of the site.

Terraces Flat Roof			
Volume	40%	60%	80%
Irradiation offset by thermal losses (GWh)	1.218	1.4	1.516
Increase compared to non-optimised case	(+9.8%)	(+8.1%)	(+4.7%)

Table 2.1: For fixed volumes we compared irradiation values offset by thermal losses for the optimised case and the non-optimised case of all roofs at the same height

In order to understand the relative improvement obtained with the Evolutionary Algorithm over conventional practice, we compare the optimised cases at 40%, 60% and 80% of the total volume configurations having the same volume but with all buildings at the same height (see Table 2.1). The corresponding heights at 40%, 60% and 80% are respectively $h_{i=1..25} = 5.6$,

$h_{i=1..25} = 8.4$ and $h_{i=1..25} = 11.2$. We notice that by punctuating the urban built form with gaps and solids a significant increase in the first objective can be achieved, which quite naturally decreases as we approach the maximum allowed volume.

Slabs Sloped Roof

In Figure 2.7 we present results for the second case: "Slabs Sloped Roofs", with three optimal cases superimposed for 30%, 50% and 70% of the maximum allowed volume. From this, we can again see where the algorithm
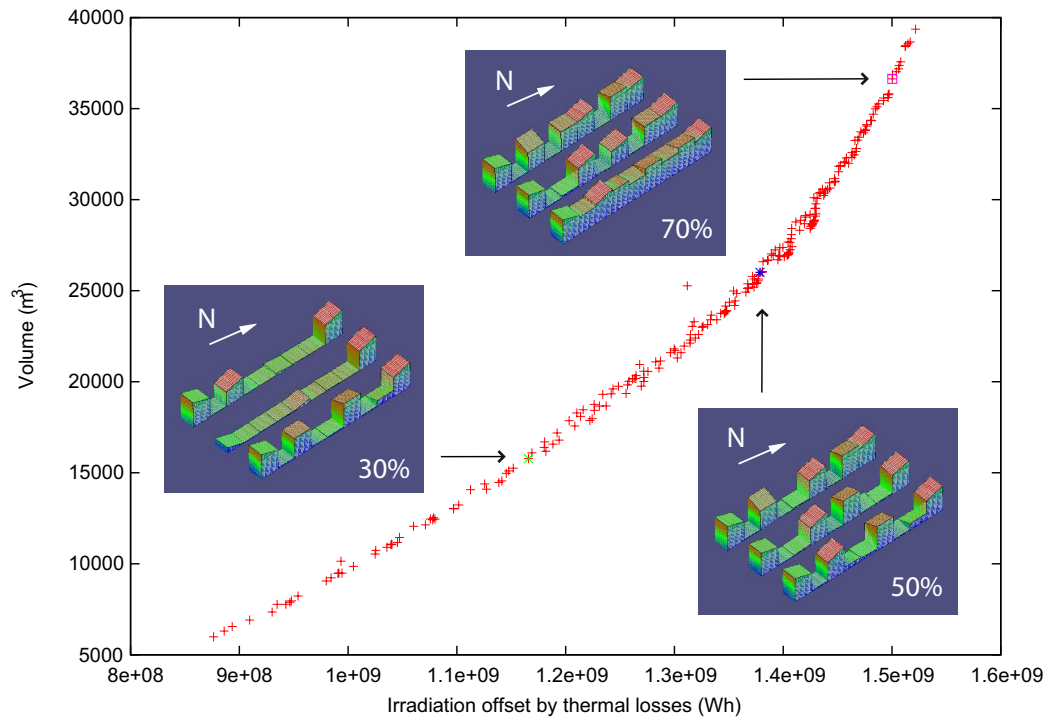
Figure 2.7: Pareto fronts of clusters of solutions for the "Slabs Sloped Roof" scenario: the irradiation offset by the thermal losses on the x-axis and the volume on the y-axis

reduces the total volume by diminishing the height of buildings. It seems to start with the buildings at the center of the parcel and then at the south end. At 30% of the total allowed volume we notice the same kind of arena shape as in the first case studied. At 50% and 70%, the center and south end are progressively filled.

We once again compare for a given volume the optimised and non-optimised cases of all parameters. In Table 2.2 we notice that the increase in the first

objective is significant compared to the non-optimised case. The trends are

Slabs Sloped Roof			
Volume	30%	50%	70%
Irradiation offset by thermal losses (GWh)	1.167	1.379	1.500
Increase compared to non-optimised case	(+21.0%)	(+18.5%)	(+11.1%)

Table 2.2: For fixed volumes we compare irradiation values offset by thermal losses for the optimised case and the non-optimised case of all west-oriented roofs at the maximum height.

less clear in respect of roof geometry (which has a less marked input on the results than building height), but we do notice that roofs at the north and south extremes of the scene are oriented towards the center of the urban form, which may favour the absorption of reflected radiation.

Terrace Courts

In Figure 2.8 we present results for the final case: "Terrace Courts", with the three optimal cases for 40%, 60% and 80% of the total maximum allowed volume superimposed. We notice that the algorithm reduces the height of buildings oriented in Slabs (bars oriented North-South) before adjusting the Terraces (bars oriented East-West). This effect might be explained by relative shadowing between buildings in the Slabs configuration. At 40% of the total allowed volume, the algorithm tends toward the Terraces configuration, which admits more solar energy to the buildings than the Slabs configuration. When increasing the volume to 60% and 80% the buildings in the Slabs configuration grow.
Once again we compare the optimised and non-optimised cases of all parameters at the the same height. The results are summarised in Table 2.3, from which we again notice a significant increase for the optimised case.

Terrace Courts			
Volume	40%	60%	80%
Irradiation offset by thermal losses (GWh)	1.528	1.679	1.768
Increase compared to non-optimised case	(+17.1%)	(+13.4%)	(+6.5%)

Table 2.3: For fixed volumes we compare irradition values offset by thermal losses for the optimised case and the non-optimised case of all buildings and roofs at the same height.
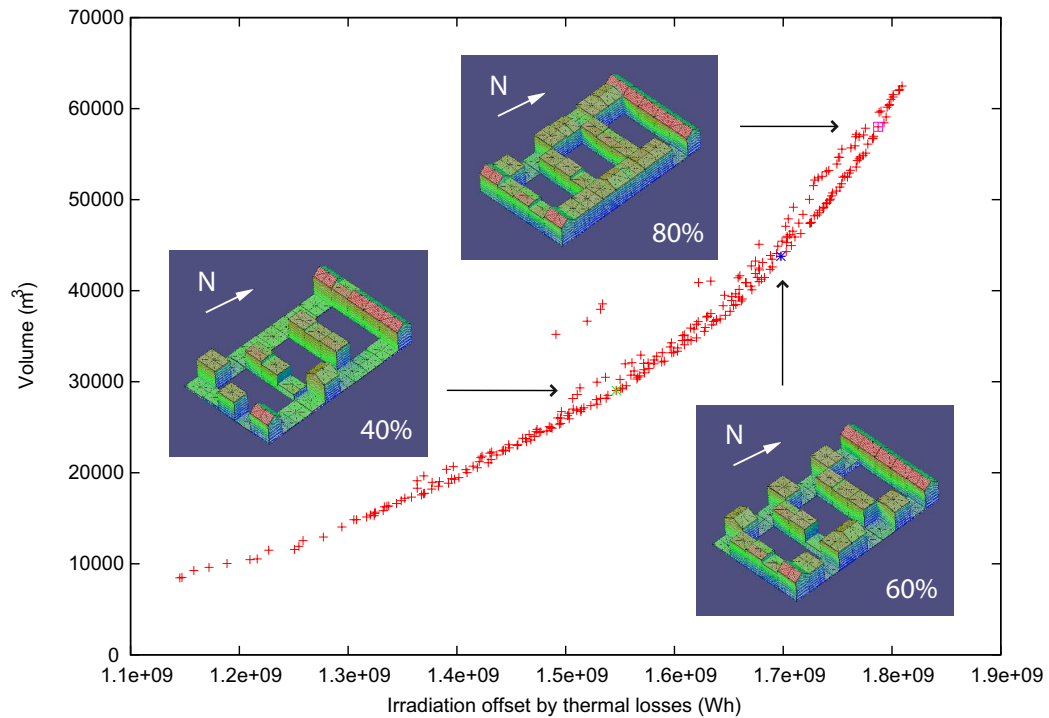
Figure 2.8: Pareto fronts of clusters of solutions for the "Terrace Courts" scenario: the irradiation offset by the thermal losses on the x-axis and the volume on the y-axis

Comparison of optimal cases

We have overlayed in Figure 2.9 the three Pareto fronts obtained for each of our scenarios. The fronts for the "Terraces Flats Roofs" and "Slabs Sloped Roofs" are roughly superimposed, indicating similar irradiation offset by thermal losses for volumes under 30000 m^3. Above this threshold, the "Terraces Flat Roofs" perform slightly better, due to relatively reduced self-shadowing. The "Terrace Courts" always perform better than the other cases. This is because its collection surface is large whilst the volume is compact, so minimising the thermal losses.

A rendering of the "Terrace Courts" at 80% of the maximum volume was generated using RADIANCE (Figure 2.9) in which we can also see the surrounding buildings that were included in the RADIANCE simulations. We notice that the "Terrace Courts" blend in well with the other building arrangements that can be found in the Matthäus district, suggesting that it is rather well integrated in an architectural sense.

Table 2.4 shows the detailed simulation results for the the three optimal ur-
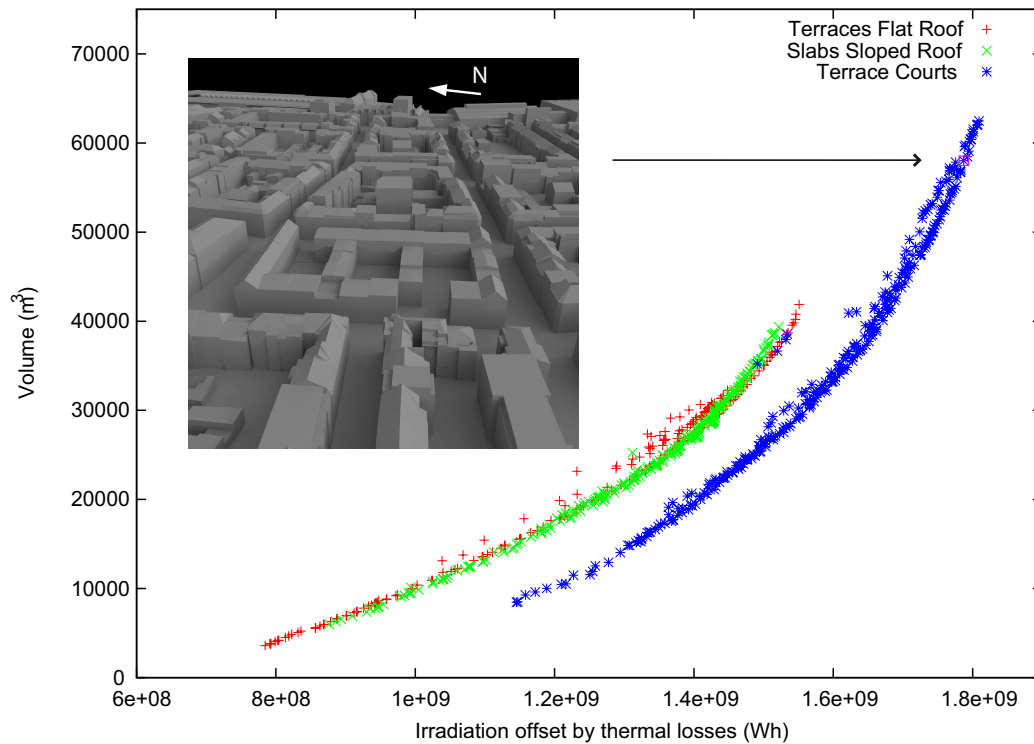
Figure 2.9: Superposition of the Pareto fronts obtained for the Terraces Flat Roof, Slabs Sloped Roof and Terrace Courts. On the left, a synthetic image rendered using RADIANCE showing Terrace Courts at 80% of the maximum allowed volume and their surroundings.

ban forms for the Terraces Flat Roofs, the Slabs Sloped Roofs and the Terrace Courts at respectively 80%, 70% and 80% of the total allowed volume. From this it appears again that the best urban configuration is Terrace Courts, in terms of energy gains and losses. In terms of relative importance we calculate that the thermal losses are equivalent on average to only about 17.6% (within 0.5% margin) of the solar potential, so that their impact in determining the optimum building shape is relatively modest. However, when having two cases receive similar irradiation the form which has lower thermal losses will be favoured.

2.4 Conclusion

In the design of urban settlements, the rational use of solar irradiation can reduce the energy demand for heating and artificial lighting. Therefore, as a first approximation minimising buildings' energy demand is equivalent to

	Terraces Flat Roofs (80%)	Slabs Sloped Roofs (70%)	Terrace Courts (80%)
Irradiation (GWh)	1.835	1.838	2.157
Thermal losses (MWh)	319	338	370
External surface area (m^2)	12956	13713	15007
Volume (m^3)	36582	36632	58007
Ground surface area (m^2)	3260	3251	4523
Irradiation per unit external surface area (kWh/m^2)	142	134	144
Thermal losses per unit ground surface area (kWh/m^2)	98	104	82

Table 2.4: Comparison for the optimised cases

maximising incident solar irradiation offset by thermal losses. We were interested to find the best urban shape that maximises the incident solar irradiation for a given volume. We proposed a methodology that involves a multi-objective Evolutionary Algorithm named MOO, with two objectives. The first objective is to maximise the solar irradiation, and the second one is to the minimise the urban shape volume. This optimisation leads to a Pareto front, which enables us to identify the cases that minimise the energy consumption for a given volume. As an application of this methodology, we parameterised three urban forms: "Terraces Flat Roofs", "Slabs Sloped Roofs" and "Terrace Courts". For each of these cases clear trends in the optimal sizing and form of buildings are discernable for different target built volumes.

Using this methodology, which has produced some interesting results, we were able to identify urban shapes which minimise our indicator of energy consumption for a given built volume in the form of Pareto fronts. However, constraints such as allowable volume may be known a priori, prior to launching the optimisation algorithm. In this case, the presented methodology may involve a great many redundant calculations, due to the evaluation of parameter combinations which lie beyond our known constraints. Resolving this was the inspiration behind the work described in the next chapter.

Chapter 3

A new hybrid Evolutionary Algorithm

> The part of this chapter describing the new Evolutionary Algorithm was published in the journal Applied Soft Computing [Kämpf and Robinson, 2009a]. The constrained application has been accepted for publication in the journal Energy & Buildings [Kämpf and Robinson, 2009b], and the comparison with another global optimisation algorithm has been accepted for publication in the Journal of Building Performance Simulation [Kämpf et al., 2009].

Evolutionary Algorithms (EA) are a family of optimisation methods based upon the principles of darwinian natural selection [Fogel, 2006, Goldberg, 1992, Mitchell, 1998]. They are population-based heuristic algorithms, where each individual represents a potential solution of the function to optimise. A population of μ individuals is randomly chosen as a starting point. The population goes through three operators to evolve: recombination between individuals, random mutation of their alleles and selection of the fittest. One iteration of the strategy is a step from a population P^n to P^{n+1}, where n is the generation number, and can be written as:

$$P^{n+1} := opt_{EA}(P^n) \tag{3.1}$$

The optimisation of P^n is defined by the operators sel (selection), mut (mutation) and rec (recombination) in the following way:

$$opt_{EA} := sel \circ (mut \circ rec)^{\lambda}, \tag{3.2}$$

where λ corresponds to the number of new individuals (children).
According to the type of EA, a phase of adaptation of the parameters or

migration of individuals might follow from their selection. The termination criterion for each iteration is met when the maximum number of function evaluations is reached. Since this is roughly proportional to the total computing time, we are able to define an (approximate) upper limit of time required for the optimisation process. When reached, the algorithm exits and returns the individual, that has performed best up to that point. The objective function value for a potential solution is often referred to as the fitness of an individual.

The first evolutionary algorithms, proposed from the mid-60s, were the Genetic Algorithms (GAs) of John Holland [Holland, 1975] at the University of Michigan, the Evolutionary Programming (EP) of Lawrence Fogel [Fogel et al., 1966] at the University of California in San Diego and independently the Evolution Strategies (ES) of Ingo Rechenberg [Rechenberg, 1973] at the Technical University of Berlin. Their work introduced a wide class of optimisation methods for difficult problems where little is known about the underlying search space. John Koza [Koza, 1992], with the introduction of Genetic Programming (GP) at the beginning of the 1990s, further enriched the Evolutionary Algorithms.

Evolution Strategies (ES) were first developed by Rechenberg and Schwefel [Rechenberg, 1973, Schwefel, 1995] and have evolved into the cumulative step-path adaptation algorithm (CSA-ES) [Beyer and Schwefel, 2002, Dirk and Alexander, 2006] and the covariance matrix adaptation algorithm (CMA-ES) [Hansen and Ostermeier, 2001, Hansen and Kern, 2004]. The variables of the function to optimise are coded using a floating-point representation and are associated in phenotypes with standard deviations for mutation purpose. CMA-ES have been used to solve many optimisation problems [Hansen and Kern, 2004] and are regarded as one of the best algorithm for real-value coded variables. However Hansen and Kern [2004] conclude that CMA-ES is outperformed by Differential Evolution only if the function to optimise is additively separable. Differential Evolution (DE) was developed by Storn and Price in 1996 [Storn and Price, 1996] and has proven to be another good candidate for real-value optimisation problem solving. DE which is based on stochastic search is very simple to implement and relies only on variables with a floating point representation. However one of its drawbacks is the need for a large population to overcome local optima. Chang et al. [2007] subsequently developed a hybrid algorithm of differential evolution (HDE) to allow for the use of a smaller population. For all kinds of DE, the results are very sensitive to the algorithm control parameters [Nobakhti and Wang, 2008], so that these parameters must be carefully chosen.

Reiterating the conclusion of Hansen and Kern [2004]:

> "Only if the function is additively separable, Differential Evolution strongly outperforms the CMA-ES.",

we therefore considered that a hybrid CMA-ES/HDE algorithm might combine the advantages of the two optimisation methods, since in real life applications we tend to face optimisation problems where the dependence of the function on its variable is unknown. This then might be a good compromise in terms of robustness and convergence speed, as it should perform well on both additively and non-additively separable functions.

In urban energy consumption minimisation problems, buildings sufficiently far in a simulated scene have weak or inexistant interactions and therefore, with respect to their variables, the objective function is essentially additively separable. But this is not necessarily the case for adjacent buildings, for which the objective function is rather non-additively separable. This reinforces the development of a hybrid optimiser which may face both additively and non-additively separable problems.

3.1 Covariance Matrix Adaptation Evolution Strategy (CMA-ES)

A detailed description of this algorithm can be found in Hansen and Ostermeier [2001] and Hansen and Kern [2004]. Each individual in the population $P = \{\vec{a_1}, \vec{a_2}, ..., \vec{a_\mu}\}$ referred to by an index $k = 1..\mu$ has a phenotype[1] $\vec{a_k} = (\vec{x_k}, \vec{z_k})$ with $\vec{x_k}, \vec{z_k} \in \mathbb{R}^n$, where $\vec{x_k}$ is the standard ES parameter vector and $\vec{z_k}$ is the associated standard deviation vector. Each element of the phenotype is known as an allele. Three matrices are needed for the algorithm: the covariance matrix $C \in \mathbb{R}^{n \times n}$, the eigenvector matrix of C named $B \in \mathbb{R}^{n \times n}$ and the diagonal matrix of the square rooted eigenvalues of C, named $D \in \mathbb{R}^{n \times n}$. The μ individuals of the initial population are randomly defined ($\vec{x_k}$ are randomly chosen within the domain boundaries of f and $\vec{z_k}$ are set to the null vector). Matrix B is set to the identity matrix, the diagonal matrix D is set to represent the domain boundaries $D_{ii} = h_i - l_i, \forall i = 1..n$. C is calculated as the product of BD and its transpose: $BD \cdot (BD)^t$. Figure 3.1 shows graphically the operators of recombination, mutation and selection for a function of two parameters (x_1, x_2). The functioning of these operators is described in the following sections.

---

[1]Evolution Strategies are known to be phenotypic algorithms as they operate directly on the parameters of the system itself, unlike Genetic Algorithms which operate at the genotypic level and need a coding/decoding step to obtain the phenotype.
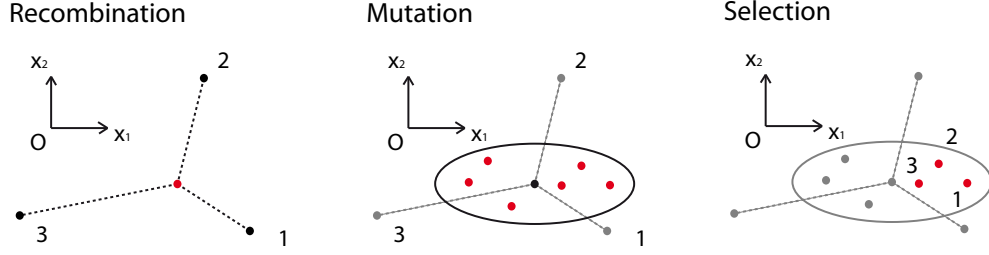
Figure 3.1: The three operators of the evolution for the CMA-ES, illustrated for an objective function in two dimensions. Three parents produce, by recombination and mutation, six children from which we select the new parents.

3.1.1   Recombination

Using the global weighted intermediate recombination method in conjunction with a sorted population (the best individual is number 1, the worst is μ), λ identical children are created with a phenotype:

$$(\vec{x_h})_i = \sum_{k=1}^{\mu} \omega_k \cdot (\vec{x_k})_i, \forall i = 1..n \tag{3.3}$$

$$(\vec{z_h})_i = 0, \forall i = 1..n \tag{3.4}$$

in which the individual index h goes from $(\mu + 1)$ to $(\mu + \lambda)$ and ω_k are the weights of the recombination, which are themselves parameters of the algorithm. In this study we take $\omega_k = \frac{\log(\mu+1)-\log(k)}{\sum_{l=1}^{\mu}(log(\mu+1)-log(l))}$ from Hansen and Ostermeier [2001], which gives more weight to the best individuals of the population.

3.1.2   Mutation

The main mechanism of the implemented operator is changing the allele values by adding random noise drawn from a normal distribution. The randomness from the normal distribution is stored in the individual phenotype and used in the adaptation phase. The mutation acts on each of the λ children with a modification of their phenotype in the following order:

$$\begin{aligned} (\vec{z_h})_i &\leftarrow N_i^h(0,1), \forall i = 1..n \\ (\vec{x_h})_i &\leftarrow (\vec{x_h})_i + \sigma_F \cdot \sum_{k=1}^{n} B_{ik} \cdot D_{kk} \cdot (\vec{z_h})_k, \forall i = 1..n, \end{aligned} \tag{3.5}$$

where $N_i^h(0,1)$ is a random number drawn from a normal distribution sampled anew for each element i of each individual $h = (\mu + 1)..(\mu + \lambda)$ and the symbol $\leftarrow$ means that $(\vec{z_h})_i$ and $(\vec{x_h})_i$ will take the values on their RHS. The global step size $\sigma_F \in \mathbb{R}_+$ is a (problem-dependent) parameter of the

algorithm.

A mutated individual may happen to be outside the box constraints, if this is the case, it is put back inside the domain by taking:

$$(\vec{x_h})_i \quad \leftarrow \quad \min\left((\vec{x_h})_i, h_i\right) \tag{3.6}$$

$$(\vec{x_h})_i \quad \leftarrow \quad \max\left((\vec{x_h})_i, l_i\right) \tag{3.7}$$

In order to provide random numbers that follow a normal distribution, we use the Ziggurat method [Marsaglia and Tsang, 2000].

3.1.3 Selection

Elitist selection is used to retain the μ best individuals of the λ children.

3.1.4 Adaptation

Three parameters of the algorithm are adapted in this phase, these are the global step size σ_F, the orthogonal matrix B and the diagonal matrix D. More precisely, the covariance matrix C, used for the determination of B and D, is adapted. The global step size $\sigma_F \in \mathbb{R}_+$ is adapted using a "conjugate" evolution path $\vec{s} \in \mathbb{R}^n$, in the following order:

$$
\begin{aligned}
\vec{s} &\leftarrow (1-c_s)\vec{s} + \sqrt{\mu_{eff} \cdot c_s(2-c_s)} \cdot B \cdot \sum_{k=1}^{\mu} \omega_k \vec{z_k}, \\
\sigma_F &\leftarrow \sigma_F \cdot exp\left(\left(\frac{s}{\overline{\chi_n}} - 1\right) \cdot \frac{c_s}{d_s}\right),
\end{aligned}
\tag{3.8}
$$

where $\overline{\chi_n} = \sqrt{n}(1-1/4n+1/21n^2)$, $c_s = \frac{\mu_{eff}+2}{n+\mu_{eff}+3}$, $d_s = 1+2\cdot max\left(0, \sqrt{\frac{\mu_{eff}-1}{n+1}} - 1\right) + c_s$, $\mu_{eff} = 1/\sum_{k=1}^{\mu} \omega_k^2$ and s is the vector norm of $\vec{s}$. The initial conjugate evolution path is $\vec{s} = \vec{0}$.

The covariance matrix $C \in \mathbb{R}^{n \times n}$ is adapted using the evolution path $\vec{c} \in \mathbb{R}^n$ in the following way:

$$
\begin{aligned}
\vec{c} &\leftarrow (1-c_c)\vec{c} + H_s \cdot \sqrt{\mu_{eff} \cdot c_c(2-c_c)} \cdot BD \cdot \sum_{k=1}^{\mu} \omega_k \vec{z_k} \\
C &\leftarrow (1-c_{cov})C + c_{cov} \cdot \frac{1}{\mu_{eff}} \cdot \vec{c} \cdot \vec{c}^{\,t} \\
&\quad + c_{cov} \cdot \left(1 - \frac{1}{\mu_{eff}}\right) \cdot \sum_{k=1}^{\mu} (BD \cdot \vec{z_k})(BD \cdot \vec{z_k})^t
\end{aligned}
\tag{3.9}
$$

where $c_{cov} = \frac{1}{\mu_{eff}} \cdot \frac{2}{\left(n+\sqrt{2}\right)^2} + \left(1 - \frac{1}{\mu_{eff}}\right) \cdot min\left(1, \frac{2\mu_{eff}-1}{(n+2)^2+\mu_{eff}}\right)$, $c_c = \frac{4}{n+4}$, $H_s = 1$ if $\frac{s}{\sqrt{1-(1-c_s)^{2(g+1)}}} < \left(1.5 + \frac{1}{n-0.5}\right)\overline{\chi_n}$ or 0 otherwise (the symbol g corresponds to the generation number). The initial evolution path is $\vec{c} = \vec{0}$. Once adapted, the orthogonal matrix B and diagonal matrix D are obtained through principal component analysis of C (i.e. $C = BD^2B^t$).

3.2   The Hybrid Differential Evolution algorithm (HDE)

Following Storn and Price [1996], Feoktistov [2006] and Chang et al. [2007], the individuals are coded with real-value representations. The population $P = \{\vec{a_1}, \vec{a_2}, ..., \vec{a_{NP}}\}$ is composed of NP individuals and their phenotype is given by $\vec{a_k} = (\vec{x_k}), \vec{x_k} \in \mathbb{R}^n$ where $\vec{x_k}$ is the parameter vector for individual $k = 1..NP$. The initial population is randomly distributed in the domain of the function to optimise. Figure 3.2 shows graphically the operators of mutation, recombination and selection for a function of two parameters (x_1, x_2). The functioning of the operators is described in the following.
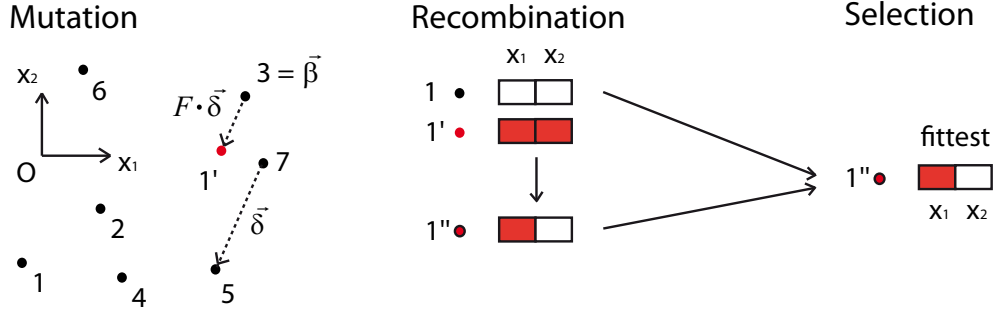
Figure 3.2: The three operators of the evolution for the HDE illustrated for an objective function in two dimensions. For the first parent, a trial individual is created and recombined with the parent to produce a child. The fittest of the parent and child is selected.

3.2.1   Recombination and Mutation

For each candidate member of the parent population $k = 1..NP$ a trial individual $\vec{w_k} \in \mathbb{R}^n$ is generated thus:

$$\vec{\omega_k} = \vec{\beta_k} + F \cdot \vec{\delta_k}, \tag{3.10}$$

where F is the differentiation constant (which controls the amplification of the differentiation), $\vec{\beta_k}$ is the base vector and $\vec{\delta_k}$ the differentiation vector. The differentiation strategy used in our study is *Rand*3 [Feoktistov, 2006] where $\vec{\delta_k} = \vec{\xi_1} - \vec{\xi_2}$ and $\vec{\beta_k} = \vec{\xi_3}$. $\{\vec{\xi_1}, \vec{\xi_2}, \vec{\xi_3}\}_k$ are randomly chosen individuals in the population sampled anew for each $k = 1..NP$.
A crossover is then carried out between the trial and corresponding candidate:

$$(\vec{\omega_k})_i \leftarrow \begin{cases} (\vec{\omega_k})_i, & if \ (rand_i(0,1) \geq C_r \ or \ R = i) \\ (\vec{a_k})_i, & otherwise \end{cases} \tag{3.11}$$

where C_r is the crossover probability, R is a randomly selected allele number defined before the crossover (this forces at least one allele to change) and $rand_i(0,1)$ is a random number between zero and one sampled anew for each allele i.

The trial individual may happen to be outside of the box constraints. If this is the case, it is put back randomly inside the domain by taking:

$$(\vec{\omega_h})_i \leftarrow rand_i(l_i, h_i), \tag{3.12}$$

where $rand_i(l_i, h_i)$ is a randomly chosen number within the upper h_i and lower l_i boundaries of allele i.

The resulting trial individuals are contained in a set of NP individuals for the selection phase.

3.2.2 Selection

The best individual between the candidate in the parent population and the corresponding trial is kept.

3.2.3 Migration

In order to reduce the population size and avoid stagnation in the region of a local optimum, Chang proposed a migration technique[2]. When the diversity ρ of the population is too small (i.e. $\rho < \epsilon_1$), all individuals are modified according to the rule:

$$(\vec{x_k})_i \leftarrow \begin{cases} (\vec{x_k})_i + \rho_1 \cdot (L_i - (\vec{x_b})_i), & if \ \rho_2 < \frac{(\vec{x_k})_i - L_i}{H_i - L_i} \\ (\vec{x_k})_i + \rho_1 \cdot (H_i - (\vec{x_b})_i), & otherwise \end{cases} \tag{3.13}$$

where $i = 1..n$, $\vec{x_b}$ is the best individual of the actual population and ρ_1, ρ_2 are two random numbers chosen between 0 and 1 and sampled anew for each element of each individual.

The diversity ρ is defined as follow:

$$\rho = \sum_{k=1}^{\mu} \sum_{i=1}^{n} \frac{\chi_{ki}}{n \cdot (\mu - 1)} \tag{3.14}$$

where:

$$\chi_{ki} = \begin{cases} 1 & if \ \left| \frac{(\vec{x_k})_i - (\vec{x_b})_i}{(\vec{x_b})_i} \right| > \epsilon_2 \quad and \quad |(\vec{x_k})_i - (\vec{x_b})_i| > (\vec{\epsilon_3})_i \\ 0 & otherwise \end{cases} \tag{3.15}$$

---

[2]not to be confused with the migration phase of island distributed EAs [Tomassini, 2005]
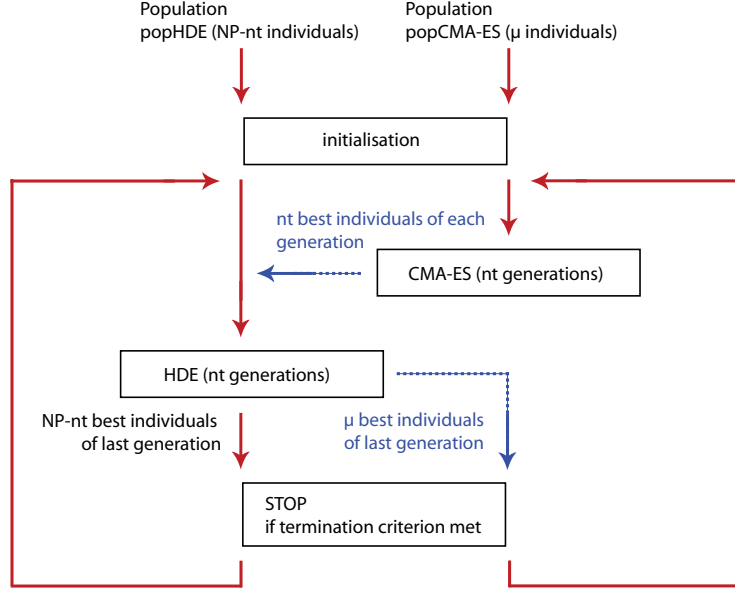
Figure 3.3: The hybrid algorithm, a coupling of CMA-ES and HDE - Two distinct populations popHDE and popCMA-ES go through evolution process (red solid lines) exchanging individuals (blue dashed lines)

with $\epsilon_2 \in \mathbb{R}_+$ and $\vec{\epsilon_3} \in \mathbb{R}_+^n$, which are respectively the relative precision and the absolute precisions vector for the problem solved. We have introduced the parameter $\vec{\epsilon_3}$, which was not originally included in the HDE, to take into account the desired number of decimal places in these variables.

3.3   The hybrid algorithm (CMA-ES/HDE)

Figure 3.3 depicts the proposed hybrid algorithm in schematic form. The HDE and CMA-ES operate in series. We distinguish two populations: popHDE and popCMA-ES that are associated with the HDE and the CMA-ES. We start with the CMA-ES with a random population for n_t steps (or generations). This then feeds the best n_t individuals at each step to the population of HDE and the missing $(NP - n_t)$ individuals in popHDE are randomly generated. We then continue with the HDE for n_t generations. We keep from the last generation of HDE the μ and $(NP - n_t)$ best individuals. If the termination criterion is met, the algorithm is stopped, otherwise it loops and switches over to the CMA-ES. For the following applications, we have chosen to run each algorithm for $nt = 10$ generations.

3.4 Unconstrained applications

To illustrate the performance of the proposed hybrid method we have used two benchmark functions: those of Ackley and Rastrigin. The Ackley function is not additively separable, unlike the Rastrigin function. A priori from Hansen and Kern [2004] the CMA-ES alone should perform best on Ackley and the HDE alone on Rastrigin. We proceed by checking this and comparing the proposed hybrid performance to the following methods: $(\mu/2_I, \lambda)$-ES, CSA-ES, CMA-ES, DE and HDE (see page 24 for references). We conduct our tests on unconstrained applications with the maximisation of solar energy potential in urban areas.

3.4.1 Benchmark functions

Benchmark functions are designed to test the performance of optimisation algorithms. They should also represent some of the complexity that can be encountered in real-world optimisation problems. Moreover, they are inexpensive to compute unlike the real-world problems.

3.4.2 Ackley function

The generalised Ackley function is defined in n dimensions by,

$$f_n(\vec{x}) = -a \exp\left(-b\sqrt{\frac{1}{n}\sum_{i=1}^{n}x_i^2}\right) - \exp\left(\frac{1}{n}\sum_{i=1}^{n}\cos cx_i\right) + a + \exp(1), \quad (3.16)$$

where $\vec{x} \in \mathbb{R}^n$, $a = 20$, $b = 0.2$ and $c = 2\pi$. Its domain is $-32.768 \leq x_i \leq 32.768, \forall i = 1..n$. This function is multi-modal with a global minimum at $\vec{x} = \vec{0}$ which is surrounded by many local minima. Figure 3.4 shows a two dimensional plot of the Ackley function.

We have tested the Ackley function for $n = 10$, repeated each case for 100 runs and compared results from the hybrid algorithm CMA-ES/HDE with DE, HDE, CSA-ES [Beyer and Schwefel, 2002, Dirk and Alexander, 2006], CMA-ES and $(\mu/2_I, \lambda)$-ES [Quagliarella et al., 1998]. The following parameters of the algorithms were chosen for a good level of performance (based on the Q-measure) after many experiments.

DE $NP = 30$, $C_r = 0.1$, $F = 0.3$

HDE $NP = 30$, $C_r = 0.1$, $F = 0.3$, $\epsilon_1 = 0.1$, $\epsilon_2 = 0.1$, $(\vec{\epsilon_3})_{i=1..n} = 1 \cdot 10^{-3}$

ES $\sigma_F = 0.2$, $\mu = 15$, $\lambda = 100$, $K = 1.0$
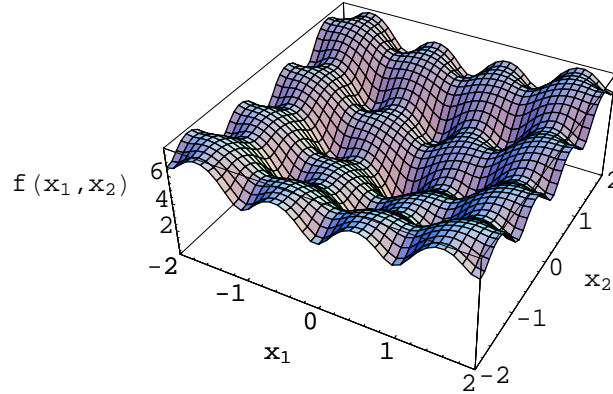
Figure 3.4: The Ackley function in two dimensions (n=2).

CSA-ES and CMA-ES $\sigma_F = 0.2$, $\mu = 5$, $\lambda = 10$

CMA-ES/HDE a combination of the parameters of CMA-ES and HDE

The results are summarised in Table 3.1. In this the first line contains the convergence measure C (the mean number of function evaluations to reach a fitness under 0.1) and its standard deviation. The second line contains the percentage of convergence P_C on a maximum of 80 thousands function evaluations and the Q-measure (Q_m), which is the ratio of convergence measure and the percentage of convergence. See Feoktistov [2006, p.84] for further details. We notice from these results (Table 3.1) that, based on the Q-measure,

	DE	HDE	ES	CSA-ES	CMA-ES	CMA-ES/HDE
C	3510 ± 151	3510 ± 151	3675 ± 201	1178 ± 137	862 ± 70	2695 ± 178
P_C (Q_m)	100% (3510)	100% (3510)	99% (3712)	99% (1190)	98% (880)	100% (2695)

Table 3.1: Convergence comparison for the Ackley benchmark function

the CMA-ES outperforms the DE on this non-additively separable function, as Hansen and Kern [2004] suggest. However, the DE is more robust than the CMA-ES, as it achieves 100% convergence.

The proposed hybrid algorithm benefits from the advantages of both algorithms. The HDE component brings a high convergence percentage (100%) whilst the CMA-ES component provides a better performance in the Q-measure than the HDE alone.
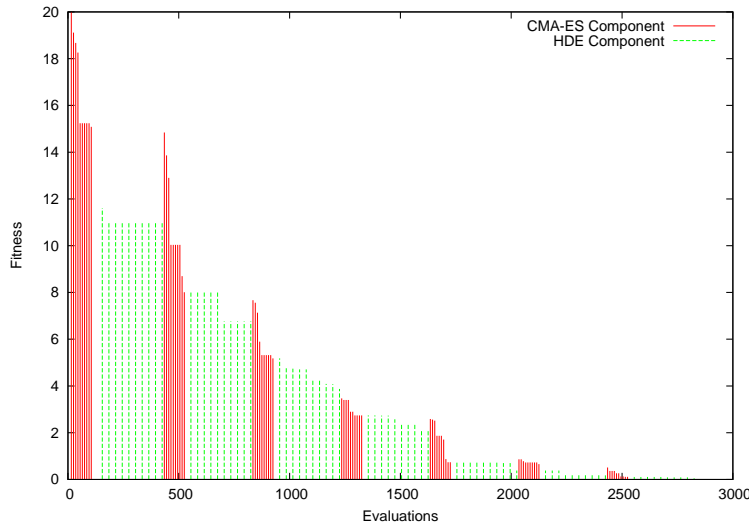
Figure 3.5: A typical run of the CMA-ES/HDE algorithm on the Ackley function with dimension n=10: the best individual fitness (or objective function value) versus the number of function evaluations

n	10	20	30	40
C	7717 ± 264	12018 ± 279	15542 ± 306	18765 ± 269
P_C	100%	100%	100%	100%

Table 3.2: Convergence for Ackley benchmark function with different dimension values (n)

If we look closer at a typical run (Figure 3.5), we notice that the CMA-ES component is more active in improving the population's best fitness than the HDE component. The average number of function evaluations needed by the CMA-ES component for the hybrid to converge to the global minimum is roughly the same as for the CMA-ES alone. The overall performance in Q-measure of the hybrid is worsened by the HDE component, but fortunately it provides a better convergence percentage.

After a first run of the hybrid algorithm, the CMA-ES component obtains the μ best individuals from the HDE, and performs a global intermediate recombination of these, followed by mutation. This operation can result in worse individuals than the initial ones as the elitist selection phase forgets about the parents. This effect is very noticeable after the first HDE component run in Figure 3.5: the best individual of the following first CMA-ES generation is worse than the last best one.

Finally, we have tested the performance of our algorithm against the dimension number n of the generalised Ackley function (Table 3.2). The CMA-ES population size is adapted according to ($\mu = 2 + \lfloor 1.5 \cdot \log(n) \rfloor, \lambda = 4 + \lfloor 3 \cdot \log(n) \rfloor$) taken from Hansen and Ostermeier [2001]; while the HDE population size is kept constant ($NP = 30$). The termination criterion is satisfied when the function returns a value under $1 \cdot 10^{-6}$, and the precision parameters for HDE are set to: $\epsilon_2 = 0.1, (\vec{\epsilon_3})_{i=1..n} = 5 \cdot 10^{-7}$. From this we conclude that our algorithm can adapt to reasonable increases in problem dimension for the Ackley function.

3.4.3   Rastrigin function

The second benchmark function is the generalised Rastrigin function of dimension n,

$$f_n(\vec{x}) = nA \sum_{i=1}^{n} x_i^2 - A \cos(\omega x_i), \tag{3.17}$$

where $\vec{x} \in \mathbb{R}^n$, $A = 10$ and $\omega = 2\pi$. Its domain is $-5.12 \leq x_i \leq 5.12$, for all $i = 1..n$ and the global minimum is at $\vec{x} = \vec{0}$. This function is highly multi-modal with many sub-peaks increasing in intensity when approaching the global minimum. Figure 3.6 shows the Rastrigin function in two dimensions.
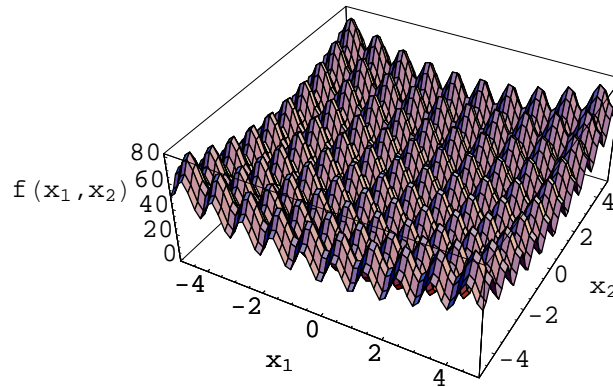
Figure 3.6: The Rastrigin function in two dimensions ($n = 2$).

We tested the Rastrigin function for $n = 10$. The parameters are the same as

for the Ackley function, except for the $(\mu/2_I, \lambda)$-ES [Quagliarella et al., 1998] where the population was increased to $(32, 200)$ for performance reasons. The population size of CSA-ES and CMA-ES should have been further increased for good convergence [Hansen and Kern, 2004], however we decided to keep it small to facilitate a better performance of the hybrid CMA-ES/HDE. The corresponding results are summarised in Table 3.3. Both the CSA-ES and

	DE	HDE	ES	CSA-ES	CMA-ES	CMA-ES/HDE
C	5949 ± 607	6543 ± 1897	17432 ± 3709	-	-	6255 ± 2020
P_C (Q_m)	95% (6262)	100% (6543)	32% (54475)	0%	0%	100% (6255)

Table 3.3: Convergence comparison for Rastrigin benchmark function

the CMA-ES have a too small population to converge to the global minimum. We also note that, thanks to its migration procedure, HDE is more robust than DE. As expected from Hansen and Kern's conclusion [Hansen and Kern, 2004], the DE outperforms the CMA-ES on this additively separable function.

The hybrid appears in the statistics to be just slightly better in the Q-measure than the HDE alone. This fact is difficult to explain as the working of EA is complex and hard to understand in details. However at least a small part of the explanation emerges from the results: when approaching the vicinity of the global minimum, the CMA-ES component of the hybrid takes the lead and provides a faster convergence to the global minimum than what the HDE component does. This effect is (barely) visible in Figure 3.7, which presents two typical runs of our hybrid algorithm with the Rastrigin function.

(a) Best run, migration procedure not necessary

(b) Worst run, migration procedure needed twice to converge to the global minimum
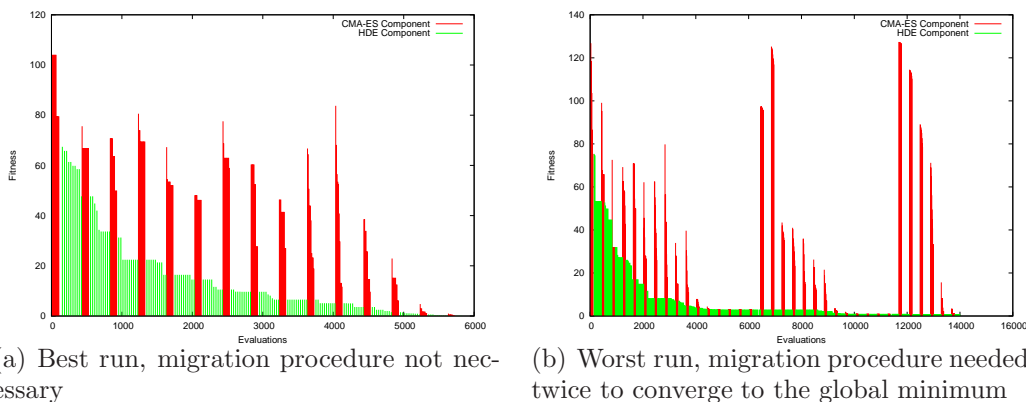
Figure 3.7: Typical runs of the CMA-ES/HDE algorithm on the Rastrigin function with dimension n=10

n	10	20	30	40
C	9104 ± 3455	33844 ± 15047	71605 ± 29932	139031 ± 51237
P_C	100%	100%	100%	100%

Table 3.4: Convergence for Rastrigin benchmark function with different dimension values

In contrast to the Ackley function, the HDE component of our hybrid is considerably more active than the CMA-ES component. The difference in the number of function evaluations to reach the global minimum for the best and worst runs gives an insight into the high standard deviation of the hundred runs. In the worst case, the migration procedure of the HDE component had to act two times to overcome local minima.

We have also tested the performance of our algorithm against the dimension number n of the generalised Rastrigin function using the same algorithm parameters as for the Ackley function. The results are summarised in Table 3.4. From this we notice that even with a small adaptation of the population size for the CMA-ES, our hybrid algorithm is robust and converges in all cases. However, the variability in convergence speed (see the standard deviation) becomes large when n increases. This is due to the migration phase in the HDE and is the cost for 100% convergence.

3.4.4   Maximisation of solar irradiation potential

The purpose of this hypothetical study is to propose an arrangement of buildings on a flat site that maximises their solar energy potential. The problem becomes particularly interesting when the number of buildings to arrange doesn't allow for a regular array (prime numbers for example) and the anisotropy of the sky leads to certain orientations being favoured over others. The period of interest chosen for the study is the winter season, when energy demands for heating and artificial lighting can be reduced. As before (see Section 2.3.2) we assume that buildings can be fitted with shading devices in the summer to avoid the negative impact of overheating. The next section deals with the parameterisation of the urban environment and the following section presents for the optimisation of absorbed solar radiation using our new hybrid algorithm.
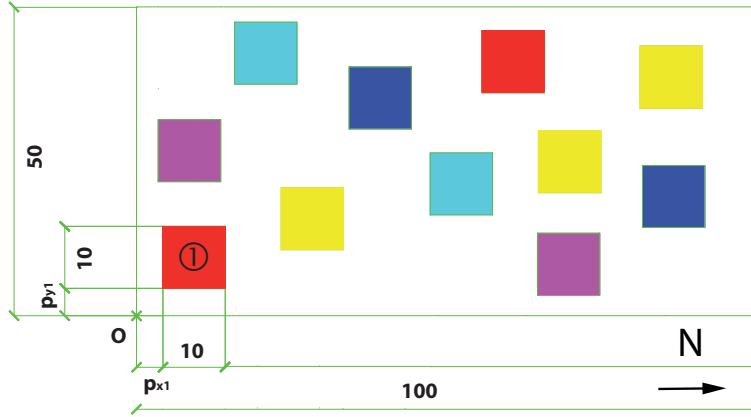
Figure 3.8: The urban environment - Eleven buildings (view from top) disposed on the field, each building is parametrised by its position relative to the origin in cartesian coordinates

Parameterisation

The parameter space is defined by the position of 11 buildings on a limited ground space of 50 m by 100 m. Each building is a parallelepiped of 10 m by 10 m on the ground and 20 m high. Figure 3.8 shows a random configuration of eleven buildings viewed from the top. We use 22 variables to define the positions of the buildings on the ground:

$$\vec{x} = (p_{x_1}, p_{y_1}, ..., p_{x_{11}}, p_{y_{11}}), \tag{3.18}$$

where $p_{xi} \in [0, 90]$ is the position in x-coordinate and $p_{yi} \in [0, 40]$ in y-coordinate of the lower left corner of the ith building.

The problem has no further constraints other than domain boundaries. In fact, it is a self-constrained problem. By this we mean that when the buildings intersect they intercept less rays from the sun and sky compared to when they are separated. By maximising the solar energy potential, the buildings tend therefore to be (maximally) separated.

Results

We have set the termination criterion of our hybrid Evolutionary Algorithm to 6000 function evaluations. Since we avoided the interruption of the algorithm part way through a component iteration, it was ceased after 6016 evaluations. Each evaluation takes approximatively 57 seconds on an Intel Centrino Duo 2 GHz equipped with 1 Gb of RAM; due to the total computing time needed only one run of the algorithm was accomplished. Figure
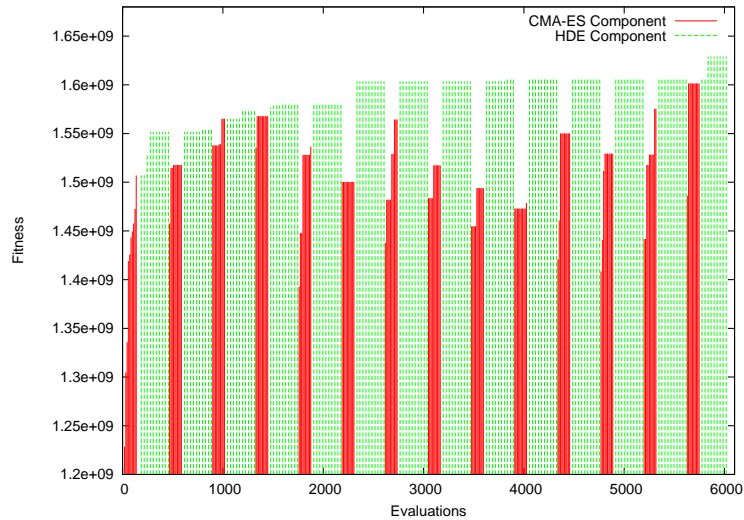
Figure 3.9: The improvements in solar energy potential of the urban configuration versus the evaluations number

3.9 presents the evolution of the best candidate with the number of function evaluations. Looking more closely at this we note that the best individual appeared after 5836 evaluations. The CMA-ES component was very helpful at the beginning, providing a quick exploration of the search space, the HDE component then proceeded to provide the best individual.

The solar energy potential of the best candidate (see Figure 3.10 for a RADIANCE image) is about 1.63 GWh during the heating period, relating to a cumulative sky for Basel (Switzerland).

For comparison purposes we have solved the same problem using the advanced optimisation software MOO [Leyland, 2002, Molyneaux, 2002] which runs under MATLAB. With this software configuration we predict an equivalent solar energy potential (1.63 GWh) and placement of buildings after 5200 evaluations.

3.4.5   Conclusion

A new hybrid Evolutionary Algorithm algorithm is proposed and compared with other selected methods (DE, HDE, ES, CSA-ES and CMA-ES) on two standard benchmark functions: Ackley and Rastrigin. From our statistical results the method exhibited the advantages of the two hybridised algorithms; the HDE component brought robustness in finding the global minimum and the CMA-ES component provided for faster convergence compared with the HDE alone.

kWh/m2
380
340
300
260
220
180
140
100
60
20
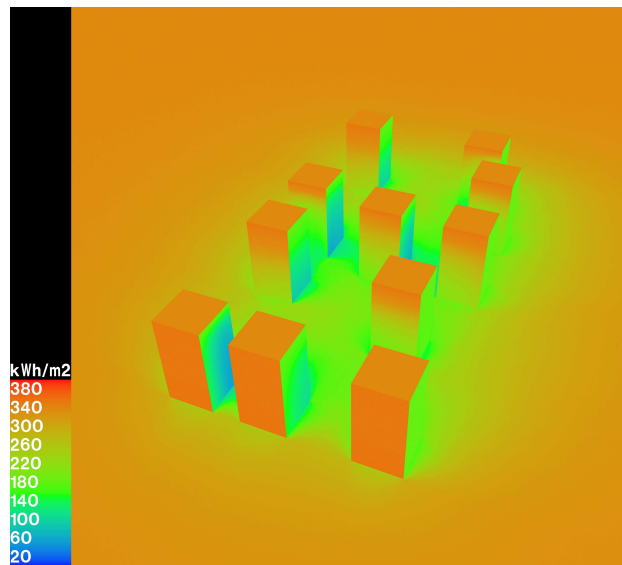
Figure 3.10: The results of the optimisation of the solar energy potential for the placement of eleven buildings in a rectangular ground. RADIANCE rendering with surface falsecolored according to incident irradiation.

In real-world optimisation applications robustness is an important issue. Therefore if the function dependence on its parameters has similarities with the Ackley or Rastrigin functions, then the proposed hybrid should be similarly robust in finding a good solution. Nevertheless, we do not know if a similar degree of robustness would be provided for dissimilar functions. It is however encouraging that an application of the hybrid to a real-life problem of solar energy potential maximisation showed good results compared to the multi-objective optimiser MOO.

3.5   Constraints handling and applications

3.5.1   Constraint handling

As shown in the introduction, the feasible domain M is written in the form:

$$M = \{\vec{x} \in \mathbb{R} \mid g_j(\vec{x}) \leq 0, \forall j \in \{1, ..., m\}\}, \tag{3.19}$$

where $g_j : \mathbb{R}^n \to \mathbb{R}, \forall j \in \{1, ..., m\}$ are m constraint functions of the parameters $\vec{x}$. In numerous examples, we have analytical constraints and time consuming evaluations. For computational reasons we want to avoid evaluating potential solutions that do not satisfy the constraints, we therefore redefined the objective function:

$$\hat{f}(\vec{x}) = \begin{cases} f(\vec{x}) & \vec{x} \in M, \\ +\infty & \text{otherwise}, \end{cases} \tag{3.20}$$

and implemented the "Modification of the Selection Operation" proposed by Feoktistov [2006, pp.34-35]. It redefines the "is better than" operator, by taking into account a pure Pareto dominance defined in a constraint function space. This latter operator is defined as follow: $\vec{x_1}$ is better than $\vec{x_2}$ if and only if $\Phi \vee \Psi$, where:

$$\begin{aligned} \Phi &= (\forall k \in \{1, ..., m\} : g_k(\vec{x_1}) \leq 0 \wedge g_k(\vec{x_2}) \leq 0) \wedge \\ &\quad (f(\vec{x_1}) < f(\vec{x_2})), \\ \Psi &= (\exists k \in \{1, ..., m\} : g_k(\vec{x_1}) > 0) \wedge \\ &\quad (\forall k \in \{1, ..., m\} : \max(g_k(\vec{x_1}), 0) \leq \max(g_k(\vec{x_2}), 0)). \end{aligned}$$

Please note that if $\Phi \vee \Psi$ is false, nothing is said about $\vec{x_2}$ (i.e. $\vec{x_2}$ is not always better than $\vec{x_1}$). The application of this comparison operator within the CMA-ES and HDE is explained below. This method of handling constraints allows individuals violating the constraints to survive in the first generations of the algorithms, and therefore to participate in the recombination process, so bringing diversity and allowing the borders of the constrained parameter space to be approached.

CMA-ES   The mutation phase is repeated on an individual as long as it remains outside of the constrained space, but for a maximum of 10 times. The comparison operator described above is applied to the population of children for sorting, prior to the elitist selection of the new generation's parents.

HDE In the selection phase, the comparison operator is used to compare the candidate with the trial (in that order). If the candidate is better than the trial, the candidate is kept, otherwise the trial is kept. This ensures that when both individuals satisfy the constraints and the objective functions are equal, the trial is preferred, bringing diversity to the population and preventing stagnation. Moreover, when both individuals do not satisfy the constraints, the candidate individual is kept only if it dominates over all constraints at the same time, allowing the trial to be selected in most cases, for the same diversity reasons.

3.5.2 Benchmark function

The following benchmark function has 13 variables and 9 linear constraints, it was designed to test different constraint handling methods [Michalewicz and Schoenauer, 1996],

$$f(\vec{x}) = 5x_1 + 5x_2 + 5x_3 + 5x_4 - 5\sum_{i=1}^{4} x_i^2 - \sum_{i=5}^{13} x_i + 15, \qquad (3.21)$$

subject to the following constraints:

$$2x_1 + 2x_2 + x_{10} + x_{11} \leq 10, \qquad -8x_1 + x_{10} \leq 0, \qquad -2x_4 - x_5 + x_{10} \leq 0,$$
$$2x_1 + 2x_3 + x_{10} + x_{11} \leq 10, \qquad -8x_2 + x_{11} \leq 0, \qquad -2x_6 - x_7 + x_{11} \leq 0,$$
$$2x_1 + 2x_3 + +x_{11} + x_{12} \leq 10, \qquad -8x_3 + x_{12} \leq 0, \qquad -2x_8 - x_9 + x_{12} \leq 0.$$

Its domain is $0 \leq x_i \leq 1$, for all $i = 1..9$ and $i = 13$ with an absolute precision $\vec{\epsilon}_{3i} = 0.01$ and $0 \leq x_i \leq 100$ for $i = 10, 11, 12$ with $\vec{\epsilon}_{3i} = 0.1$. The function is quadratic with a global minimum at $f(1, 1, 1, 1, 1, 1, 1, 1, 1, 3, 3, 3, 1) = 0$. The topology of the feasible region and the characteristic of the objective function are quite significant measures of the difficulty of problems according to Michalewicz and Schoenauer [1996]. In this benchmark function even though the objective function is only quadratic, the topology of the nine linear constraints makes it difficult to resolve with no access to the objective function value outside of the constrained domain.

Results

On a total of hundred simulations, 39 runs converged to the global minimum (considered by a fitness under 0.2) within 4207 ± 1328 evaluations on an evaluation limit of 10000. This performance is relatively poor compared to other methods that *do* evaluate the objective function outside of the constrained

domain [Runarsson and Yao, 2000], but the choice of our constraint handling method, which does *not* necessitate an objective function evaluation, was made for computational cost and robustness reasons. Due to its recombination and mutation operators, the CMA-ES/HDE tends to explore the interior of the domain boundaries, making it difficult to approach the boundaries where the global minimum is found. However, thanks to the constraint handling procedure within the mutation phase of the CMA-ES algorithm, we observe that the border of the domain can sometimes be approached and the global minimum successfully identified. This result is rather encouraging as in general in real-world applications the global minimum is not exactly at the domain boundaries, making the problem less hard for the CMA-ES/HDE.

3.5.3   Manhattan style grid

In this application a hypothetical city comprised of cuboidal shapes is created with the objective of maximising the annual irradiation incident on all buildings. The initial configuration is shown in Figure 3.11. Each building
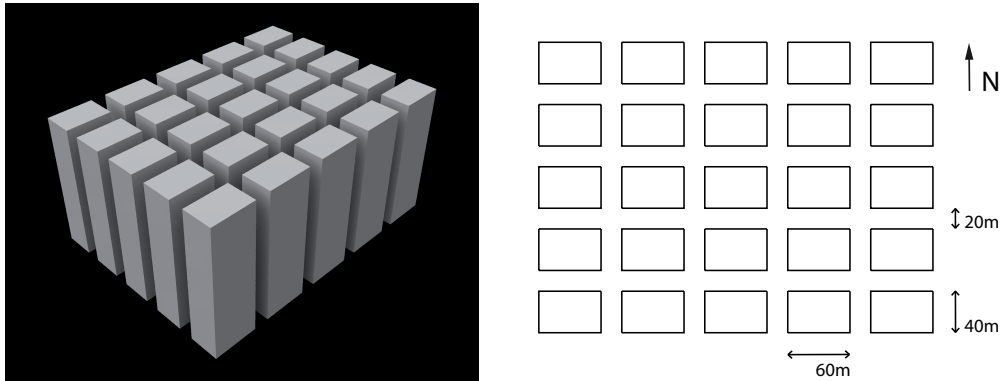
Figure 3.11: A RADIANCE generated image of the Manhattan style grid (left), a schematic view from top (right)

may have its height varied so that there are in total 25 parameters:

$$\{\vec{x} \in \mathbb{R}^{25} \mid x_i \in [0, 123], i = 1..25\} \tag{3.22}$$

Those parameters are the number of floors (a maximum of 123) in each building. The parameters are rounded to the nearest integer before the evaluation and the floors are considered to be 3m high each. Simulating all possibilities would require 124^{25} evaluations of the solar potential, which is not feasible. To reduce the cost of the evaluation process to a reasonable minimum, reflected radiation is ignored.

The constrained parameter space is defined by the total built volume remaining within 10% of half of the maximum $(25 \cdot 40 \cdot 60 \cdot 123 \cdot 3/2 \pm 10\% \text{ m}^3)$. The constraints expressed in mathematical terms give:

$$\underbrace{v(\vec{x}) - v(\vec{x}_{max}) \cdot 50\% \cdot 110\%}_{g_1(\vec{x})} \leq 0, \qquad (3.23)$$

$$\underbrace{-v(\vec{x}) + v(\vec{x}_{max}) \cdot 50\% \cdot 90\%}_{g_2(\vec{x})} \leq 0, \qquad (3.24)$$

where $\vec{x}_{max} = (123, ..., 123)$ and $v(\vec{x})$ is the volume corresponding to parameters in $\vec{x}$. We thus have two linear constraints, giving a range of possible volumes.

Results

A candidate solution, presented in Figure 3.12, was found after some 12000 evaluations. Buildings at the northern edge of this grid are all at maximum
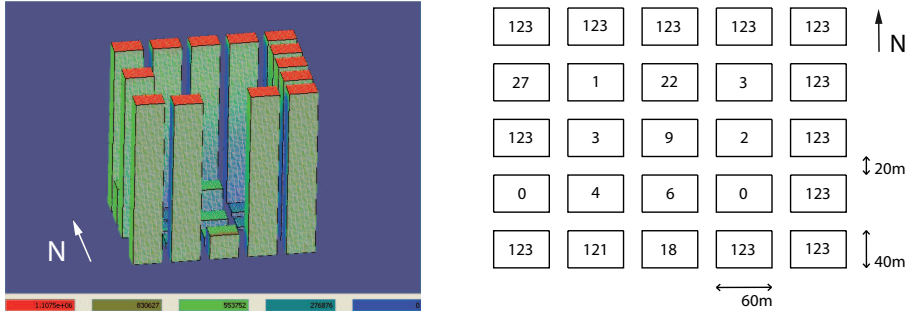
Figure 3.12: Optimal case for the Manhattan style grid after 12000 evaluations, on the left the model with an irradiance map in Wh, on the right a two-dimensional representation with the number of floors of each building

height, whereas buildings at the east and particularly south and west edges are irregular, with some at or approaching the maximum height and some considerably lower. This arrangement provides solar access for the lower interior buildings and (more particularly) for the southern facades of the building at the northern edge.

Figure 3.13(a) shows the evolution of the fitness (annual solar irradiation) of the candidates along with the evaluations made in the evolutionary algorithm. The CMA-ES part of the algorithm provides a steep rise in fitness at the beginning of the simulation, whilst the HDE part goes deeper in fine-tuning the solution.

(a) The fitness (solar energy potential) evolution within the evolutionary algorithm for the Manhattan style grid

(b) Corona and Stairs shapes
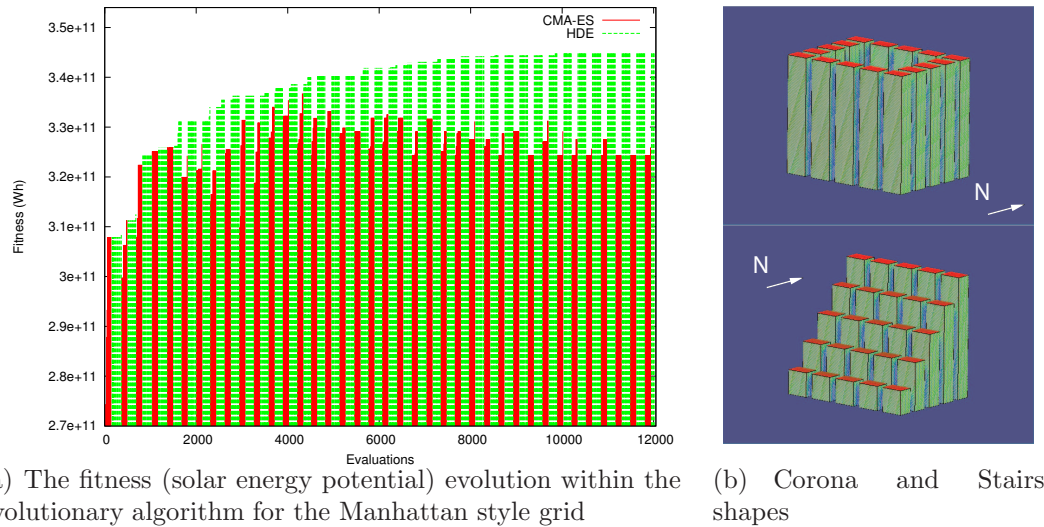
Figure 3.13: The results and comparison for the Manhattan style grid

Parameters	Irradiation (GWh)	Volume ($\cdot 10^7$ m^3)
Stairs shape (floors are multiple of 22, see 3.13(b))	282.2 (82%)	1.188
Corona shape (border buildings with 105 floors, internal ones with 1 floor)	319.5 (93%)	1.216
Optimal shape after 12000 evaluations	344.9 (100%)	1.217

Table 3.5: Irradiance values comparison for the optimised case, the corona and stairs cases

In Table 3.5, we can see that the improvement gained with our optimisation algorithm relative to two subjectively chosen variants - the corona and stair shaped layouts shown in Figure 3.13(b); both of which satisfy the constraints mentioned earlier. Relative to the corona shape the optimised shape (which wouldn't necessarily be arrived at by intuition) yields an 8% improvement for a similar built volume; whereas relative to the stairs layout the improvement is 22%. This is interesting because conventional site planning guidance suggests that buildings should be progressively stepped-up towards the North of a site, to maximise solar access [Littlefair et al., 2000].

3.5.4   A photovoltaic extension of a Mansion

An extension of a Mansion was planned as part of an architectural studio design project, for which it was intended to install photovoltaic (PV) panels

on the newly created building surfaces. In this the objective was to orient and tilt the roof surfaces so that they would receive the maximum available irradiation throughout the year, with reflected radiation once again being neglected for computation reasons. The scene is shown in Figure 3.14, in which the extension is decomposed into triangles on the schematic plan. Each
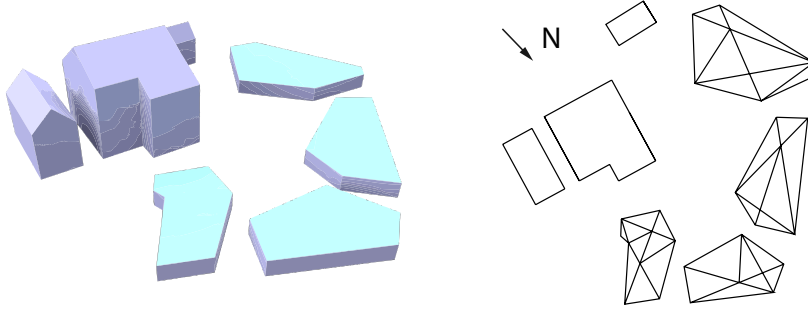
Figure 3.14: A projection and schematic plan viewed from top of the Mansion and its extension (decomposed in triangles on the 2D schematic plan)

triangle vertex may take a height of between 3 and 6 *m*. In total there are 31 parameters:

$$\{\vec{x} \in \mathbb{R}^{31} \mid x_i \in [3, 6], i = 1..31\} \tag{3.25}$$

A key constraint is that the roof must maintain a convex shape, as observed from above. In other words, the height of each internal point must be greater than or equal to that of the external point(s) to which it is connected. In total there are 32 constraints, which are not detailed here in mathematical form.

Results

For this case a candidate solution, shown in Figure 3.15, was found after 12000 evaluations. Compared to flat roofs at heights of 3 m and 6 m, the improvement is about 10% in annual irradiation (see Table 3.6). With an annual irradiation of 1.234 GWh and an average photovoltaic efficiency of 10%, the gain is equivalent to 11.6 MWh electrical energy which is non-negligible. Roof-integrated PV would appear to be viable in this case.
An interesting alternative to the above fitness function might be based on the proportion of the total envelope for which an irradiation threshold (eg. 800 kWh $\cdot$ m^{-2} for facades and 1000 kWh $\cdot$ m^{-2} for roofs) is exceeded, as a basis of determining the viability of solar energy (eg. PV) conversion systems.
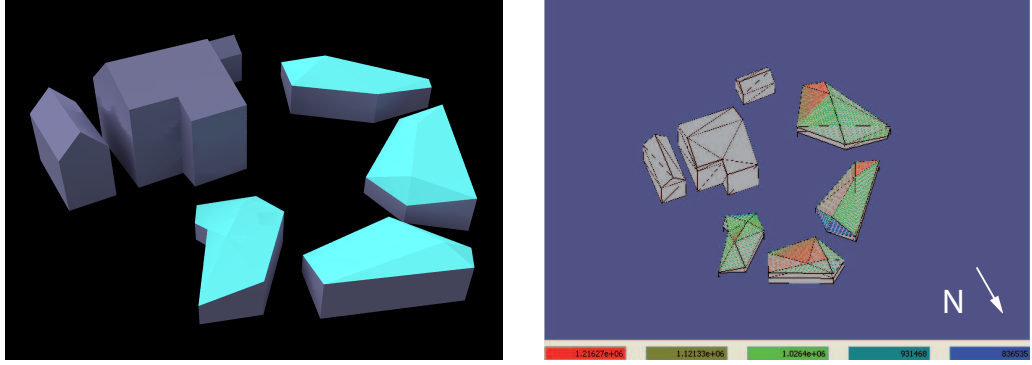
Figure 3.15: Optimal case for the photovoltaic extension after 12000 evaluations

Photovoltaic extension of a Mansion	
Parameters	Irradiation (GWh)
Minimal values $h_i = 3m, i = 1..31$	1.118 (91%)
Maximal values $h_i = 6m, i = 1..31$	1.131 (92%)
Optimal values after 12000 evaluations	1.234 (100%)

Table 3.6: Irradiation values comparison for the optimised case and flat roofs

3.5.5 2D Fourier series

In this hypothetical application, the idea was to use a two dimensional (2D) Fourier series to describe the geometry of a roof as a continuous function with relatively few terms. Once again we seek to maximise the utilisation of solar irradiation throughout a year, this time on both the roof and the vertical facades. Figure 3.16 shows a roof shape a described by a 2D Fourier series. For this application, the two dimensional Fourier series is expressed in terms of sines and cosines with N and M impairs:

$$
\begin{aligned}
h(x,y) = \ & \sum_{k=-\frac{N-1}{2}}^{\frac{N-1}{2}} \sum_{l=-\frac{M-1}{2}}^{\frac{M-1}{2}} \quad C_{kl} \cdot e^{\left(2\pi i k \frac{x}{L_x \frac{N}{N-1}} + 2\pi i l \frac{y}{L_y \frac{M}{M-1}}\right)} \qquad (3.26) \\
= \ & \sum_{k=-\frac{N-1}{2}}^{\frac{N-1}{2}} \sum_{l=0}^{\frac{M-1}{2}} \quad A_{kl} \cdot \cos\left(2\pi k \frac{x}{L_x \frac{N}{N-1}} + 2\pi l \frac{y}{L_y \frac{M}{M-1}}\right) \\
& \qquad\qquad + B_{kl} \cdot \sin\left(2\pi k \frac{x}{L_x \frac{N}{N-1}} + 2\pi l \frac{y}{L_y \frac{M}{M-1}}\right),
\end{aligned}
$$

where $h : \mathbb{R}^2 \to \mathbb{R}$ gives the height as a function of the position (x,y) in the plane, $x \in [0, Lx], y \in [0, Ly]$, L_x and L_y delimit the domain of interest in x and y, $C_{kl} \in \mathbb{C}$ are coefficients of elements in the Fourier basis and
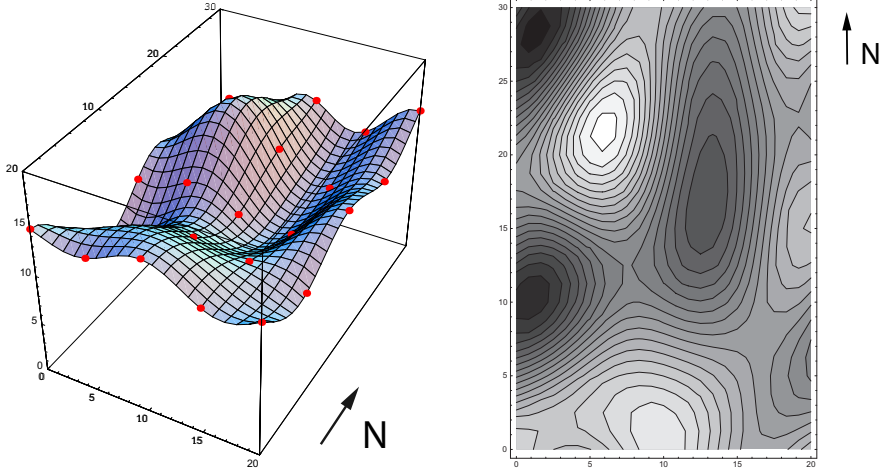
Figure 3.16: A roof represented by a 2D Fourier series (left), a contour plot representing the height (right).

$A_{kl}, B_{kl} \in \mathbb{R}$ are the amplitudes of the sines and cosines.

By definition, the function $h(x, y)$ is periodic in x and y. The period is $T_x = L_x \frac{N}{N-1}$ and $T_y = L_y \frac{M}{M-1}$ respectively for x and y. The multiplication by the factors $\frac{N}{N-1}$ and $\frac{M}{M-1}$ is introduced in order to avoid repetition in the domain of interest $x \in [0, Lx]$ and $y \in [0, Ly]$.

By considering the Fourier series in (3.26) as a backward discrete Fourier transform we have a continuous function that can pass through a grid of $N \cdot M$ regularly spaced points in the domain of interest. Such points are shown in Figure 3.16, with the corresponding backward Fourier transform superimposed (for $N = M = 5$). It can be shown that the coefficients A_{kl} for $l = 0$ are symmetric with k, so that $A_{k0} = A_{-k0}$. Likewise the coefficients B_{kl} for $l = 0$ are antisymmetric with k, i.e. $B_{k0} = -B_{-k0}$. Therefore to describe a surface that goes through $N \cdot M$ points, we need $N \cdot (M-1)/2 + (N-1)/2 + 1$ amplitudes for A_{kl} and $N \cdot (M-1)/2 + (N-1)/2$ for B_{kl}; which also gives $N \cdot M$ amplitudes.

This observation allows us to use directly the amplitudes of the sines and cosines as parameters in the optimisation process[3].

For our numerical application, the domain boundaries were chosen to be $L_x = 20$ m, $L_y = 30$ m and $N = M = 5$; giving 25 parameters. The amplitude A_{00} is the base amplitude, which is a constant value throughout the domain. It was chosen to vary between 0 and 10 m. The other amplitudes

---

[3]Note that an alternative could have been to work with the $N \cdot M$ grid-point heights, and to smoothen the roof with a backward Fourier transform in order to produce a continuous and differentiable function.
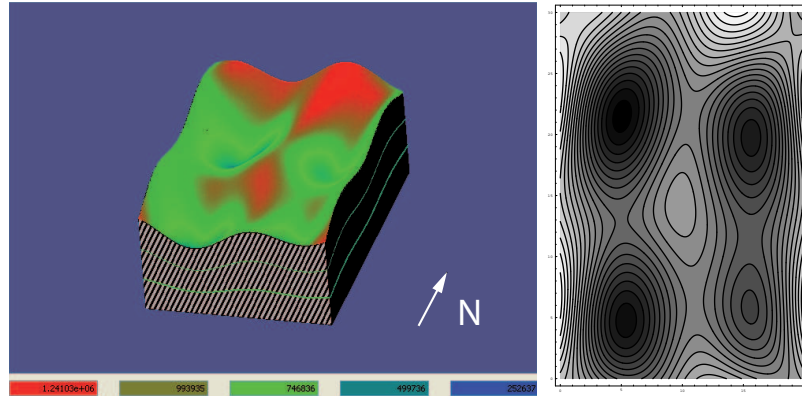
Figure 3.17: Result for small amplitudes after 12000 evaluations: 3D view (on the left) and contour plot (on the right)

are limited between a lower and an upper limit; in total three cases are tested:

1. $A_{kl}, B_{kl} \in [-\frac{1}{2}, \frac{1}{2}]$ but $A_{00} \in [0, 10]$

2. $A_{kl}, B_{kl} \in [-1, 1]$ but $A_{00} \in [0, 10]$

3. $A_{kl}, B_{kl} \in [-2, 2]$ but $A_{00} \in [0, 10]$

A minimal cut value was chosen in the height of the surface at 0 meters, so that when the surface goes below the ground (placed at 0 meters), it is not taken into account in the irradiation calculation. Further constraints dictate that the volume under the surface must remain within 10% of 80% of the maximum allowed volume, which is defined by a parallelepiped of 10 m by 20 m by 30 m (i.e. 10 m·$L_x \cdot L_y$). In mathematical form these constraints are similar to those of the first application (Equations 3.23 and 3.24).

Results

The results, after 12000 evaluations, are shown in Figures 3.17, 3.18 and 3.19. We observe that the volumes for the optimal cases are close to the maximum allowed value of 5280 m^3 (see Table 3.7), suggesting that the volume that intercepts rays should be as large as possible. It is also noteworthy that in each case depressions are created in the volume about its centre and there is a tendency to maximise the peaks to the North end of the building. There seems to be an attempt, with this continuous trigonometric function, to emulate the staggered arrangement of example 1, which maximises solar access to south facing collecting surfaces. Note that, as with example 1, incident irradiation on facades is also taken into account.
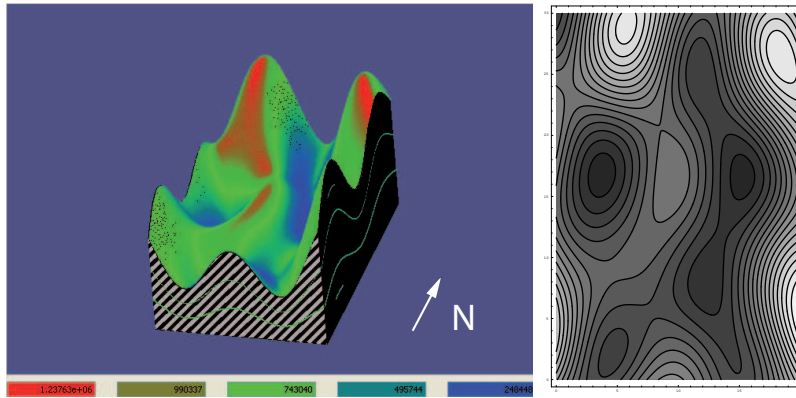
Figure 3.18: Result for medium amplitudes after 12000 evaluations: 3D view (one the left) and contour plot (on the right)
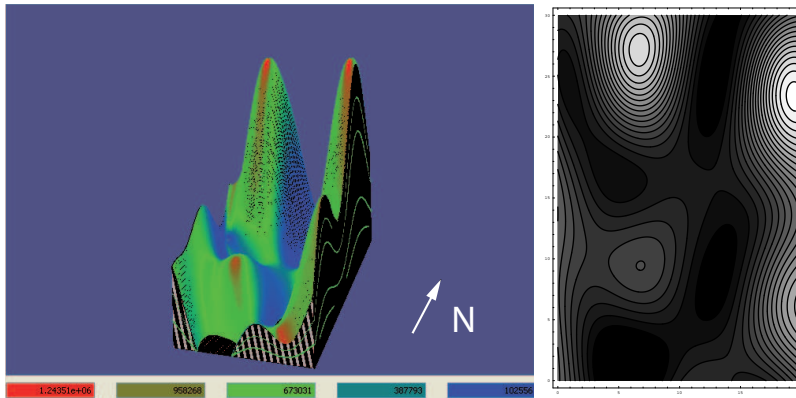
Figure 3.19: Result for large amplitudes after 12000 evaluations: 3D view (on the left) and contour plot (on the right)

Parameters	Irradiation (GWh)	Volume (m^3)
Flat roof ($A_{kl}, B_{kl} = 0$ except $A_{00} = 8.8$)	1.1292 (68%)	5280
Small amplitudes ($A_{kl}, B_{kl} \in [-\frac{1}{2}, \frac{1}{2}]$ except $A_{00} \in [0, 10]$) - Figure 3.17	1.2728 (76%)	5234
Medium amplitudes ($A_{kl}, B_{kl} \in [-1, 1]$ except $A_{00} \in [0, 10]$) - Figure 3.18	1.4075 (84%)	5222
Large amplitudes ($A_{kl}, B_{kl} \in [-2, 2]$ except $A_{00} \in [0, 10]$) - Figure 3.19	1.6685 (100%)	5131

Table 3.7: Optimal irradiation after 12000 evaluations for roof forms defined by a Fourier series compared that of a flat roof enclosing a similar volume

The dimensions $L_x = 20$ m times $L_y = 30$ m are arbitrary and the calculation in RADIANCE is scale free; so that the resultant forms are equally applicable to proportionally smaller or bigger buildings.

3.5.6   Conclusion

In recent years there has been considerable interest in studying urban forms which maximise the utilisation of solar energy within the urban context, whether by passive or active means. The methodologies employed thus far have been based on evaluating a small sample of subjectively chosen configurations from within the essentially infinite number of theoretically possible combinations. The probability of identifying an urban form which optimises solar radiation utilisation is therefore somewhat small. To resolve this we have used a hybrid Evolutionary Algorithm that was refined in order to handle constraints. By way of example three different problems have been investigated: a group of cuboid shaped buildings within an urban grid; a small group of geometrically more complex buildings adjacent to a large existing building; a building of rectangular plan whose volume has been parameterised as a Fourier series.

From this, we have found that:

- the new algorithm consistently converged to a good solution whilst taking constraints into account,

- the solar energy available for utilisation may be increased by up to 20% (with respect to an initial subjectively chosen form),

- the forms of these solutions tend to be highly non-intuitive (and correspondingly unlikely to be arrived at by subjective selection).

Concerning the latter point, it is hoped that computational tools of this nature might provide a useful source of inspiration to architects, from which to derive an architectural solution to a given design problem.

3.6 Comparison with another global optimisation algorithm

Many heuristics are in use today and some experiments are generally required to discover which algorithm performs best on a selected family of problems. The aim of this section is to provide a comparison between the performance of the hybrid CMA-ES/HDE algorithm and an alternative optimisation algorithm on both benchmark functions and simulation-based optimisation of buildings. For the alternative algorithm the hybrid PSO/HJ, which has been already applied to building energy performance optimisation with Energy-Plus was chosen. The hybrid PSO/HJ was ranked the best amongst nine optimisation algorithms tested with EnergyPlus, using two sets of parameters [Wetter and Wright, 2004]. Moreover it is part of a Generic Optimisation Program "GenOpt" that is freely available and customisable [Wetter, 2004]. We begin this section by explaining the principles of the algorithms selected and then go onto describe the parameters used. We then present an extended selection of benchmark functions that vary from convex to highly multi-modal, on which the comparison will be made. Those functions have an analytical form and are therefore inexpensive to compute, so that we can use statistical measures of the performance of the algorithms. Results from this may give some insights into which algorithm is best suited to a particular response function, and furthermore into the selection of the algorithms parameters that are best adapted to those functions. Finally, we use the two algorithms and their selected parameters on a more computationally expensive real-world problem that involves the minimisation of the annual primary energy consumption of a building. In order to vary the complexity of the corresponding objective function, we defined two different buildings (with one thermal zone and several thermal zones) at three locations representing three different climates. The buildings' performance is simulated with EnergyPlus version 2.2. As our cost function evaluations are computationally expensive and the available computing resources limited, we compare the algorithms performance for a prescribed number of objective function evaluations.

3.6.1 Hybrid PSO and HJ algorithm

The Particle Swarm Optimisation algorithm was initially proposed by Eberhart and Kennedy [1995]. It is a population-based algorithm, in which each individual is called a particle. Those particles evolve within generations mimicking the social behaviour of flocks of birds or schools of fish. They change their location going towards a point of lower objective function value known from previ-

ous iterations, so modelling cognitive behaviour, but also towards regions of space where other particles had a lower objective function value, so modelling social behaviour. For the cognitive behaviour, a corresponding acceleration is given as a parameter algorithm, modifying the speed of the particle proportionally to the difference vector between the particle and the local best point. For the social behaviour, another acceleration is given as parameter, modifying the speed according to the difference vector between the particle and the global best point. The global best point is taken in the neighbourhood of the particle.

This heuristic is a global optimisation algorithm that generally finds a good solution at the expense of many function evaluations. The implemented version of the algorithm uses a constriction coefficient, which reduces the velocity of the particles. Moreover, it is placed on a mesh, meaning that even though the variables are considered as continuous in the algorithm, when the evaluation of the objective function takes place, the coordinates of the nearest mesh point are used to compute the objective function. The distance between the mesh points is given by a step size for each variable. Since the particles are put on a rectangular grid, the von Neumann neighbourhood is used.

The HJ algorithm is a member of the family of Generalised Pattern Search algorithms. It searches along each coordinate direction for a decrease in the objective function. The initial mesh size for the search is given by a step size for each variable and when no improvement in the objective function is achieved, the step size is divided by a mesh size divider. When the local search around the current point finds a better point, the algorithm attempts to perform a global search move continuing in the same direction. As far as the global search finds a better point, it continues moving in the same direction until it fails, in which case the local search is restarted around the last best point. The local search and the algorithm ends once the maximum number of step reductions is attained. For this algorithm, convergence to a stationary point (a point at which the gradient is zero) is guaranteed for unconstrained, differentiable problems [Torczon, 1997, Lewis and Torczon, 1999, Audet and Dennis, 2003]. However, on a multi-modal objective function the algorithm may get stuck at a local minimum.

The idea of the hybridisation is to use the PSO as a global optimisation algorithm, which gets close to the global minimum and then refine the position of the attained minimum using the HJ algorithm. Practically, the PSO algorithm is executed for a user-specified number of generations, and then the HJ uses as its initial search point the best individual obtained by the PSO algorithm. For the coupled PSO/HJ, because the PSO algorithm evaluates the cost function only a finite number of times, the proofs of Torczon [1997], Lewis and Torczon [1999], Audet and Dennis [2003] that establish conver-

gence to a local minimum on differentiable functions still apply. However, as for other metaheuristic algorithms, for multimodal functions convergence can only be established for a local but not a global minimum. For a detailed description of the hybrid or each algorithm separately please refer to Wetter [2004].

To optimise the benchmark functions, five algorithm parameter sets were used for the PSO algorithm. Four are taken from Wetter and Wright [2004] and the last one from Bui et al. [2007], as summarized in Table 3.8. The set

	particles	c_1 cognitive acceleration	c_2 social acceleration	λ maximum velocity gain	κ constriction coefficient
Variant 1	16	2.8	1.3	0.5	0.5
Variant 2	16	2.8	1.3	0.5	1
Variant 3	36	2.8	1.3	0.5	0.5
Variant 4	36	2.8	1.3	0.5	1
Variant 5	100	2.05	2.05	0.2	1

Table 3.8: Parameters used for the PSO algorithm within the hybrid PSO/HJ algorithm for the benchmark functions

for which the PSO algorithm performs best, in terms of identifying benchmark functions' optima, will then be used for the real-case applications with EnergyPlus. For the HJ algorithm we use as parameters $r = 2$, $s = 0$, $t = 1$ and $m = 4$, where r is the mesh size divider, s is the initial mesh exponent, t is the mesh size exponent increment and m is the number of step reductions.

Constraint handling

The same constraint handling procedure as described in Section 3.5.1 was used for the two algorithms. Its implementation in each of the algorithms is described in the following paragraphs.

PSO When the particles' positions are updated, if a variable is outside of the domain boundaries, it is put back within the domain in the following way: $x_i \leftarrow 2 \cdot l_i - x_i$ if $x_i < l_i$ and $x_i \leftarrow 2 \cdot h_i - x_i$ if $x_i > h_i$. The procedure is repeated as long as the variable remains outside of the domain boundaries. The best local and global particles are selected using the comparison operator, which takes into account total domination over the constraints when comparing two individuals not satisfying the constraints. If the best particles are better than the new proposed ones, they will remain the best ones, otherwise the new ones become the new best ones.

HJ   In the global and local search, if a proposed variable is outside of the domain boundaries, we assign $f(\vec{x}) = \infty$, so that the iterate is rejected. Moreover, the new solution is compared to the former one using the comparison operator, keeping the new one only if it is better.

3.6.2   Parameters of CMA-ES/HDE

In this study, we use the same parameters as those used in previous runs of the hybrid. That is: for the CMA-ES $\sigma = 0.2$ and for the HDE the *rand3* strategy was used, along with $NP = 30$, $F = 0.3$ and $Cr = 0.1$. The relative precision for the HDE migration phase was chosen to be $\epsilon_2 = 10\%$. The absolute precisions $\vec{\epsilon_3} \in \mathbb{R}_+^n$ (one for each variable) are problem dependent and selected as $\frac{1}{32}$ of the problem step sizes, which corresponds to half the finest grid size of the PSO/HJ algorithm described in the previous section.

3.6.3   Benchmark functions

Five benchmark functions were used with different complexities for the optimisation algorithms. The first two are the Ackley and Rastrigin functions already described in Section 3.4.1. For the Ackley function, the step size for the optimisation algorithms was chosen to be 0.5, which corresponds to twice the frequency of the cosine perturbations. We have also chosen this step size for the Rastrigin function.

The third benchmark function is the generalized Rosenbrock function for dimension n,

$$f_n(\vec{x}) = \sum_{i=1}^{n-1} 100 \cdot (x_i^2 - x_{i+1})^2 + (1 - x_i)^2. \tag{3.27}$$

Its domain is $-2.048 \leq x_i \leq 2.048$, for all $i = 1..n$. In two dimensions, this function is unimodal and banana shaped but slightly asymmetric, the minimum being at $\vec{x} = (x_1, x_2) = (1, 1)$. However, for dimensions higher than three, the function is no longer unimodal and has a local minimum in the neighbourhood of $\vec{x} = (-1, 1, ..., 1)$ [Shang and Qiu, 2006] in addition to the global minimum at $f(\vec{1}) = 0$. In this case, a step size of 0.1 was chosen. The fourth benchmark function is the Sphere function of dimension n,

$$f_n(\vec{x}) = \sum_{i=1}^{n} x_i^2. \tag{3.28}$$

Its domain is $-1 \leq x_i \leq 1$, for all $i = 1..n$ and the global minimum is at $f(\vec{0}) = 0$. This function, for which we use a step size of 0.5, is completely

symmetric along every axis.

The last benchmark function is the constrained function described in Section 3.5.2.

3.6.4   Real-world applications with EnergyPlus

As noted earlier we have used the simulation software EnergyPlus version 2.2 to compute the objective function for real-world optimisation problems. The parameters varied during the optimisation were the window position, HVAC control temperatures and the temperatures used for system sizing. Two different benchmark buildings within the United States were used, each for the three locations, Chicago (IL), Miami (FL) and San Francisco (CA). In each case our aim is to minimize the primary energy consumption,

$$f(\vec{x}) = Q_h(\vec{x})/\eta_h + E_{el}(\vec{x})/\eta_{el}, \qquad (3.29)$$

where $\vec{x}$ is the vector containing the independent parameters, Q_h is the total annual on site energy consumption for heating and domestic hot water production (in J), η_h is the energy conversion efficiency for the heating system primary resource, E_{el} is the total annual electricity consumption (in J) and η_{el} is the energy conversion efficiency for electricity. We have taken source energy factors from Deru and Torcellini [2007] which are the inverse of the efficiencies in Equation 3.29 (see Table 3.9).

	Chicago	Miami	San Francisco
Gas	1.092	1.092	1.092
Electricity	3.546	3.317	3.095

Table 3.9: Source energy factors used in our study

Small Office Building

The first set of numerical experiments uses the DOE benchmark case of a single story office building with one thermal zone. The floor area is 511 m^2 and the floor height is 3.05 m. The envelope properties vary with climate according to ASHRAE 90.1-2004. The original window to wall ratio is 18%, which corresponds to a window of height 0.55 m which is distributed throughout the entire length of the wall. This ratio will vary throughout the study. The infiltration rate is 0.5 h^{-1} when fans are off and 0.15 h^{-1} otherwise, due to a higher pressure in the building. The HVAC system consists of packaged single zone air conditioning units and a gas furnace. Twenty people occupy
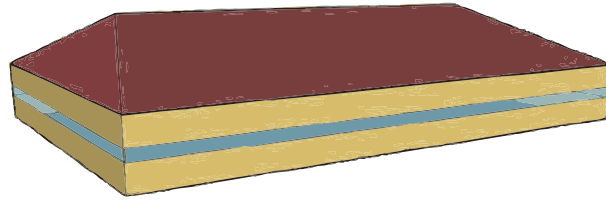
Figure 3.20: A projection of the Small Office Building simulated with the initial windows position

the office during working hours, with an appliance load of 8.07 W/m^2. The interior lights have a peak power consumption of 10.8 W/m^2, of which 40% are in the central part of the building and controlled by the working hours schedule. The remaining 60% have a dimming control that uses two measurement points placed, respectively, at a distance of 3 m from the south and north windows. No shading devices or overhangs are present in the building. Figure 3.20 shows a projection of this small office building.

Parameters   The thirteen parameters for the study are shown in the Table 3.10. There are eight parameters describing the windows' lower and upper positions for each facade. The minimum allowed value for the lower window position is 0.8 m, which corresponds to a standard desk height for reasons of daylight utilisation. The maximum allowed value for the lower window position is 1.25 m, which corresponds to the eye height of a seated person (see Watson and Crosbie [2004]) and hence permits a view to the outside world. For the upper window position, the minimum value was set to accommodate the minimal window size of 0.55 m. The maximum value for the upper window position was selected to be 2.2 m, which takes into account the slab height and the space needed for ventilation and air conditioning equipment. In addition to the window size and position, we varied the cooling supply air temperature used when sizing the system. A higher value results in larger flow rates which increases the fan energy use but reduces the chiller electricity consumption. The last four parameters are the control set points for the night and week-end temperature set-back for heating and cooling. The temperature set points during the day on weekdays and Saturdays in winter and summer are 21°C and 24°C. The domain of the parameters corresponding to the setback temperatures was adapted to include those.
To automatically size the HVAC system, EnergyPlus requires both the supply air temperature and absolute humidity to be specified. As the supply air temperature is varied over a large range, we compute the absolute humidity,

Parameter description	Symbol and Domain
North, east, south and west window lower positions (m)	$x_1, x_3, x_5, x_7 \in [0.8, 1.25]$
North, east, south and west window upper positions (m)	$x_2, x_4, x_6, x_8 \in [1.35, 2.2]$
Cooling supply air temperature used for system sizing($°C$)	$x_9 \in [12, 18]$
Heating setback night set point temperatures for Weekdays & Saturdays ($°C$)	$x_{10} \in [13, 21]$
Heating setback whole day set point temperatures for Sundays & Holidays ($°C$)	$x_{11} \in [13, 21]$
Cooling setback night set point temperatures for Weekdays & Saturdays ($°C$)	$x_{12} \in [24, 36]$
Cooling setback whole day set point temperatures for Sundays & Holidays ($°C$)	$x_{13} \in [24, 36]$

Table 3.10: The thirteen parameters for the Small Office Building study and the Large Office Building study

which is input to the sizing algorithms of EnergyPlus as follows:

$$\omega = 6.875 \cdot 10^{-4} x_9 - 2.5 \cdot 10^{-4}, \tag{3.30}$$

where w is the moisture content of the cooling supply air (kg/(kg dry air)). This leads to a supply air relative humidity of about 90%.
The step sizes for the optimisation algorithms were chosen to be 0.05 for the window positions x_1 to x_8 and 0.25 for the temperature set points x_9 to x_{13}.

Remark In our early optimisation experiments, the optimiser selected in all cases the minimum supply air temperature of 12°C as the optimum, because this led to the smallest fan power consumption. The reason was that the small office building had a direct evaporating coil model in which the COP is a function of the coil supply air inlet temperature but is independent of the coil supply air outlet temperature. Therefore, this model was not detailed enough to find the optimum supply air temperature, as decreasing the supply air temperature would otherwise decrease the COP. To overcome this limitation, we replaced the HVAC system of the small office building that is part of the DOE Commercial Building Benchmark files with that from the large office building. This HVAC system is described in the next section.

Constraints There are four linear constraints to ensure a minimum window height of 55 cm, which is the standard window size in the DOE benchmark building description files. The constraints are:

1. $g_1(\vec{x}) = x_1 - x_2 + 0.55 \leq 0$

2. $g_2(\vec{x}) = x_3 - x_4 + 0.55 \leq 0$

3. $g_3(\vec{x}) = x_5 - x_6 + 0.55 \leq 0$

4. $g_4(\vec{x}) = x_7 - x_8 + 0.55 \leq 0$
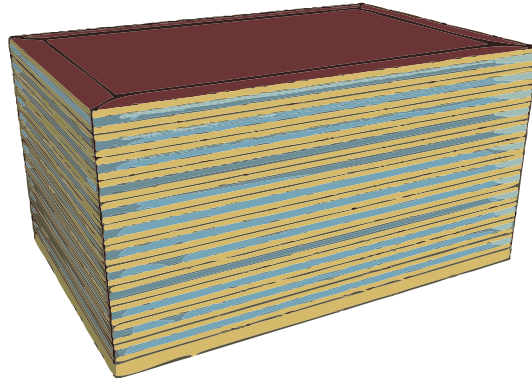
Figure 3.21: A projection of the Large Office Building simulated with the initial windows position

Large Office Building

The second set of numerical experiments uses a 12 story office building with a basement. The floor area is 42757 m^2 and its aspect ratio is 1.5. The envelope thermal properties vary with climate according to ASHRAE Standard 90.1-2004. The window to wall area ratio is 40% which corresponds, for the floor height of 3.05 m, to a window size of 1.22 m. Each floor of the building, except for the basement, is subdivided into five thermal zones. For each floor there are four 4.5 m deep perimeter zones with an infiltration rate of 0.3 h^{-1} when fans are off and 0.15 h^{-1} when fans are on. There is also one central zone with an infiltration rate of 0.15 h^{-1} when fans are off and 0.075 h^{-1} when fans are on. The HVAC system is a variable air volume flow system with reheat. The internal gains are composed of lights (10.8 W/m^2), electrical plug loads (8.07 W/m^2) and the heat release by the presence of 195 people. No shading devices are present, but daylighting control is used in all perimeter zones. A projection of the building is shown in Figure 3.21.

Parameters   The same thirteen parameters as for the Small Office Building were used (see Table 3.10). In the standard case defined in the DOE Benchmark Description files, the parameters for the window positions are of 0.91 m and 2.13 m respectively for the lower and upper extremities of the window. The window positions x_1 to x_8 are interpreted as relative to each floor equipped with windows, which excludes the basement. In other words, all windows simulated on a facade have the same dimensions given by the first eight parameters.

Constraints   The same four linear constraints as for the Small Office Building are used for this Large Office Building case.

Remark   Even though the same parameters and linear constraints as for the Small Office Building were used, we expect a more complex objective function because it has, for each floor, separate thermal zones for each facade as well as an interior thermal zone.

3.6.5   Results

We measured the time required for one simulation of EnergyPlus version 2.2 on a Linux machine equipped with a Quad-Core AMD Opteron 2.3 GHz processor and 1 GB of RAM. The Small Office Building takes about 80 seconds to complete and the Large Office Building about 900 seconds. We selected a *limit of 3000 evaluations*, leading to a reasonable 17 hours of simulation time for the Small Office Building using the four cores available in parallel. For the Large Office Building, using four such processors (16 cores available in parallel), requires 2 days of simulation time. In comparison with this simulation time, the computing time overhead associated with the optimisation algorithm is negligible. Please note that the CMA-ES/HDE will remain close to the limit of 3000 evaluations, as it will not get interrupted during a population evaluation. However, the PSO/HJ algorithm takes the 3000 evaluations as the limit for the PSO algorithm and then the solution is refined by the HJ algorithm which stops itself when no improvement is found with the finest grid spacing allowed. Typically, the improvement by the HJ requires only a few hundred evaluations and therefore the total number of evaluations is not far from the limit established.

Benchmark functions

The tests with the benchmark functions were conducted with 10 and 20 problem variables, as our real-world experiment with EnergyPlus will be in this range. In order to obtain useful statistics for the different algorithms, one hundred runs were carried out for each objective function, in which we varied the seed of the pseudo-random number generator. Figure 3.22 presents the lowest objective function value found by the hundred runs of the algorithms in the form of Box-Whisker plots. The median of the set is represented by the solid horizontal line in the box, the box itself includes the values lying between the first and third quartiles of the set (50% of the values) and outlier

values that are within 1.5 of the inter-quartile range to the whiskers. The remaining outliers that are not within 1.5 of the inter-quartile range are represented by dots.

For the Ackley function, the CMA-ES/HDE algorithm consistently performs best by getting closer to the global minimum compared to the PSO/HJ algorithm, even considering all outliers. For all runs and all parameters, the PSO remains stuck in the neighbourhood of a local minima. The HJ then refines the position of the local minimum and obtains its exact position, which improves the function value, but only insignificantly. Therefore, the different objective function values arrived at by the PSO/HJ algorithm correspond to local minima. This is not the case for the CMA-ES/HDE algorithm, for which there is no guarantee to find a stationary point. We notice that increasing the number of particles for the PSO (going from PSO/HJ 1 to PSO/HJ 5) improves the probability of finding a better local minimum and indeed of approaching the global minimum as the parameter range for this function is large. We note that our choice of limiting the number of function evaluations to 3000, in view of the typically rather large computing time of a building simulation, leads to a limited performance of the PSO algorithm, which usually requires more function evaluations to provide good performance [Parsopoulos and Vrahatis, 2002]. However for the CMA-ES/HDE, the previous obtained (Section 3.4.2) 100% of convergence (considered by a fitness below 0.1) of the Ackley function with 10 variables after 2695±178 evaluations was repeated in this experiment.

In the case of the Rastrigin function, the CMA-ES/HDE performs best for dimension 10. The median value is comparable to that of PSO/HJ 5, but its spread is smaller as the algorithm more often gets closer to the global minimum. However, in Section 3.4.3, we observed that the CMA-ES/HDE algorithm would have needed 6255±2020 evaluations for 100% convergence with 10 variables. For dimension 20, the CMA-ES/HDE suffers even more from the low number of total evaluations and the PSO/HJ performs better, particulary the PSO/HJ 3.

For the Rosenbrock function, the CMA-ES algorithm is always inferior to the PSO/HJ algorithm. The HJ part of the PSO/HJ algorithm can almost always improve the solution and get to the global minimum with an initial step size of 0.1 and 4 step reductions, thereby the box representing 50% of the runs collapses to a line where the objective function value is zero. However, had we selected more step reductions, then the step size would have been sufficiently small for the algorithm to converge to a minimum, as can formally be proven [Torczon, 1997, Lewis and Torczon, 1999]. We note that for the PSO/HJ 5, the PSO brings the solution sufficiently close to a minimum for the HJ to always find the local minimum around $f(\vec{x}) = 4$, or the
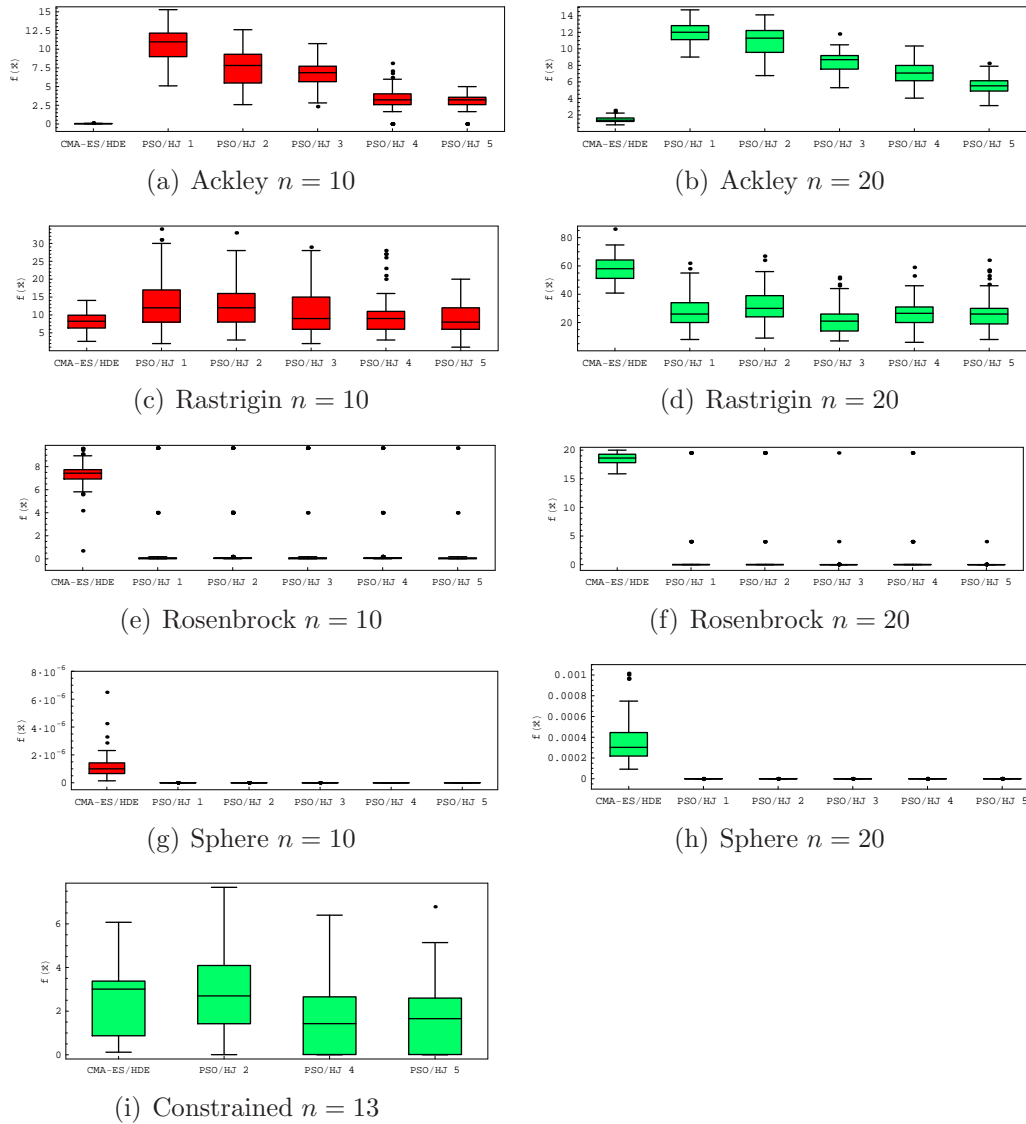
Figure 3.22: Comparison of different algorithms with benchmark test functions, Box-Whisker plots of one hundred best candidates shown by their objective function value $f(\vec{x})$.

global minimum around $f(\vec{x}) = 0$.

For the Sphere function, both hybrid algorithms perform well. The PSO/HJ algorithm always converges exactly to the global minimum. Indeed, as this function is uni-modal and the global minimum on the grid defined for the algorithm, the HJ always converges. The CMA-ES/HDE algorithm gets very close to the global minimum, but searches around it due to the nature of its recombination and mutation operators.

For the constrained function, the variants 1 and 3 of the PSO/HJ algorithm, with a constriction coefficient $\kappa = 0.5$, were not able to get inside the constrained space during our tests. The PSO was concentrating rapidly on a region outside of the constrained space and got stuck there as the speed of particles reduced quickly with generations. The other variants of the PSO algorithm could at least find one point within the constrained space that attracted the particles. When particles could reach in the vicinity of the global minimum, the HJ algorithm led to its exact position, as it is on the grid defined by the algorithm. In this constrained example, the global minimum sits at the domain boundaries, and even though it is not a stationary point of the function, the HJ algorithm approach it thanks to its constraint handling procedure. The CMA-ES/HDE performed less well than variants 4 and 5 of the PSO/HJ. Due to its recombination and mutation operators, it tends to explore the interior of the domain boundaries. However thanks to the constraint handling procedure within the mutation phase of the CMA-ES algorithm, it can also touch the border of the domain. Even though the number of function evaluations is not the same for the two hybrid algorithms, as the HJ algorithm stops itself when no further improvement is found, clear trends can be identified. In particular it is possible to identify which algorithm is best suited to a certain kind of objective function. For example, the CMA-ES/HDE algorithm performs best on highly multi-modal functions such as Ackley and Rastrigin, as the algorithm was designed for just these kinds of functions. On the other hand, for functions with one or two minima such as Rosenbrock or Sphere, the PSO/HJ very frequently converges to the global minimum. In those cases, the PSO algorithm explores the parameter space and when the best particle approaches the global minimum, the HJ algorithm is able to find its exact position. The real-world experiment in building performance optimisation presented in this paper should favour one algorithm over the other according to the shape of the objective function.

Real-world application with EnergyPlus

From the results obtained for the benchmark test functions, the parameters of variant number 5 were adopted for the PSO/HJ algorithm.

Small Office Building The results for the objective function minimisation (see Equation 3.29) are summarized in Figure 3.23. In each case the primary energy consumption has been normalised per unit floor area to allow for an easier comparison between the different buildings. For illustration purposes, Box-Whisker plots were prepared using 5 runs at each location. Please note that the quartiles are not statistically significant in this latter plot. For the
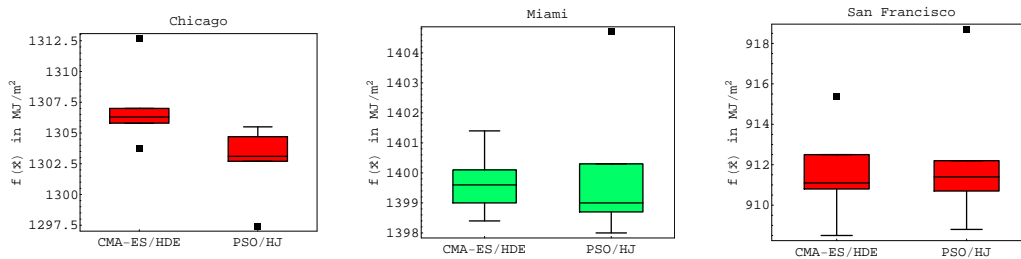
Figure 3.23: Primary energy consumption (in MJ/m^2) for the optimised Small Office Building, Box-Whisker plots for 5 runs at each location.

Chicago climate the PSO/HJ performs the best. However, using a Wilcoxon rank sum test [Mann and Whitney, 1947] the difference between the two is slightly significant (W=23, p-value=0.016). For the Miami climate, the difference between the two algorithms is not significant (W=14, p-value=0.42). For the San Francisco climate, likewise the Miami climate, the difference is not significant (W=12, p-value=0.58). Finally, the difference in primary energy consumption between the extreme cases corresponds to around 1% or less of the median value, which may be regarded as negligible.

Even though the annual primary energy use is similar between the algorithms, it is interesting to understand the possible differences between the optimal parameter values. For this, by way of illustration, we have selected for each algorithm the worst cases for the Chicago climate, the best cases for the Miami climate and close to median cases for the San Francisco climate. The corresponding variable values are presented in Table 3.11. We have also included the parameters corresponding to the standard case, which were given in the DOE benchmark description files. On closer inspection of the best candidates found by the two algorithms in Table 3.11, we notice that the parameter values can be rather different. In order to understand this, we examine below the results for each climate case in turn.

Chicago (IL) case For the Chicago (IL) case the North, East and West window sizes are consistently around the minimum allowed value. Table 3.12

	x_1 North window	$x_2 - x_1$	x_3 East window	$x_4 - x_3$	x_5 South window	$x_6 - x_5$	x_7 West window	$x_8 - x_7$	x_9	x_{10}	x_{11}	x_{12}	x_{13}
Initial parameters	1.25	0.55	1.25	0.55	1.25	0.55	1.25	0.55	14.0	13.0	13.0	33.0	33.0
Chicago (IL)													
CMA-ES/HDE	0.90	0.60	1.03	0.61	1.09	0.60	1.18	0.56	15.1	17.5	13.0	26.1	34.6
PSO/HJ	0.95	0.55	1.05	0.55	1.11	0.55	1.20	0.55	15.3	18.0	13.0	25.8	30.7
Miami (FL)													
CMA-ES/HDE	0.86	0.73	0.84	1.36	0.84	1.36	1.09	1.11	12.0	18.6	16.8	27.1	31.6
PSO/HJ	0.88	0.73	0.80	1.40	0.85	1.35	1.05	1.05	12.0	15.2	19.8	27.0	34.8
San Francisco (CA)													
CMA-ES/HDE	0.91	0.65	1.21	0.77	0.89	0.58	1.23	0.59	12.0	18.5	13.3	24.0	29.9
PSO/HJ	1.07	0.56	1.25	0.67	0.90	0.55	1.25	0.55	12.0	18.5	14.8	24.0	29.0

[a]Please refer to Table 3.10 for details about the parameters

Table 3.11: Results for the Small Office building optimisation, worst cases for Chicago, best cases for Miami, close to median cases for San Francisco[a]

Energy type and use (MJ/m²)	initial	CMA-ES/HDE	PSO/HJ
Electricity			
Interior Lighting	100.7	97.28 (-3.4%)	98.10 (-2.6%)
Interior Equipment	128.8	128.8	128.8
Cooling	45.89	33.52 (-27.0%)	32.43 (-29.3%)
Natural Gas			
Heating	138.8	142.2 (+2.4%)	146.2 (+5.3%)
Electricity			
Fans	76.05	55.38 (-27.2%)	53.01 (-30.3%)
Pumps	11.3	6.46 (-42.8%)	6.11 (-45.9%)
Heat Rejection equipment (cooling tower)	8.45	4.99 (-40.9%)	4.70 (-44.4%)
Total primary energy use	1468	1313 (-10.6%)	1305 (-11.1%)

Table 3.12: Details about the Chicago Small Office building's site energy consumption in MJ/m²

shows a breakdown of the energy consumption for the different systems in the building, for both the initial and optimised cases. From this we notice that for the optimised cases we save energy for both the cooling and ventilation compared to the initial case. However, more natural gas was consumed in heating, which may indicate that it is more beneficial to reduce electricity consumption as its source-site factor is about three times that of natural gas.

To produce Figure 3.24 we used the optimal parameters identified by the PSO/HJ algorithm shown in Table 3.11, but varied the variable x_9 to cover its domain. From this we find that the PSO/HJ algorithm correctly identified the minimum for this ninth parameter in the subspace shown by this Figure. As expected, we notice an increase in fan energy use if the supply temperature is raised, starting at the optimal value for x_9. This is because with a higher cooling supply air temperature, a higher mass flow rate is required to provide the same cooling load. Below the optimal value for x_9, we have a constant value for fan energy use, because for $x_9 < 15.3°$C, the sizing of the heating system determines the minimum mass flow rate. This behaviour cannot is not observed for San Francisco and Miami, in which the fan size was determined exclusively by the cooling load.

Looking more closely at the EnergyPlus input file, we notice that the ASHRAE 90.1-2004 regulation leads to poorly performing double glazed windows (2× 3 mm clear glass, 6 mm air gap) having a U-value of 3.26 W/(m²K). To understand the implications of this, we re-ran the optimisation after replacing the window construction with a better performing double glazed window. The new glazing consists of a double glazed window of 6 mm clear glass, with a gap of 13 mm filled with Argon. The outer layer also has a low emissivity coating. The new windows lead to a reduction in the objective function
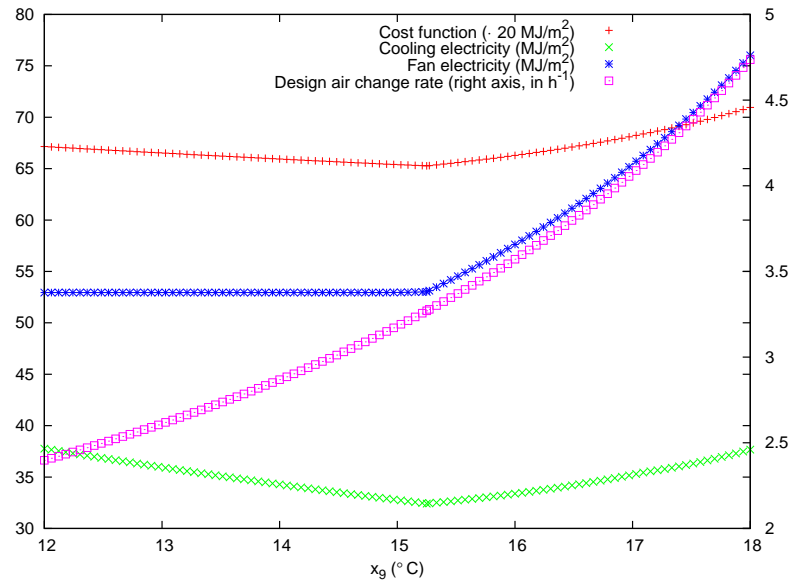
Figure 3.24: Variation of the objective function with x_9 around the best candidate found for the Small Office Building in Chicago with PSO/HJ

relative to the initial cases (without optimisation) equivalent to about 6% primary energy. Moreover, the optimised case with new glazing has larger windows which may be preferred by the occupants (see Table 3.13).

From Table 3.11, we also notice that for Chicago the optimal night set back temperature for heating was not at its lowest allowed value, which seems counter intuitive. To understand this, we examined results from two simulations. The first one was based on the optimal parameters found by the CMA-ES/HDE algorithm and the second one used the same parameters but this time with the night set back temperature set to its lowest allowed value of 13°C. This reduction in night set back temperature led to an increase in primary energy consumption of 9.7%. By way of explanation, in Figure 3.25 we plot results for a particular day in which the performance of the optimal case was better than the one with the night set back at its lowest value. During that day, the power consumption for fans and heating were higher for the case with lower night set back temperature. This higher fan power can be explained by the auto-sizing algorithm used by EnergyPlus: during the night, the temperature of the building will decrease more, resulting in a bigger heat load for the first hour in the morning. Therefore, a larger fan is needed to provide the relatively larger amount of heating energy that is required after the set point change.

	x_1 North window	$x_2 - x_1$	x_3 East window	$x_4 - x_3$	x_5 South window	$x_6 - x_5$	x_7 West window	$x_8 - x_7$	x_9	x_{10}	x_{11}	x_{12}	x_{13}	$f(\vec{x})$ MJ/m^2
Initial parameters	1.25	0.55	1.25	0.55	1.25	0.55	1.25	0.55	14.0	13.0	13.0	33.0	33.0	1381
Chicago (IL) equipped with Double Glazing and Low Emission coating														
CMA-ES/HDE	0.84	0.75	0.91	1.26	0.88	1.16	0.95	0.79	13.4	17.3	13.8	26.2	30.4	1200
PSO/HJ	0.96	0.77	0.98	1.19	0.90	1.15	1.18	0.72	13.9	17.3	13.1	26.0	28.8	1199

[a]Please refer to Table 3.10 for details about the parameters

Table 3.13: Results for the Small Office building optimisation in Chicago with double glazing and low emission coating after 3000 evaluations, parameter values[a]
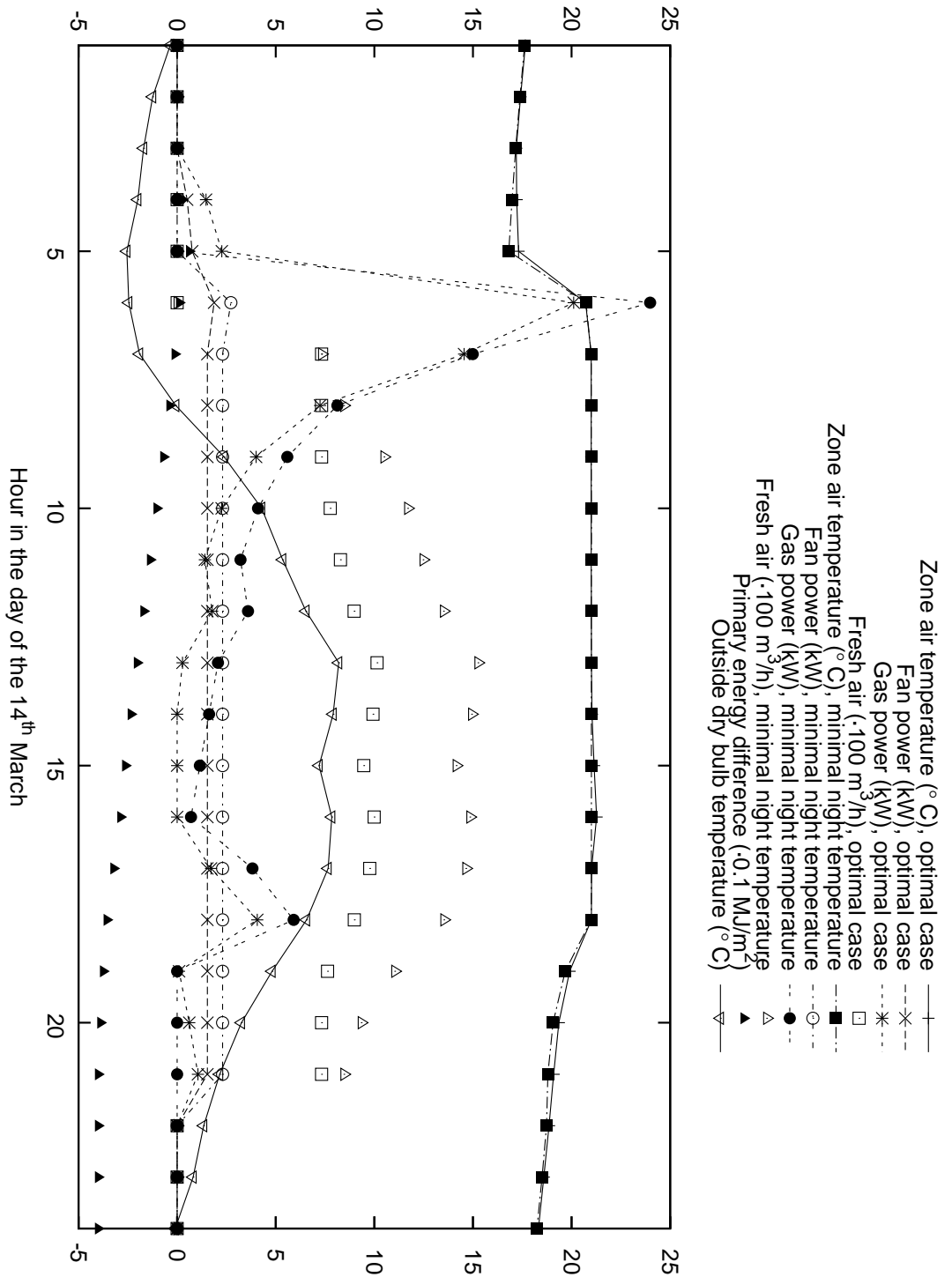
Figure 3.25: Comparison between the optimal point found for Chicago by the CMA-ES/HDE and the same parameters with the night set back temperature changed to 13°C. The day chosen was the 14th March.

The higher gas consumption was at first surprising, because the minimum outside air mass flow rate for ventilation was fixed according to the expected occupancy, and independent of the fan size. Furthermore, a larger fan adds more heat to the air stream. However, the EnergyPlus input file is such that the economizer control attempts to maintain a mixed air temperature of 16°C between the 1st October and the 31st March. Since in the case of the lowest night temperature there is a higher air flow rate (due to a larger fan), more outside air is needed to reduce the mixed air temperature to 16°C. Consequently more gas is needed to reheat the mixed air to the building's supply air temperature.

From the above analysis, we conclude that the way the economizer was modeled in the DOE benchmark files used for this study was oversimplified for the heating season. However, for the summer, a mixed air temperature of 13°C was used, which is reasonable to take advantage of night cooling. Moreover, the temperature schedule used for the auto-sizing algorithms should ramp up to the daytime set point, instead of having a change that looks like a step function. If the room air set point temperature for heating had been ramped up over a period of 3 hours, then compared to a constant night set back temperature of 13°C, a reduction in the objective function of 9.4% would have been achieved, which is substantial.

Miami (FL) case For Miami the optimised cases have large windows (Table 3.11) especially for the East, South and West facades. The cooling supply air temperature is set to the lowest bound (12°C). The winter heating set back temperatures are close to the initial set point of 21°C, but these seem non-intuitive for the PSO/HJ algorithm, as the set-back temperature for Sundays and Holidays is higher than that for weekdays and Saturdays. To understand this, we analysed the office temperatures for these two periods. During Sundays and Holidays, the minimum achieved room temperature was 19.6°C. For Weekdays and Saturdays during the night time, the minimum temperature was 19.3°C. Therefore, any heating temperature set point below these temperatures will have the same effect, which explains the non-intuitive values. The summer cooling set back temperatures, on the other hand, do follow our intuition. The maximum room temperature at night during weekdays and Saturdays achieves the set point temperature. However the maximum temperature during Sundays and Holidays was 30.4°C. Therefore any set point above this temperature leads to equivalent energy use, which explains the differences between the set points found by the CMA-ES/HDE and the PSO/HJ.

Table 3.14 shows the energy use for the different systems in the building for

Energy type and use (MJ/m^2)	Miami (FL) initial	CMA-ES/HDE	PSO/HJ
Electricity			
Interior Lighting	102.4	88.60 (-13.5%)	88.75 (-13.3%)
Interior Equipment	128.8	128.8	128.8
Cooling	120.1	110.5 (-8.0%)	110.5 (-8.0%)
Natural Gas			
Heating	0.96	1.41 (+46.9%)	1.39 (+44.8%)
Electricity			
Fans	85.56	63.60 (-25.7%)	63.50 (-25.8%)
Pumps	19.5	15.7 (-19.5%)	15.7 (-19.5%)
Heat Rejection equipment (cooling tower)	17.1	13.9 (-18.7%)	13.8 (-19.3%)
Total primary energy use	1571	1398 (-11.0%)	1398 (-11.0%)

Table 3.14: Details about the Miami Small Office building's site energy consumption in MJ/m^2

the optimised cases and the initial case. For the optimised cases energy for cooling is reduced but natural gas consumption is slightly increased, which is, however, negligible for the Miami climate. Fan electrical consumption shows the biggest savings. By reducing the cooling supply air temperature to its minimum value, the optimiser reduced the necessary mass flow rate for an equivalent cooling load.

San Francisco (CA) case   As with the Chicago case, for San Francisco the windows are set to around the minimum allowed height. The cooling supply air temperature is also at its lowest value ($12°C$), allowing for a reduction in fan power. Table 3.15 shows the energy use for the different systems in the

Energy type and use (MJ/m^2)	San Francisco (CA) initial	CMA-ES/HDE	PSO/HJ
Electricity			
Interior Lighting	99.78	93.56 (-6.2%)	95.83 (-4.0%)
Interior Equipment	128.8	128.8	128.8
Cooling	40.14	19.55 (-51.3%)	19.06 (-52.5%)
Natural Gas			
Heating	35.03	26.52 (-24.3%)	24.15 (-31.1%)
Electricity			
Fans	47.36	32.86 (-30.6%)	32.25 (-31.9%)
Pumps	13.0	5.48 (-57.8%)	5.36 (-58.8%)
Heat Rejection equipment (cooling tower)	11.1	4.76 (-57.1%)	4.66 (-58.0%)
Total primary energy use	1091	911 (-16.5%)	911 (-16.5%)

Table 3.15: Details about the San Francisco Small Office building's site energy consumption in MJ/m^2

building. For the optimised cases we save about half the energy for cooling compared to the initial case. Perhaps of more interest is that for a similar

	Chicago (IL)	Miami (FL)	San Francisco (CA)
Standard parameter set	1689	1718	1440
Best candidate with CMA-ES/HDE	1347.7 (-20.2%)	1596.2 (-7.1%)	1014.5 (-29.6%)
Best candidate with PSO/HJ	1348.2 (-20.2%)	1596.0 (-7.1%)	1015.2 (-29.5%)

Table 3.16: Results for the optimisation of the Large Office building in different locations after 3000 evaluations, yearly primary energy consumption in MJ/m^2

reduction in total primary energy consumption, the CMA-ES/HDE results in larger windows and therefore reduces lighting energy use, but it also results in an increase to all other energy end uses compared to the solution found by the PSO/HJ algorithm. This indicates what may be a multi-modal objective function with two almost equivalent minimum objective function values but different independent parameters.

Large Office Building   For the Large Office Building, considering the large simulation time of about 800 seconds for each function evaluation and the similar reduction in primary energy consumption obtained by different runs, we chose to perform the optimisation only once for each algorithm. The results for the objective function minimisation are summarized in Table 3.16. We have added a further digit to the yearly energy consumption to clarify the actual difference between the two algorithms, which is insignificant in terms of energy consumption. As for the Small Office Building, the most significant improvement was achieved for San Francisco. For the Large Office Building, we expected a more complex objective function because it has, for each floor, separate thermal zones for each facade as well as an interior thermal zone. We might therefore expect this problem to favour the CMA-ES/HDE as with the Ackley or Rastrigin benchmark functions. However, there is no discernable difference between the two tested optimisation methods, based on a single run of these algorithms.

Table 3.17 shows that both algorithms found similar parameters. We show in Figure 3.26 the evolution of the objective function with the number of evaluations for San Francisco. This Figure shows that the HDE component of the CMA-ES/HDE is most effective in improving the solution, as is the PSO component in the PSO/HJ. With both algorithms, a plateau has been reached after around 2200 evaluations. The apparent divergent behaviour of the CMA-ES algorithm was already observed on the Rastrigin function in Kämpf and Robinson [2009a]. At each generation, the CMA-ES algorithm selects the new parents amongst the children, and those children may have a worse fitness than the actual parents. It appears that such a small populated

	x_1 North window	$x_2 - x_1$	x_3 East window	$x_4 - x_3$	x_5 South window	$x_6 - x_5$	x_7 West window	$x_8 - x_7$	x_9	x_{10}	x_{11}	x_{12}	x_{13}
Standard	0.91	1.22	0.91	1.22	0.91	1.22	0.91	1.22	14.0	13.0	13.0	33.0	33.0
Chicago (IL)													
CMA-ES/HDE	1.22	0.55	1.01	0.56	1.15	0.55	1.22	0.59	12.1	14.6	13.0	24.8	34.4
PSO/HJ	1.21	0.55	1.00	0.55	1.00	0.55	1.15	0.55	12.8	14.6	13.0	24.5	33.5
Miami (FL)													
CMA-ES/HDE	1.22	0.55	1.18	0.75	1.17	1.02	1.24	0.70	12.0	17.3	16.2	24.3	35.8
PSO/HJ	1.18	0.56	1.25	0.73	1.23	0.97	1.25	0.68	12.0	17.6	16.0	24.3	36.0
San Francisco (CA)													
CMA-ES/HDE	1.20	0.69	1.17	0.69	1.20	0.55	1.19	0.58	12.0	14.4	13.0	24.5	34.9
PSO/HJ	1.25	0.78	1.25	0.68	0.95	0.55	1.25	0.56	12.0	13.0	13.0	24.5	35.8

Table 3.17: Results for the Large Office building optimisation in different locations after 3000 evaluations, parameter values[a]

[a]Please refer to Table 3.10 for details about the parameters
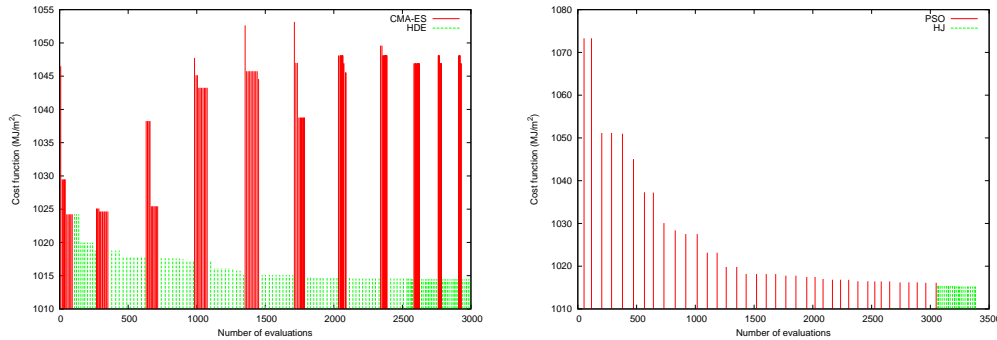
Figure 3.26: The improvement in objective function as a function of the number of evaluations for the Large Office in San Francisco, on the left for the CMA-ES/HDE and on the right for the PSO/HJ

CMA-ES algorithm with $\mu = 5$ and $\lambda = 11$ is not suited to this kind of function, which justifies the hybrid approach, as this knowledge comes after the optimisation. Moreover, this behaviour of the CMA-ES algorithm does not impact on the robustness of the hybrid, but rather brings diversity to the population of the HDE during the exchange of individuals.

3.6.6 Conclusion

The novel hybrid evolutionary algorithm CMA-ES/HDE was compared with the established performance of the PSO/HJ. The first set of numerical experiments involved benchmark functions with different complexities (Ackley, Rastrigin, Rosenbrock, Sphere and Constrained). The CMA-ES/HDE performed better than the PSO/HJ on difficult multi-modal functions such as those of Ackley and Rastrigin for a parameter space of dimension 10 and within a limit of 3000 evaluations. However, when the problem dimension was increased to 20, the CMA-ES/HDE performed less well than the PSO/HJ algorithm for the Rastrigin function, which indicates a limit of the algorithm for complex functions when using a low number of function evaluations. For the non-convex Rosenbrock function in dimensions 10 and 20 the PSO/HJ performs best, because the HJ algorithm very often finds the global minimum once the PSO algorithm has reached a basin of attraction of the global minimum. The uni-modal Sphere function is best solved by the HJ part of the PSO/HJ, which always converges exactly to the global minimum. Even though the CMA-ES/HDE algorithm does not reach the exact position of the global minimum, it gets very close to it. The uni-modal constrained function favours the PSO/HJ, moreover indicating algorithm parameters that should

be preferred.

We then tested the algorithms' performance for minimising the energy use of small and large office buildings simulated by EnergyPlus. Thirteen parameters were varied, representing window positions, HVAC system design variables and control set-points. The optimal configuration led to a reduction of primary energy consumption of up to 30%. The optimal values represented a trade-off that one can obtain by sizing the windows properly in order to save electricity for artifical lighting, and by setting the HVAC sizing and control temperatures to reduce energy for fans, pumps and air conditioning systems. Similar performance was obtained by the two algorithms CMA-ES/HDE and PSO/HJ for the small office building, but for one climate the PSO/HJ provided slightly better results. Similar performance was also obtained for the large office building, based on a single run of each algorithm. However, the resultant parameter sets were different, indicating that the objective function is multi-modal or locally just a flat landscape. We can conclude then that even though the performance of the optimisation algorithms tested was significantly different for benchmark functions, this was not the case for the experiments with EnergyPlus. Even though the total number of function evaluations was not the same between the two hybrid algorithms, as the HJ algorithm stops itself when no further improvement is found in the objective function, clear trends were identified regarding the performance of the hybrid algorithms with benchmark functions. Highly multi-modal objective functions were best solved by the CMA-ES/HDE algorithm and objective functions with one or two minima by the PSO/HJ algorithm. The objective function of the building performance optimisation problem seemed to lie somewhere between these extremes, as no algorithm was significantly favoured over the other.

Through those experiments we gain confidence in our hybrid Evolutionary Algorithm, as it compares well in terms of the performance simulated with EnergyPlus with another well-known optimisation algorithm. In principle our algorithm might be further improved by adding a HJ component after a run of the CMA-ES/HDE algorithm.

3.7   Summary

In this chapter, we proposed a hybrid of two heuristic optimisation algorithms: CMA-ES and HDE. The hybrid showed superior results on the Rastrigin and Ackley benchmark functions relative to each individual method. This hybrid was also applied to a variety of maximisation problems of the urban solar potential without constraints. A constraint handling procedure

was then proposed and tested on both a benchmark function and a solar potential maximisation problem. Finally we compared the hybrid with another global optimisation algorithm, the PSO-HJ. We found that they showed similar results on a real-world problem of building energy consumption minimisation using EnergyPlus, but that for complex multi-modal function the CMA-ES/HDE tends to perform better.

Chapter 4

Explicit physical modelling at the urban scale

> The part of the thesis describing the Thermal Model was published in the journal Energy & Buildings [Kämpf and Robinson, 2007].

A new holistic urban resource flow modelling tool is being developed by our research group based on similar principles to that of its predecessor SUNtool. In comparison with SUNtool, this new tool *CitySim* is designed for application at the range of scales from the individual building to the neighbourhood (several tens of buildings), to the entire town or city of several tens of thousands. CitySim is also based on a more rigorous family of physical and statistical models. The conceptual structure of CitySim's solver (which is currently biased towards the modelling of energy flows) is shown in Figure 4.1. The radiation model is the same as that SUNtool, based on the simplified radiosity algorithm of Robinson and Stone [2005]. Work towards the present thesis has contributed to a simplified building thermal model, as well as models of HVAC and Energy Conversion System. Those models represent the core of CitySim's solver and allow for the prediction of the energy performance of many buildings at the same time, taking into account radiant interactions between them. The thermal microclimate model for temperature, velocity and pressure calculation in the urban environment is under development, and therefore is not coupled with CitySim at the moment, which is why in Figure 4.1 the arrow is dotted. Furthermore, the protoype stochastic models have also yet to be integrated. As an intermediate step occupants' presence and behaviour is represented by deterministic rules and profiles.
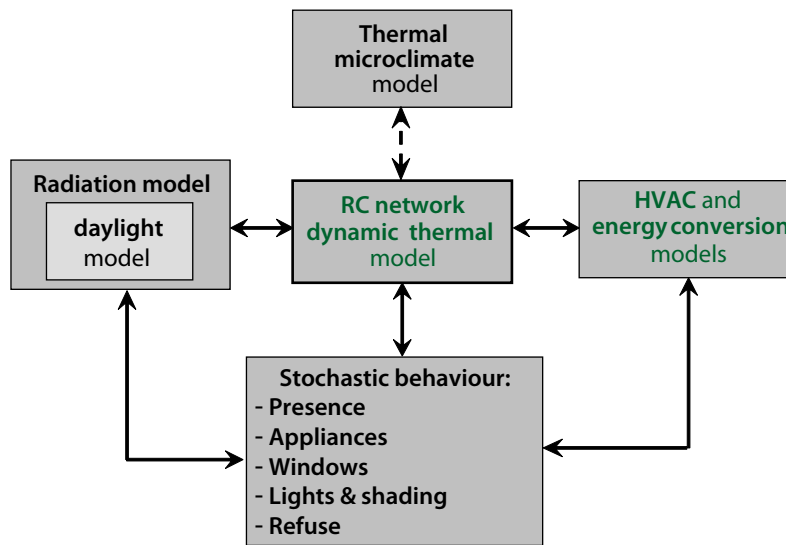
Figure 4.1: The solver of CitySim with the different models involved.

4.1 The thermal model

In order to simulate the flows of energy and matter at the urban scale and to evaluate urban environmental performance, it is necessary to simulate buildings' energy consumption. Since we aim to simulate energy demand for a large number of buildings for which we have relatively little descriptive information, it is desirable to ensure that we have compatibility between: the data available; the complexity of the selected modelling approach; reasonable simulation time. To this end we have chosen to explore simplified methods for dynamic simulation of thermal energy flows in our buildings.

Methods for the calculation of transient heat transfer in buildings can be broadly classified as follows:

1. Explicit solution of the heat diffusion equation, by finite difference [e.g. Clarke, 2001] or response function [e.g. Gough, 1982] methods.

2. Model reduction techniques, such as the grey box method due to Déqué et al. [2000].

3. Model simplification techniques, such as the resistance-capacitance (RC) network [e.g. Lefebvre et al., 1987] and admittance [Milbank and Lynn, 1974] methods.

Of these, the explicit solution methods are too onerous for our purposes, both computationally and in terms of data requirements (and associated

uncertainties). The reduction technique is intrinsically limited to the cases from which the reduced model was derived, and so lacks generality - we seek a model that will have applicability to a wide range of circumstances. The thermal model included in SUNtool was based upon one such reduction technique: the grey box approach [Déqué et al., 2000]. It has the advantage of using relatively few parameters to characterise the thermal behaviour of buildings, but it also has some disadvantages:

- The class of possible simulated buildings is finite and was created by the authors using parametric studies. Simulation of a building that does not belong to a predefined category, may entail significant errors.

- The temperature output by the model is restricted to the air node (convective) so that we cannot access information relating to the wall temperature (radiant). This radiant temperature can be important for the modelling of air conditioning control systems, as it is needed for the evaluation of occupants' thermal comfort.

- The source code is not freely available, we cannot make modifications or adaptations.

- The simulation of multiple zones is sequential. So that the prediction of the energy demands of these zones requires several iterations and a consequent accumulation of rounding errors.

The most promising candidate therefore, is the family of simplified models. These offer a good compromise between simplicity (yet with reasonable accuracy and generality), data requirements and computational expense. Of these the harmonic methods tend to be somewhat conservative (at least that is for the period normally used in their implementation), in that the assumption of a repeated climatic harmonic tends towards under/overestimation of plant sizes, energy consumption and indoor temperature. In principal, models which are based on an electrical analogy suffer no such drawback.

In this section, we start by the derivation of the electrical analogy from the energy conservation equation. We then proceed to describe the evolution of the complexity of this model to ensure its validity to model both a single space and an enclosure with an arbitrary number of spaces.

4.1.1 From energy conservation to the electrical analogy

Electrical analogy models are derived from the energy conservation equation:

$$\frac{\partial u(\vec{x}, t)}{\partial t} - \nabla \cdot \vec{j}(\vec{x}, t) = s(\vec{x}, t), \tag{4.1}$$

where $\vec{x} \in \mathbb{R}^3$ represents the position (m), $t \in \mathbb{R}$ the time (s), $u(\vec{x}, t) \in \mathbb{R}$ the internal energy (J), $\vec{j}(\vec{x}, t) \in \mathbb{R}^3$ the energy flow rate (W) and $s(\vec{x}, t) \in \mathbb{R}$ the energy generation rate (W). Integrating the former equation over a volume V, we have:

$$\int_V \frac{\partial u(\vec{x}, t)}{\partial t} dV - \int_V \nabla \cdot \vec{j}(\vec{x}, t) dV = \int_V s(\vec{x}, t) dV. \tag{4.2}$$

In this, the internal energy can be written as: $u(\vec{x}, t) = \rho(\vec{x}, t) \cdot C_p(\vec{x}, t) \cdot T(\vec{x}, t)$, with ρ being the material density (kg/m³), C_p the material specific heat capacity ($J \cdot kg^{-1} \cdot K^{-1}$) and T the material temperature (K). Considering an integration volume in which ρ, C_p are constant and using the Divergence theorem, we obtain the following equation:

$$\rho \cdot C_p \cdot \frac{d\bar{T}_V(t)}{dt} V - \int_{\partial V} \vec{j}(\vec{x}, t) \cdot d\vec{S} = S_V, \tag{4.3}$$

where S_V is the energy generation rate (W) in the volume V and $\bar{T}_V$ is the volume V averaged temperature. Let us now consider a volume enclosed within n surfaces, with perpendicular energy flow rates $\vec{j}(\vec{x}, t) \cdot \vec{S}_i = j_{\perp,i}(t)$ on each delimiting surface $i = 1..n$, so that:

$$\rho \cdot V \cdot C_p \cdot \frac{d\bar{T}_V(t)}{dt} - \sum_{i=1}^{n} j_{\perp,i}(t) \cdot S_i = S_V \tag{4.4}$$

For a solid material: considering Fourier's law for determining the energy flow rate ($\vec{j}(\vec{x}, t) = -\lambda_V \cdot \nabla T(\vec{x}, t)$), we have that:

$$j_{\perp,i}(t) \cdot S_i \approx -\lambda_V \cdot \frac{T_{S_i} - \bar{T}_V(t)}{\Delta x_i} \cdot S_i, \tag{4.5}$$

where λ_V is the thermal conductivity ($W \cdot m^{-1} \cdot K^{-1}$) of material in the volume V, T_{S_i} is the temperature at surface i and Δx is the distance between a point at temperature $\bar{T}_V$ (generally the geometrical centre of the volume V) and surface i. The linear approximation of the spatial derivative is valid only if Δx_i remains small. In other words, for an infinite number of small volumes in contact with other volumes, the approximation becomes exact.
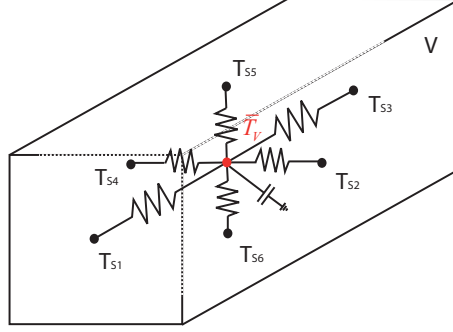
Figure 4.2: The electrical analogy on a parallelepiped volume V

For a fluid material: considering experimental convection coefficients hc_i $(\mathrm{W} \cdot \mathrm{m}^{-2} \cdot \mathrm{K}^{-1})$ and neglecting their temperature dependency, for surface $i = 1..n$ we have:

$$j_{\perp,i}(t) \cdot S_i \approx -hc_i \cdot S_i \cdot (T_{S_i} - \bar{T}_V(t)). \tag{4.6}$$

The final equations for a volume V delimited by n surfaces respectively for a solid and a fluid are then:

$$\rho V C_p \cdot \frac{d\bar{T}_V(t)}{dt} + \sum_{i=1}^{n} \frac{\lambda_V}{\Delta x_i} S_i \left(T_{S_i} - \bar{T}_V(t)\right) = S_V \tag{4.7}$$

$$\rho V C_p \cdot \frac{d\bar{T}_V(t)}{dt} + \sum_{i=1}^{n} hc_i \cdot S_i \left(T_{S_i} - \bar{T}_V(t)\right) = S_V \tag{4.8}$$

On closer examination of Equations 4.7 and 4.8, we see where the analogy with electrical networks stands. Considering temperature as being analogous to voltage for a parallelepiped volume (see Figure 4.2), the former equations reduce to Kirchoff's current law at a node with one capacitor and six resistors. The capacitor's capacitance C_V and resistors' conductances $G_{i,V}$ being given by:

$$C_V = \rho V C_p \tag{4.9}$$

$$G_{i,V} = \begin{cases} \frac{\lambda_V}{\Delta x_i} S_i & \text{for a solid} \\ hc_i \cdot S_i & \text{for a fluid} \end{cases} \tag{4.10}$$

where C_V is the volume capacitance $(\mathrm{J}/(\mathrm{kg} \cdot \mathrm{K}))$ and $G_{i,V}$ is the volume conductance (W/K) to surface i.

Each volume described by Equation 4.7 or 4.8 is defined as a temperature node in the literature. The volume capacitance C_V is a measure of its associated thermal inertia. According to different values of the volume capacitance, the temperature node is [Carter, 1990]:
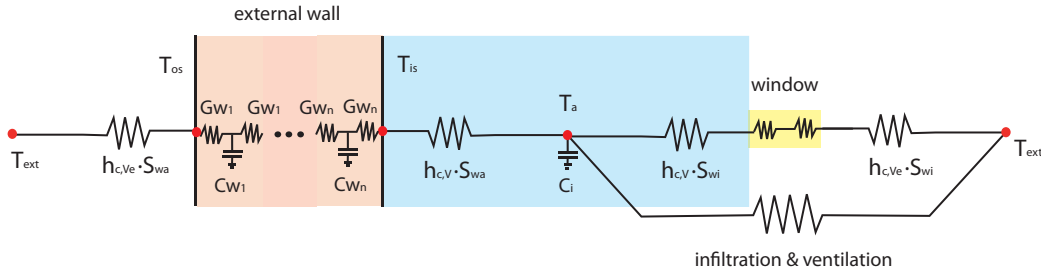
Figure 4.3: The volumes taken into account in a building application

1. with thermal mass, the general case

2. with zero-mass, where the volume capacitance is neglected ($C_V \rightarrow 0$)

3. at a prescribed varying temperature, where the volume capacitance is very large ($C_V \rightarrow \infty$)

Knowing the equations of the electrical analogy for heat transfer, we can now proceed to their application in the building domain.

4.1.2 The electrical analogy applied to buildings

In building applications, a typical zero-mass node is a window pane, its capacitance is so small compared to other elements in the building that it can be neglected. A typical node at a prescribed varying temperature is the external air temperature, it is supposed to be unaffected by the building and derives from measured or simulated meteorological data.

Let us now consider a room in a building. It can in principle be decomposed into many volumes (or nodes) connected to each other. The more nodes we have, the more precise can be the determination of the nodes'/volumes' temperature. However, for each node we need physical information (capacitance and conductances), which may not be precise and could add uncertainty to the final result. A trade-off must be found between the number of nodes and the available information and computing resource.

Considering a single air volume separated from the external air by a wall and a window, Figure 4.3 represents an equivalent electrical network. The different volumes taken into account are (from left to right): the external air node at a prescribed varying temperature, the different wall layers, the air/furniture node, the zero-mass window node and again the external air node.

The internal wall part of surface S_{wa} is at uniform temperature T_{is} and in contact with the internal air node T_a through the convective conductance

$h_{c,V}$. Likewise, the external wall part of surface S_{wa} is at uniform temperature T_{os} and in contact with the outdoor air temperature node T_{ext} via the convective conduction coefficient h_{c,V_e}.

The window of surface S_{wi} may likewise be considered as a wall sandwiched between the nodes T_a and T_{ext}. An equivalent infiltration/ventilation conductance can be calculated knowing the mass flow rate of air exchange between the inside air node and the external air node.

The different subvolumes of the wall shown in Figure 4.3 (one for each wall layer) are not always explicitly represented in the thermal building simulation according to the required precision. The less precise approximation is to consider the wall as only one global volume (or node) and neglect its capacitance and the air volume one. Such an approach is referred to as steady-state. It is commonly used for heating needs determination, considering a constant internal air volume temperature. A slight improvement to the steady-state approach is to take into account the air volume capacitance and still neglect all others (see [Page, 2007, p.97]). However, on that basis, by increasing the number of wall subvolumes we find more realistic models:

> A two node model, taking into account the air volume and wall volume capacitances (see Fraisse et al. [2002], Crabb et al. [1987], Nielsen [2005]).

> A three node model, taking into account the air volume capacitance and dividing the wall volume into two parts, with an internal wall capacitance and an external wall capacitance (see Tindale [1993]).

> A many node model, subdividing the walls' volume into three or more nodes per homogeneous element (see [Clarke, 2001, p.67]).

As stated earlier, our objective is to simulate the thermal behaviour of a whole city or city district (potentially comprised of several thousand buildings), therefore we need a simplified model that is sufficiently accurate and that can produce results within a reasonable amount of computing time. For this reason, we have chosen to explore the Two Node model.

4.1.3   The two node model

Two nodes for a whole building have been used frequently in the past [Fraisse et al., 2002, Crabb et al., 1987, Nielsen, 2005]. One mass node describes the heavy materials (walls, ceilings, floors), while the other describes the light materials (ambient air and room furniture). We have started with a basic two node model taken from Nielsen [2005] and refined it to suit our needs by adding two
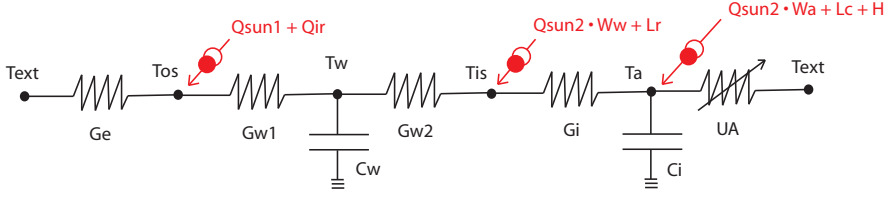
Figure 4.4: The two node thermal model as an equivalent electric circuit

temperature nodes (an internal and external walls' surface temperature) that explicitly take into account radiant and convective energy exchanges. Figure 4.4 shows the equivalent electrical circuit of our physical model, which is a simplification of Figure 4.3. The external wall volume is represented by the wall node T_w, a capacitance Cw and two resistors given by their conductance values $Gw1$ and $Gw2$. Considering a multilayered external wall, Cw is its total capacitance (the sum of the capacitances of each of its layers). The accessibility factor (the potential to mobilize the capacitance by the internal part of the building) is used in order to appropriately place the capacitance Cw in the lumped external walls, as proposed by Lorenz and Masy [1982]:

$$Gw1 = \frac{\sum_{i=1}^{l} Cw_i}{\sum_{i=1}^{l} Cw_i \cdot \left(-\frac{1}{Gw_i} + \sum_{j=1}^{i} \frac{2}{Gw_j} \right)} \tag{4.11}$$

$$Gw2 = \frac{1}{\sum_{i}^{l} \frac{1}{Gw_i} - \frac{1}{Gw1}} \tag{4.12}$$

The air and furniture volume is represented by the air node T_a, a capacitance Ci and two resistors given by their conductance values G_i and UA. The latter conductance lumps the window and infiltration/ventilation conductances from Figure 4.3. The external air temperature is represented by T_{ext}, which is linked to the walls' outside surface temperature T_{os} through the conductance of an external air layer G_e. Likewise the external walls' internal surface temperature T_{is} is linked to the air node T_a through the conductance of an internal air layer G_i.

We consider several different source terms at wall surfaces and at the air node (in red in Figure 4.4):

- Qir is the infrared energy flux (W) exchange at the outside surfaces of the wall

- $Qsun1$ is the shortwave energy flux (W) exchange at the outside surfaces of the wall

- $Qsun2$ is the shortwave energy flux (W) that enters the room, which is separated between a fraction that is allocated to the air node W_a and the rest W_w which is allocated to the walls' surfaces

- Lc is the convective heat flux (W) due to people and machines

- Lr is the radiant heat flux (W) due to people and machines

- H is the delivered convective heat flux (W)

Starting with Kirchoff's current law at each node (even zero-mass nodes), we have a system of four equations that can be summarised in the form of Equation 4.13. Note that the infrared exchange term Q_{ir}, which depends upon T_{os} to the fourth power, can be linearized using Piccard's rule (first order Taylor development).

$$\underbrace{\begin{pmatrix} Ci & 0 \\ 0 & Cw \end{pmatrix}}_{C} \underbrace{\begin{pmatrix} T'_a(t) \\ T'_w(t) \end{pmatrix}}_{\vec{T}'(t)} = \underbrace{\begin{pmatrix} -UA(t) - \kappa_2 & \kappa_2 \\ \kappa_2 & -\kappa_2 - \kappa_1(t) \end{pmatrix}}_{A(t)} \underbrace{\begin{pmatrix} T_a(t) \\ T_w(t) \end{pmatrix}}_{\vec{T}(t)} + \underbrace{\begin{pmatrix} u_a(t) \\ u_w(t) \end{pmatrix}}_{\vec{u(t)}}$$

$$(4.13)$$

where the air and wall source terms are:

$$\begin{pmatrix} u_a(t) \\ u_w(t) \end{pmatrix} = \begin{pmatrix} UA(t) \cdot T_{ext}(t) + \frac{\kappa_2}{G_{w2}} \cdot (Q_{sun2}(t) \cdot w_w + L_r(t)) \\ \frac{\kappa_2}{G_i} \cdot (Q_{sun2}(t) \cdot w_w + L_r(t)) \end{pmatrix} +$$

$$\begin{pmatrix} Q_{sun2}(t) \cdot w_a + L_c(t) + H(t) \\ \frac{\kappa_1(t)}{G_e(t)} \cdot (G_e(t) \cdot T_{ext}(t) + Q_{sun1}(t) + Q_{ir}(t)) \end{pmatrix} \quad (4.14)$$

with $\kappa_1(t)$ and κ_2 being respectively the total conductance between $T_{ext}(t)$ and T_w (left part of Figure 4.4), T_a and T_w:

$$\kappa_1(t) = \left(\frac{G_e(t) \cdot Gw1}{G_e(t) + Gw1} \right), \qquad \kappa_2 = \left(\frac{G_i \cdot Gw2}{G_i + Gw2} \right).$$

The set of differential equations (4.13) along with initial conditions gives the evolution of the system with time.

4.1.4   Numerical methods

Different methods for solving Equation 4.13 are described in Carter [1990]. These include explicit Euler methods, implicit Euler methods, modal spectral methods [Lagonotte et al., 1999], and Fourier series methods. In the special case of a two node model, an analytical solution can be found [Nielsen, 2005,

Crabb et al., 1987] which eliminates numerical errors. It involves finding eigenvalues and eigenvectors of the matrix $A(t)$ in Equation 4.13 at each discretised time step. However this method is time consuming and is not suitable for higher numbers of nodes as for a bigger matrix eigenvectors are found iteratively.

The first order Differential Equation 4.13 was solved using the implicit Euler scheme (chosen for stability reasons), the solution is given in Equation 4.15 in which time is discretised with a time step Δt. The uppercase index represents the corresponding time step number.

In order to calculate the zone temperature we need to solve the linear equation system, with T_a^n and T_w^n as unknowns.

$$C \cdot \vec{T}^{n-1} + \Delta t \cdot \vec{u}^n = (C - \Delta t \cdot A^n) \cdot \vec{T}^n \qquad (4.15)$$

A LU decomposition/backsubstitution scheme was used to solve the linear system [Press et al., 2002]. When A changes little within a time step, we can keep the LU decomposition of A and use only the backsubstitution, to save computing time.

The heating needs to achieve an inside air set point temperature after a time step is determined from Equation 4.15. We start by expressing the vectors with their components and putting everything on the left-hand side.

$$C \left(\begin{array}{c} T_a \\ T_w \end{array} \right)^{n-1} - C \left(\begin{array}{c} T_a \\ T_w \end{array} \right)^n + \Delta t \cdot A \left(\begin{array}{c} T_a \\ T_w \end{array} \right)^n + \Delta t \cdot \left(\begin{array}{c} u_a^n \\ u_w \end{array} \right)^n = 0$$

This set of equations is a linear system in which everything is known except T_w^n and u_a^n, in the latter being used to define air heating needs. We isolate T_w^n from the second equation of the linear system and replace it in the first equation of the linear system, which leaves us with one equation and u_a^n as an unknown. Finally we isolate H^n, expressed from u_a^n (see Equation 4.14) and obtain Equation 4.16 for the heating value at time step n. This heating value is the ideal convective heat flux that should be provided to the room in order to obtain a target temperature.

$$\begin{aligned} H^n \;=\; & \frac{Ci}{\Delta t} \cdot (T_a^n - T_a^{n-1}) - (-UA^n - \kappa_2) \cdot T_a^n - u_a^n + \qquad (4.16) \\ & \kappa_2 \cdot (\Delta t \cdot (-\kappa_2 - \kappa_1^n) - Cw)^{-1} \cdot (Cw \cdot T_w^{n-1} + \Delta t \cdot \kappa_2 \cdot T_a^n + \Delta t \cdot u_w^n) \end{aligned}$$

The cooling value at time step n is obtained in the same way.

The preceding equations allow for room temperature estimation, but also for ideal convective heat flux determination in order to attain a target temperature, during a single time step.

4.1.5   Using the two node model: one thermal zone

In this approximation, we assume that the walls enclose a single volume. The easiest way to thermally simulate the building envelope is to consider it homogenuous in terms of thermophysical properties. The limits of this approximation become evident when considering a real building, as we have different thermophysical properties for the walls, roofs and floors. A further simplification is that all walls' internal surfaces are assumed to have the same temperature; likewise the external surfaces. In reality this is not straightforward to implement as a south facade insolated by the sun should have a corresponding higher temperature than north facade.
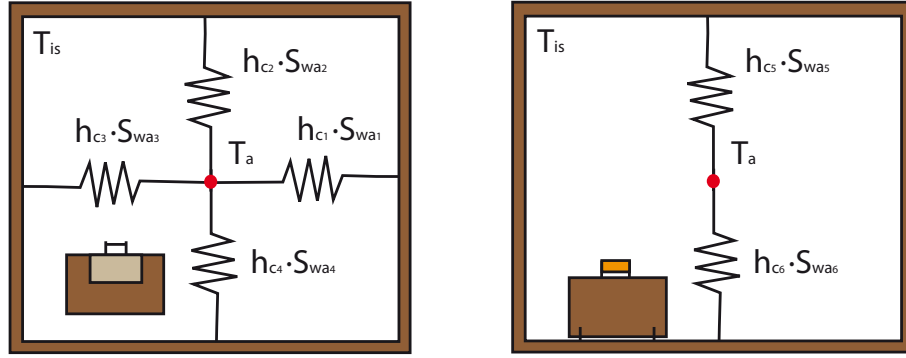
Figure 4.5: The lumping of the different walls, a view from top (left) and a view from the side (right)

Figure 4.5 shows a schema of a single zoned building, viewed from the top and from the side. Conductances from a volume node to different surfaces at the *same* temperature can now be lumped together. For instance, we can define the total conductance G_i (W/K) between T_a and T_{is} from Figure 4.5:

$$G_i = \sum_{i=1}^{6} h_{ci_i} \cdot Swa_i, \tag{4.17}$$

where Swa_i is the ith wall surface in the zone (m) and h_{c_i} the corresponding air-wall convection coefficient (W/(m^{2}K)).
In the same manner we define the total conductance G_e (W/K) between T_{os} and T_{ext}:

$$G_e = \sum_{i=1}^{6} h_{ce_i} \cdot Swa_i, \tag{4.18}$$

where Swa_i is the ith wall surface in the zone (m) and h_{ce_i} is the corresponding external air-wall convection coefficient (W/(m^{2}K)).

Finally we consider that UA is the sum of the conductances between the air/furniture node and the external air node through zero-mass elements (windows) and infiltration/ventilation. For this, the infiltration/ventilation conductance can be calculated knowing the mass flow rate of the air exchanged between our zone and the external environment:

$$UA = G_{wi} + \dot{m}_{inf} \cdot Cp + \dot{m}_{vent} \cdot Cp = G_{wi} + \frac{n_{inf}}{3600} V \rho Cp + \frac{n_{vent}}{3600} V \rho Cp, \quad (4.19)$$

where G_{wi} is the window U-value, $\dot{m}_{inf}$ and $\dot{m}_{vent}$ are respectivley the infiltration and ventilation mass flow rates (kg/s), Cp is the air specific heat capacity (J/(kg $\cdot$ K)), ρ is the air density (kg/m^3), and n_{inf} and n_{vent} are respectively the infiltration and ventilation air exchange rates (h^{-1}) at the air node volume V.

Model verification

During the 1980s and 1990s significant effort was invested to develop techniques for the validation of building thermal simulation programs. For an overview see Bloomfield et al. [1992] or Bartholomew and Robinson [1998]. The principle methods of model validation include: code checking, analytical tests [Bland, 1992], intermodel comparisons [Judkoff and Neymark, 1994] and empirical comparisons [Lomas et al., 1997]. Code checking has been carried out in our case by careful inspection and by comparing results from MATLAB and C++ implementations of the same model. Since analytical solutions do not exist for the set of heat transfer mechanisms in a fully enclosed space, these have been ignored. Empirical validation is potentially very powerful (depending upon measurement uncertainties), but is restricted by a small number of cases for which high quality datasets exist. For both convenience and versatility therefore, a method of intermodel comparisons has been used to test the predictive accuracy of our simplified model. Although there is no such thing as a truth model, following the extensive and continued validation studies that have been carried out on ESP-r [Clarke, 2001], we assume that this is a good candidate with which to compare our results.

For this an hypothetical test room has been defined (see Figure 4.6). To avoid potential differences in treatment of ground conduction it has no link to the ground and is effectively floating above it (we even receive ground reflected radiation at the external plane of the floor). The room is considered unoccupied and without furniture, the infiltration rate is set to a constant value of 0.25 h^{-1}, and there is no deliberate ventilation.

Eight types of room were tested, using test reference year (TRY) climate
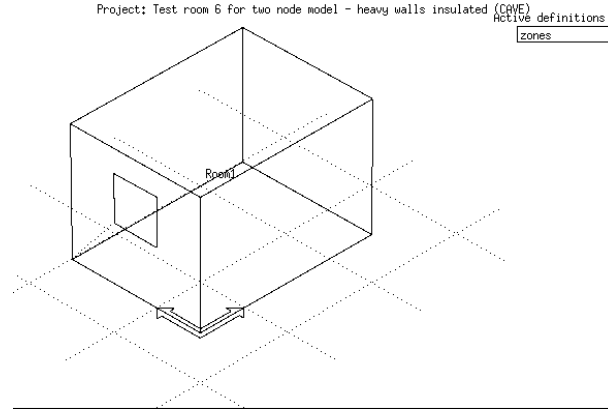
Figure 4.6: The test room, 3m · 4m · 2.7m

data for Geneva. The parameters changed for comparison with our two node model are summarized in Table 4.1. To ensure the equivalence of inputs

Label	Window	Walls composition (outside to inside)	U-Value $\mathrm{W \cdot m^{-2} \cdot K^{-1}}$	Inertia $\mathrm{kJ \cdot m^{-2} \cdot K^{-1}}$
Room1	no window	Heavy concrete (0.2m)	3.12	274
Room2	$1m^2$ south	Heavy concrete (0.2m)	3.12	274
Room3	$3.6m^2$ west	Heavy concrete (0.2m)	3.12	274
Room4	$8.64m^2$ south	Heavy concrete (0.2m)	3.12	274
Room5	$1m^2$ west	Concrete (0.1m), Insulation (0.1m), Plaster (0.012m)	0.32	104
Room6	$1m^2$ west	Insulation (0.1m), Heavy concrete (0.2m)	0.35	295
Room7	$1m^2$ west	Insulation (0.1m), Heavy concrete (0.2m), Carpet on the floor	0.35	296
Room8	$1m^2$ west	Brick (0.112m), Air Gap (0.025m), Glasswool (0.1m), Breeze block (0.12m)	0.31	290

Table 4.1: Different comparisons carried out with our two node model and ESP-r

between the models, we extracted from the ESP-r climate file the outside temperatures (to define T_{ext}) and the wind speeds and wind directions. The convective term G_e is also calculated using the wind speed, wind direction and external temperature as inputs, as described in [Clarke, 2001, p.261].

The simulation time step was chosen to be 1 hour, and the time invariant CIBSE Guide values for internal convective heat transfer coefficients were selected for reasons of simplicity and modelling compatibility. After each simulation with ESP-r, we extracted from the corresponding results database the absorbed shortwave irradiance on the outside walls ($Qsun_1$), the shortwave irradiance transmitted through the windows ($Qsun_2$) and the longwave exchange between the outside walls and the external environment (defined

as a rural site) (Q_{ir}).

To enable us to observe an accumulated discrepancy between the models we determine the heating energy demands relative to some datum. The results are summarized along with their relative difference in Table 4.2, based on a datum of 20°C for the heating period. The results are consistently within 7% of those of ESP-r, which is rather encouraging.

Label	ESP-r (kWh)	Two Node model (kWh)	Relative difference
Room1	9688	9573	1.2%
Room2	9526	9391	1.4%
Room3	9333	9054	3.0%
Room4	8950	8366	6.5%
Room5	1468	1443	1.7%
Room6	1738	1746	0.5%
Room7	1738	1739	0.1%
Room8	1370	1352	1.3%

Table 4.2: Energy needed in heating period to reach 20°C

Our model is sensitive to the size of the windows, the larger the window is, the more energy is needed compared to ESP-r (cases 1 to 4). This is because we lump together the different surfaces enclosing the room and their associated internal convective heat transfer coefficients. In accordance with the CIBSE guide, we use a convection coefficient (h_c) of 1.5 for downward, 3.0 for horizontal and 4.3 for upward flow directions. In our test case, these give an area-weighted mean convection coefficient of 2.96. Depending upon the receiving surfaces, the shortwave radiation inside the room is then convected to the air at a different rate compared to that observed in the results from ESP-r.

To judge the ability of the simplified model to faithfully model the dynamic behavior of our buildings, we have produced time series and x,y scatter plots of the indoor air temperature (T_a) calculated by each model. For the time series plots we have chosen to show the beginning of a hot period of the year, where the room needs some heating, but also some cooling (set point temperature for heating: 20°C, set point temperature for cooling: 26°C). The resulting graphs are shown in Figure 4.7 and 4.8. We have chosen to show only the dynamic behaviour of Room 4 from the first four rooms as the type of behaviours are similar - we observe only the effects of a slightly increased magnitude in temperature difference between the two models (due to an increase in temperature amplitude which exaggerates the differences between the models) as glazing ratio increases. Likewise, we have chosen to show only Room 6 (of room numbers 6 and 7), as the differences between the two dynamic behaviours are rather modest.

The dynamic behavior seems to follow well that of ESP-r for Room 4 when
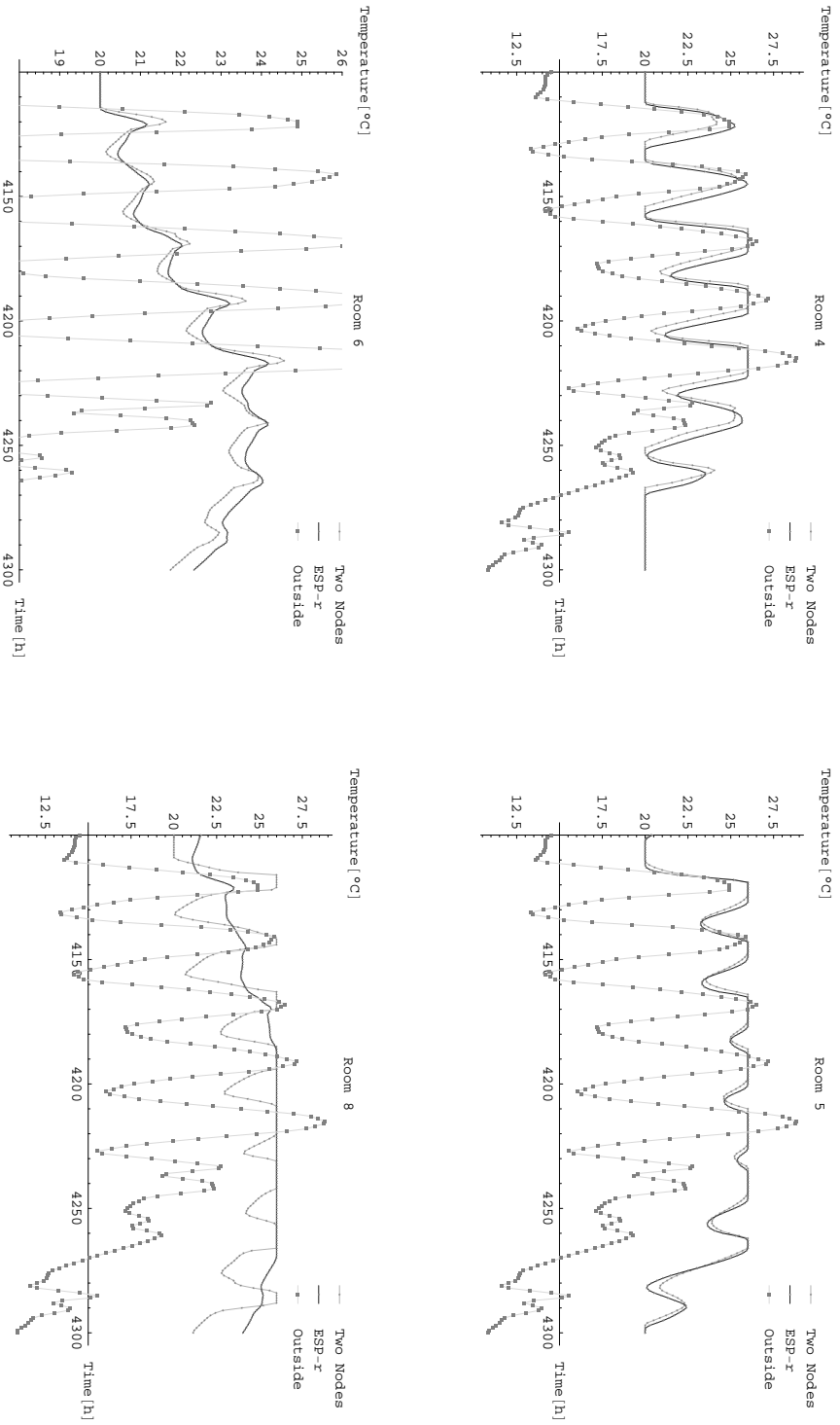
Figure 4.7: The dynamic behavior in four typical types of rooms
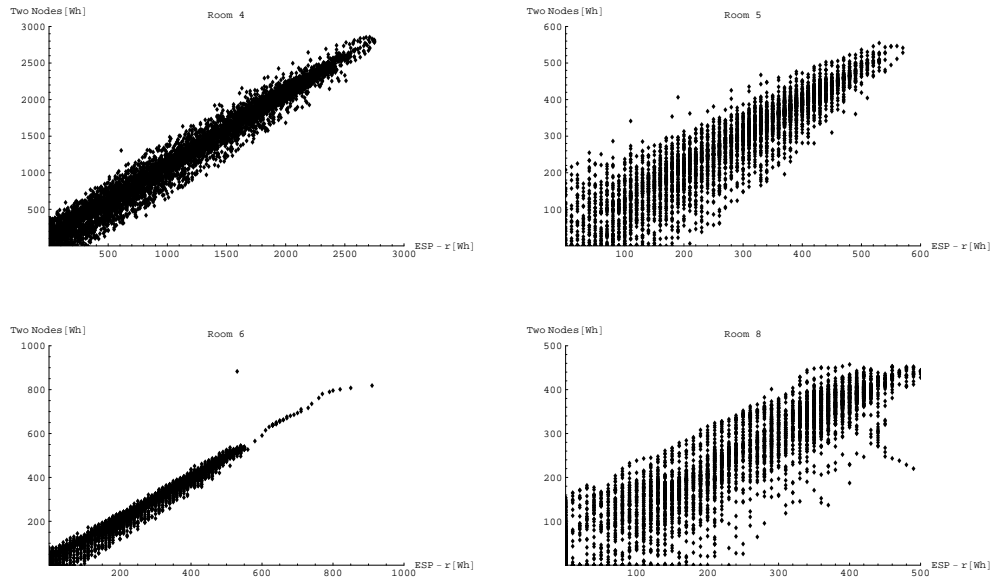
Figure 4.8: x,y scatter plots of the heating needs in four typical types of rooms

looking at Figure 4.7, but when looking at its corresponding x,y scatter plot in Figure 4.9, we can see that the phase difference between the two models can give rise to significant instantaneous temperature differences (albeit symetric about x=y). In addition to errors in heat transfer coefficient we observe that a small portion of the internal surfaces is reacting rapidly to the changes of temperature within the room, and should therefore be included in the quick reacting capacitance associated with the air node. One approach would be to lump a more detailed model (many nodes) to a two node model to improve the evaluated values of the capacitances Ci and Cw, but this would be incompatible with the aim of our work, of avoiding too much complexity in the model input parameters.

In the case of a light structure (case 5), the model is performing well.

In the case of a well insulated heavyweight zone (cases 6 and 7), the overall energy consumption in the heating period is very comparable to the calculations of ESP-r, but the two node model doesn't reproduce the convective exchange due to a heated carpet by the sun (in cases 6 and 7 the heating needs are the same for the two node model). However, the dynamic behavior of Room 6, is well reproduced.

In the last case (8), the energy consumption is predicted with good accuracy (a relative difference of less than 1.5%, which is probably much less than the
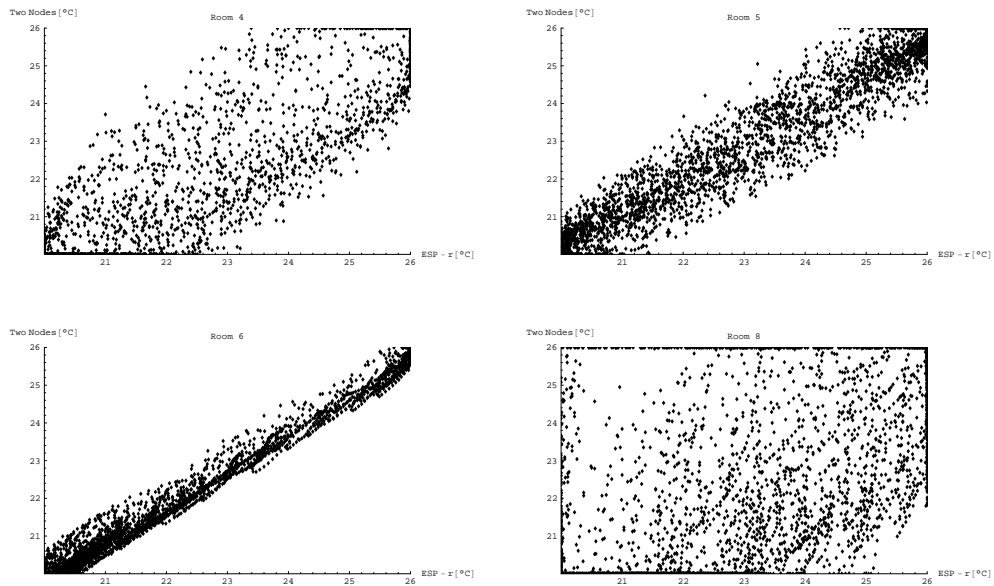
Figure 4.9: x,y temperature scatter plots of the dynamic behavior in four typical types of rooms

uncertainty in the model parameters), but the dynamic behaviour is not at all well represented. We come here to a limit of the two node model. As it has only one node (or one time constant) for the heavy part of the zone, it reproduces badly the behaviour of two walls separated by an insulating material. In such cases we need two different nodes (or two different time constants) to reproduce the dynamics. As a result, we model a global mean behavior of the two heavy parts of the external walls, which is too responsive (we have a low conductance to the mass node so that the surface response dominates - see Tindale [1993]). To overcome that limitation, a three node model will be proposed in the future for modern buildings with two heavy parts in the walls.

Finally, in all cases we observe two general trends. The variance in heating energy demand tends to reduce with its magnitude (the model performs well at zero or low solar intensities when heating demands are largest). The scatter in results is symmetric about the $x, y = 1$ line. Consequently, statistics such as temperature frequency distributions should be well reproduced. Furthermore, for large numbers of buildings, experiencing different radiant environments and stochastic internal heat gains, the consequence of these (rather small) random energy demand errors will be diminished; particularly when aggregate loads for a site are predicted.
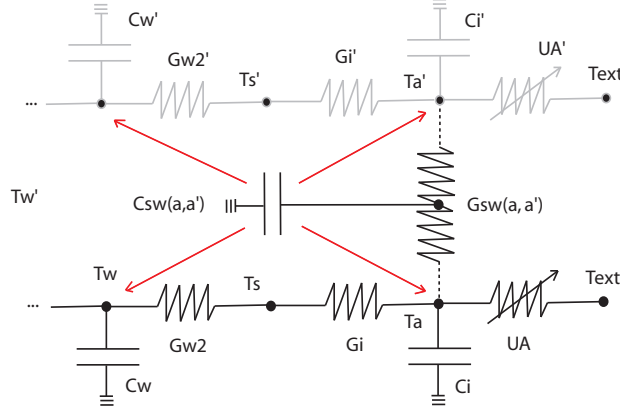
Figure 4.10: The thermal physical model for many zones in a building

4.1.6 Using the two nodes model: n thermal zones

An extension of the two node model was suggested by Achterbosch et al. [1985] by linking the air nodes of each zone together with those of neighbouring zones in a building. The corresponding link was made via separating wall resistances. However, this method neglects the separating wall thermal inertia, which could be important in buildings with thermally heavyweight partitions. To resolve this we introduce a new way of connecting the zones together (see Figure 4.10). With this approach, the air nodes are connected together via the separating wall resistance and the thermal inertia of the separating wall is subdivided and allocated to the neighbouring zones' capacitances (Ci and Ci', Cw and Cw'). We distribute the thermal inertia to the air and wall nodes of the adjacent rooms, under the assumption that the separating wall is in contact with both the air and the external wall. An interzonal airflow coupling could also be catered for in the separating wall conductance G_{sw}.

Kirchoff's current law at each node can be re-written for n-zones indexed by i and j in the form:

$$\begin{pmatrix} C_1 & 0 \\ 0 & C_2 \end{pmatrix} \cdot \begin{pmatrix} \vec{T}'_a(t) \\ \vec{T}'_w(t) \end{pmatrix} = \begin{pmatrix} D & E \\ F & G \end{pmatrix} \cdot \begin{pmatrix} \vec{T}_a(t) \\ \vec{T}_w(t) \end{pmatrix} + \begin{pmatrix} \vec{u}_a(t) \\ \vec{u}_w(t) \end{pmatrix}, \quad (4.20)$$

where,

$$(C_1)_{ij} = \begin{cases} Ci_i + \frac{1}{4} \sum_j Csw_{ij} & \text{if } i = j \\ 0 & \text{elsewhere} \end{cases}$$

$$(C_2)_{ij} = \begin{cases} Cw_i + \frac{1}{4} \sum_j Csw_{ij} & \text{if } i = j \\ 0 & \text{elsewhere} \end{cases}$$

$$(D)_{ij} = \begin{cases} -UA_i - \kappa_{2i} - \sum_j Gsw_{ij} & \text{if } i = j \\ Gsw_{ij} & \text{elsewhere} \end{cases}$$

$$(E)_{ij} = -(F)_{ij} = \begin{cases} \kappa_{2i} & \text{if } i = j \\ 0 & \text{elsewhere} \end{cases} \qquad (G)_{ij} = \begin{cases} -\kappa_{2i} - \kappa_{1i} & \text{if } i = j \\ 0 & \text{elsewhere} \end{cases}$$

with $\vec{T}_a$ being the vector containing the inside air temperature of the n-zones and $\vec{T}_w$ the wall temperature vector for the n-zones, $\vec{u}_a$ is the vector containing source terms on the air nodes for the n-zones and $\vec{u}_w$ is the vector containing the source terms on the wall nodes. Finally, Gsw_{ij} represents the conductance of the separating wall between zone i and j and Csw_{ij} is the corresponding capacitance.

Numerical methods

To solve the Differential Equation 4.20, the same Euler implicit scheme was used, as matrix A is relatively small (so that the solving procedure remains efficient) even for a building with many floors and many zones per floor.
The heating demands for each zone $\vec{H}_i$ are calculated using relation 4.21 which is a generalisation of Equation 4.16. The cooling demands are obtained in a similar way.

$$\begin{aligned} \vec{H}_i^n &= \frac{1}{\Delta t} \cdot Ci \cdot (\vec{T}_a^n - \vec{T}_a^{n-1}) - D \cdot \vec{T}_a^n - \vec{u}_a^n \\ &\quad - E \cdot (Cw - \Delta t \cdot G)^{-1} \cdot (Cw \cdot \vec{T}_w^{n-1} + \Delta t \cdot F \cdot T_a^n + \Delta t \cdot \vec{u}_w^n) \end{aligned} \qquad (4.21)$$

Model verification

The verification was again carried out by comparing our results with ESP-r. The single room of our two node model validation was replicated to define a whole (hypothetical) building (see Figure 4.11). The outside walls are taken as Room5 in the two node case and the internal walls are composed of a light mix concrete finished with plaster (5mm light plaster, 10cm light mix concrete, 5mm light plaster). We have tested different scenarios for weighting the subdivision of the separating wall thermal inertia to the air and wall nodes. An even repartition between the four air and wall nodes for the adjacent zones was found to give the best results for the cases studied in this work. The heating demands are compared in Table 4.3, from which we observe that we consistently under-estimate the annual energy demands. For edge zones this error is typically less than 5% (1,3,4,6,7,9,10 and 12), but for the middle zones (2, 5, 8 and 11) where interzonal energy exchanges dominate, the errors are more significant. This implies that our means of resolving for interzonal energy exchanges is still in error. Nevertheless the global heating
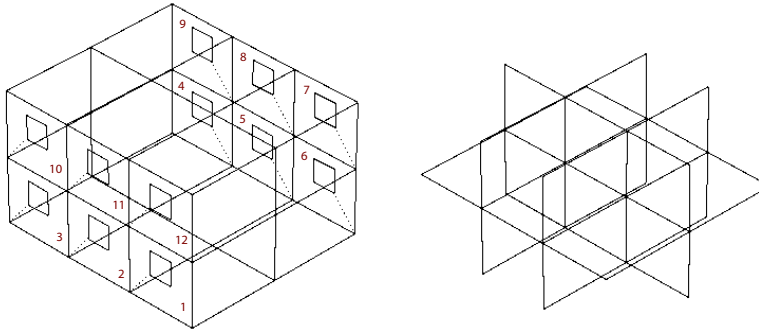
Figure 4.11: The test building composed of 12 zones of the type Room5, on the right a view of the separating walls

Table 4.3: Energy needed in the heating period to reach 20°

Label	ESP-r (kWh)	Two Node model (kWh)	Relative difference
Room1 (Ground Floor, West)	788	754	4.6%
Room2	633	561	12.8%
Room3	829	798	4.0%
Room4 (Ground Floor, East)	901	866	4.1%
Room5	700	620	12.8%
Room6	851	816	4.3%
Room7 (First Floor, East)	859	831	3.4%
Room8	712	635	12.1%
Room9	907	880	3.0%
Room10 (First Floor, West)	839	816	2.9%
Room11	647	579	11.8%
Room12	800	772	3.6%
Total	9467	8927	6.0%

needs (for the whole building) with our two node model are reasonable close to ESP-r's (the relative difference is just 6%) which we consider acceptable to fullfill our needs. Finally we compare the dynamic behaviour of Rooms 1, 2, 9, 11 in Figure 4.12 (they represent the whole set by symmetry). From these we can see that the dynamic behavior is well estimated by our model compared to ESP-r.

4.1.7 Conclusion

As we aim to simulate energy demand of buildings for which we have relatively little descriptive information, we have chosen to explore simplified methods for dynamic simulation of thermal energy flows in our buildings. For this, a simplified two node model based on the analogy between heat and electricity was proposed. It can be used for a single enclosure in a building, or multiple thermal zones. The complexity of the selected modelling approach
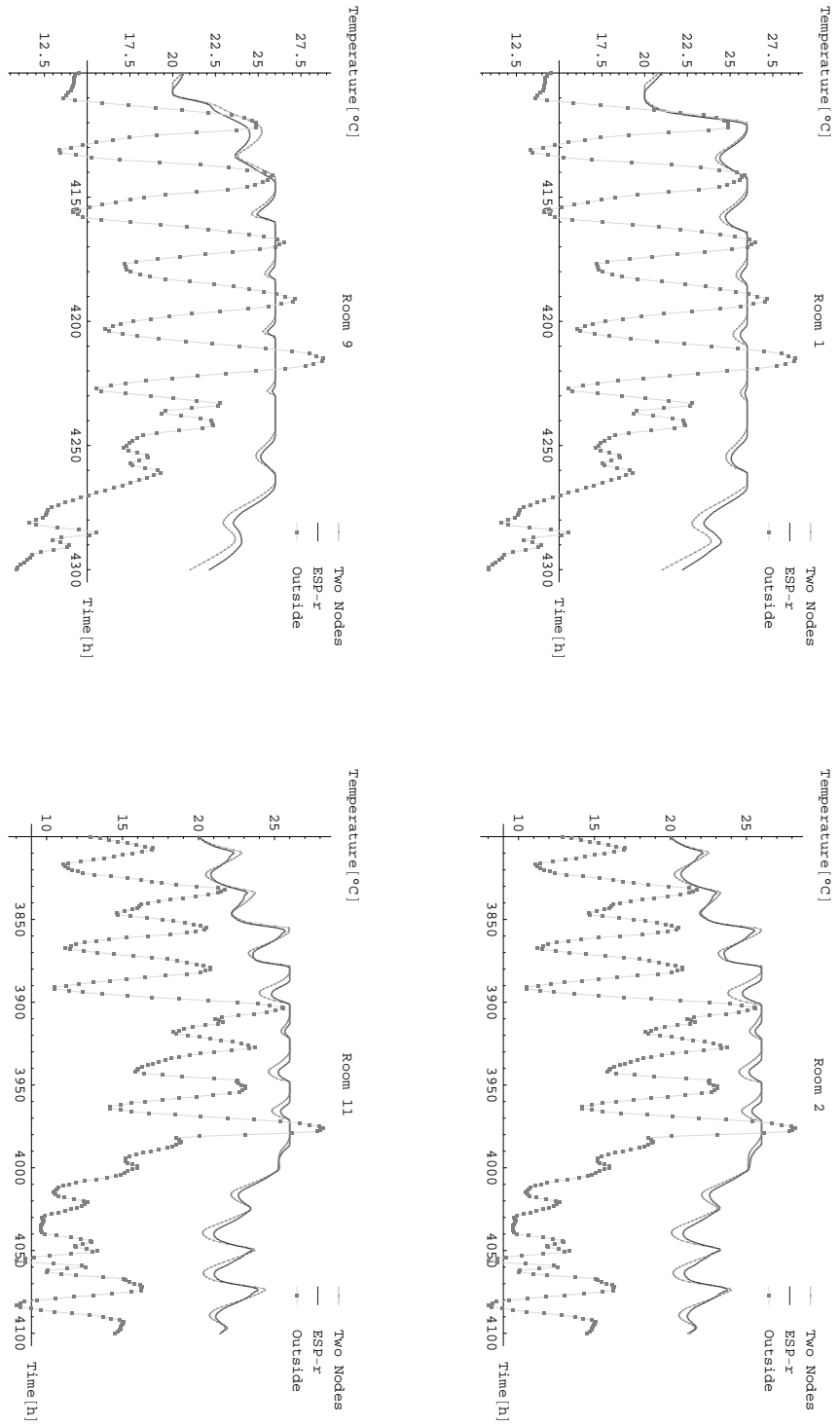
Figure 4.12: Comparison of dynamic behavior within four zones of the hypothetical building

is reasonable and likewise the simulation time.

The two node model for one room has been shown to give reasonably good results for a variety of typical wall constructions. The extension of the model to handle multi-zone buildings also seems to reproduce with good accuracy the results obtained by the dynamic thermal simulation program ESP-r. When coupled with appropriate models, the energy demands of a city district can be efficiently simulated using the presented model with minimal information regarding the buildings geometry, materials and operation.
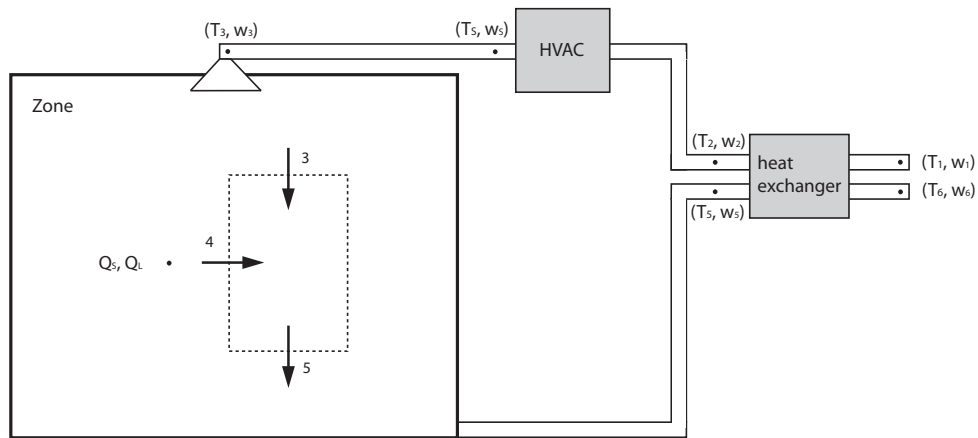
Figure 4.13: A thermal zone equipped with HVAC system

4.2   HVAC Model

Although in Europe only a relatively small proportion of buildings are serviced with Heating, Ventilation and Air-Conditioning (HVAC) systems, the energy demands of these buildings is higher compared to those without them. Furthermore we wish to develop a tool that is sufficiently general to model the range of building types. For this reason we have developed a class of models to simulate HVAC plant.

The HVAC model is based upon the psychrometry of humid air. We consider the air as being composed of two major components: dry air and moisture. The quantity of moisture being small compared to that of air, we assume that the mixture follows the Ideal Gas law and Dalton's law of partial pressures [Jones, 2000, p.3]. An air-conditioned zone is shown schematically in Figure 4.13.

Seven points are considered on the path of the air in the ducts of Figure 4.13. For each point, the air temperature and moisture content are given. The system takes outside fresh air at known state (T_1, ω_1), which then passes through an air heat/moisture exchanger, providing a new state (T_2, ω_2) to the HVAC unit. This unit provides a state (T_S, ω_S), after which the air absorbs the latent heat loads (Q_L) and sensible heat loads (Q_S) and reaches the final state (T_5, ω_5).

The final state T_5 should lie within a user defined comfort zone; the system controls the moisture content at the exit of the air conditioner (ω_S) so that the moisture content in the room (ω_5) also lies within the comfort zone. This comfort zone is defined by default as being between 20° and 26°C in the range of relative humidity 30% to 70%. A further constraint is that the mass flow

rate must be sufficient to satisfy the zone occupants' fresh air requirements. The energy and moisture to be provided to the HVAC system in order to achieve comfort in the thermal zone is equal to the enthalpy difference between (T_2, ω_2) and (T_S, ω_S). The first section deals with the assumptions made and the basic equations behind the model. The second section concerns the determination of the supply state (T_S, ω_S), after which the third section deals with ways of providing the enthalpy difference between (T_2, ω_2) and (T_S, ω_S).

4.2.1 Model assumptions and equations

The mass flow rate of dry air (in kg/s) is assumed constant throughout the system and corresponds to $\dot{m}$. This, shown in the following equation, means that we consider no air leakage in the ducts.

$$\dot{m}_1 = \dot{m}_2 = \dot{m}_3 = \dot{m}_5 = \dot{m}_6 := \dot{m} \tag{4.22}$$

We introduce a performance coefficient β[1] of the heat exchanger, which is approximated using temperature differences by neglecting the energy content of the water vapour:

$$\beta = \frac{T_5 - T_6}{T_5 - T_1} = \frac{T_2 - T_1}{T_5 - T_1}. \tag{4.23}$$

Knowing the outside air temperature T_1, the inside air temperature T_5 and the heat exchanger coefficient β, we can determine the supply temperature at the internal exit of the heat exchanger T_2.

Mass conservation

The mass conservation equation for the moisture content (in kg/kg dry air) provides us with three equations. Equation 4.24 takes into account potential condensation in the heat exchanger, which is represented by the min function. Equation 4.25 is the mass conservation in the ducts at the end of the HVAC supply. Equation 4.26 is the mass balance of moisture due to people present in the room.

$$\dot{m}\omega_2 = \dot{m} \cdot \min(\omega_1, \omega(T_2, 100\%, P_{atm})) \tag{4.24}$$

$$\dot{m}\omega_3 = \dot{m}\omega_S \tag{4.25}$$

$$\dot{m}\omega_5 = \dot{m}\omega_3 + \frac{Q_L}{L_v} \tag{4.26}$$

In the previous equations, we have:

---

[1]Data permitting, an alternative model such as the NTU-effectiveness could be employed.

Q_L is the latent heat load in the control volume (W),

L_v is the latent heat of vaporisation of water (in J/kg), and

$\omega(T_2, RH, P_{atm})$ is the moisture content (in kg/(kg dry air) of air at temperature T_2 and relative humidity RH).

The former element is calculated using the Ideal Gas Law:

$$P \cdot V = \frac{m}{M} \cdot R \cdot T, \qquad (4.27)$$

where P is the pressure (Pa), V is the volume (m^3), m is the mass (kg), M is the molar mass (kg/mol), R is the ideal gas law's constant (8.314 J/(K·mol)) and T is the temperature (K). Starting with the definition of the moisture content, which is the ratio of the mass of vapour m_v and dry air m_a, we obtain:

$$\omega = \frac{m_v}{m_a} = \frac{P_v \cdot V \cdot M_v/(R \cdot T)}{P_a \cdot V \cdot M_a/(R \cdot T)} = \frac{P_v}{P_a} \cdot \frac{M_v}{M_a}. \qquad (4.28)$$

The molar mass of air M_a is equal to 28.97 g/mol and the molar mass of water vapour M_v is 18.02 g/mol. The vapour pressure P_v can be written in terms of the product of the relative humidity RH and the saturated vapour pressure P_{ss}. Furthermore the dry air pressure P_a is the reference atmospheric pressure P_{atm} reduced by the vapour pressure, which leads to:

$$\omega(T, RH, P_{atm}) = \frac{\frac{M_v}{M_a} \cdot RH \cdot P_{ss}(T)}{P_{atm} - RH \cdot P_{ss}(T)}. \qquad (4.29)$$

The saturated vapour pressure P_{ss} is given as an empirical function of temperature in Murphy and Koop [2005].

Enthalpy conservation

The enthalpy $h(T, \omega)$ used in psychrometry is expressed in kJ per kg of dry air, and defined as the sum of the enthalpy of dry air and the enthalpy of vapour. Combining the expressions for the enthalpy of dry air and vapour in Jones [2000, p.23], we find the following expression:

$$h(T, \omega) = \begin{cases} (1.007 \cdot T - 0.026) + \omega \cdot (2501 + 1.84 \cdot T) & 0°\text{C} < T < 60°\text{C} \\ (1.005 \cdot T) + \omega \cdot (2501 + 1.84 \cdot T) & -10°\text{C} < T \leq 0°\text{C} \end{cases}$$
$$(4.30)$$

A discontinuity in the previous equation is found at $T = 0°$C. This enthalpy formulation may be used to approximate the heat (latent and sensible) associated with a change of state of air, using the principle of conservation

of enthalpy. Applying this to the control volume of the thermal zone with sensible and latent heat gains, between point 3 and 5, leads to the following two equations:

$$Q_S \;=\; \dot{m} \cdot (h(T_5, \omega_3) - h(T_3, \omega_3)) = \dot{m} \cdot (T_5 - T_3) \cdot Cp_a(\omega_3) \quad (4.31)$$
$$Q_L \;=\; \dot{m} \cdot (h(T_5, \omega_5) - h(T_5, \omega_3)) = \dot{m} \cdot (\omega_5 - \omega_3) \cdot Cp_v(T_5), \quad (4.32)$$

where $Cp_a(\omega_3)$ is the specific heat of air with a moisture content ω_3 and $Cp_v(T_5)$ is the specific heat of water vapour at temperature T_5.

The temperature drop or rise in the ducts is expressed by the temperature difference between point 3 and point S (supply):

$$\Delta T = T_3 - T_S. \tag{4.33}$$

4.2.2 Supply state determination

In the previous system, we begin with a knowledge of the outside air state (T_1, ω_1), the indoor temperature at the previous time step (T_5), the indoor set point temperature (T_5'), the sensible (Q_S) and latent (Q_L) heat loads and finally the room supply air temperatures for heating and cooling (T_3). From this, the temperature T_2 is calculated from Equation 4.23, using the value of T_5 from the previous time-step. The moisture content w_2 is calculated using equation 4.24. The room supply air temperature T_3 is set to the heating supply temperature or cooling supply temperature according to the sign of Q_S. At that point we must make a first assumption in order to predict the mass flow rate. We assume initially that the HVAC system does not alter the moisture content (i.e. $\omega_3 = \omega_2$). The mass flow rate will then be corrected at the end of the algorithm, according to the estimated value of ω_3. The mass flow rate $\dot{m}$ of the system is calculated according to:

$$\dot{m} = \max \left(\frac{Q_S}{h(T_5', \omega_3) - h(T_3, \omega_3)}, \rho_{air} \cdot n_p \cdot L_p \cdot 10^{-3} \right) \tag{4.34}$$

The first term in the parenthesis arises from Equation 4.31 and the second is the minimum fresh air requirements for n_p people in the thermal zone, considering an individual requirement L_p of 8 litres per second per person.

In order to compute the humidification or dehumidification that the HVAC system should provide we first calculate, using Equations 4.31 and 4.32, a state without moisture conditioning (T_5', ω_5') in which we maintain the assumption that the HVAC system does not act on the moisture content (i.e. $\omega_3 = \omega_2$). This allows us to evaluate the moisture in excess or insufficient to provide a state in the comfort zone for temperature T_5', that must be removed

from or added to ω_2. Using that virtual state, we can compute what should be the room's supply moisture content ω_3.

For the heating case, Algorithm 1 shows in pseudo-code the calculation of the room's supply moisture content (ω_3). The interpretation of the algorithm is

---

Algorithm 1 Determination of the room's supply moisture content (ω_3) for heating case

---

1: Heating Case
2: **if** $\omega_5' < \omega(T_5', 30\%, P_{atm})$ **then**
3:　　Humidification
4:　　$\omega_3 = \omega(T_5', 30\%, P_{atm}) - \omega_5' + \omega_2$
5: **else if** $\omega_5' > \omega(T5, 70\%, P_{atm})$ and $\omega_5' < \omega(26, 70\%, P_{atm})$ **then**
6:　　Heating with no dehumidification
7:　　$\Delta T_{HVAC} = T(\omega_5', 70\%, P_{atm}) - T_5'$
8:　　$\omega_3 = \omega_2$
9: **else if** $\omega_5' > \omega(26, 70\%, P_{atm})$ **then**
10:　　Dehumidification
11:　　$\omega_3 = \max(\min(\min(\omega(26, 70\%, P_{atm}) - \omega_5' + \omega_2, \omega(T_3, 100\%, P_{atm})),$
12:　　$\omega(T_5', 70\%, P_{atm}) - \omega_5' + \omega_2),\ 0)$
13: **else**
14:　　No moisture control
15:　　$\omega_3 = \omega_2$
16: **end if**

---

straight forward, however the function $T(\omega, RH, P_{atm})$ must be defined. This is simply the reciprocal of the function $\omega(T, RH, P_{atm})$ in Equation 4.29, and returns the temperature corresponding to a relative humidity RH and a moisture content ω. Please note that the algorithm provides ω_3, and that according to Equation 4.25, it is equal to ω_S. Moreover, according to Equation 4.33, T_S is calculated knowing the room supply air temperature (T_3) and the temperature drop or rise due to the ducts (ΔT). On this basis we can deduce the supply state (T_S, ω_S) for heating purpose. Finally we need to recalculate the mass flow rate according to equation 4.34 in order to take into account the correct value of room's supply moisture content ω_3.

For the cooling case, Algorithm 2 shows in pseudo-code the calculation of the room's supply moisture content (ω_3). In the presence of an evaporative cooling system, we consider an adiabatic change in (T_2, ω_2) (i.e. constant enthalpy) to reach a new state with a moisture content at the highest possible value in the considered comfort zone (30% to 70% of relative humidity) for the set point temperature. However, if that moisture content is larger than the maximum moisture content at the supply air temperature, then this lat-

---

Algorithm 2 Determination of the room's supply moisture content (ω_3) for cooling case

---

1: Cooling Case
2: **if** Evaporative Cooling **then**
3:    H2 = enthalpyDryAir(T2) + w2*enthalpyWaterVapour(T2)
4:    $\omega_2' = \min(\omega(T_5, 70\%, P_{atm}) - \omega_5' + \omega_2, \omega(T_3 + \Delta T, 100\%, P_{atm}))$
5:    $T_2' = (H2 + 0.026 - \omega_2' * 2501.0)/(1.007 + \omega_2' * 1.84)$
6:    **if** $T_2' < T_3$ **then**
7:       $T_2' = T_3$
8:       $\omega_2' = (H2 - 1.007 * T_2' + 0.026)/(2501.0 + 1.84 * T_2')$
9:    **end if**
10:    **if** $\omega_2' > \omega_2$ **then**
11:       evaporation $= \omega_2' - \omega_2$
12:       $T_2 = T_2'$
13:       $\omega_5' = \omega_2' + \omega_5' - \omega_2$
14:       $\omega_2 = \omega_2'$
15:    **end if**
16: **end if**
17: **if** $\omega_5' > \omega(T_5, 70\%, P_{atm})$ **then**
18:    Dehumidification
19:    $\omega_3 = \max(\min(\omega(T_5, 70\%, P_{atm}) - \omega_5' + \omega_2, \omega(T_3, 100\%, P_{atm})), 0)$
20: **else if** $\omega_5' < \omega(T_5, 30\%, P_{atm})$ **then**
21:    Humdification
22:    $\omega_3 = \omega(T_5, 30\%, P_{atm}) - \omega_5' + \omega_2$
23: **else**
24:    $\omega_3 = \min(\omega_2, \omega(T_3, 100\%, P_{atm}))$
25: **end if**

---

ter is taken into account in order to avoid unwanted condensation in the cooling coil. In the event of humidification or dehumidification the moisture calculations are similar to that of the heating case. Likewise for the determination of the supply state and the correction of the mass flow rate, which are derived in exactly the same way.

4.2.3   Determination of the HVAC loads

The energy needs of the HVAC system to reach the comfort zone are calculated using the air enthalpy difference between the points (T_2, ω_2) and (T_S, ω_S), in which the latter point was determined in the former section. Four different cases can be distinguished in Figure 4.14 to move from one point to

another on Carrier's psychrometric chart [Jones, 2000].   From which we can
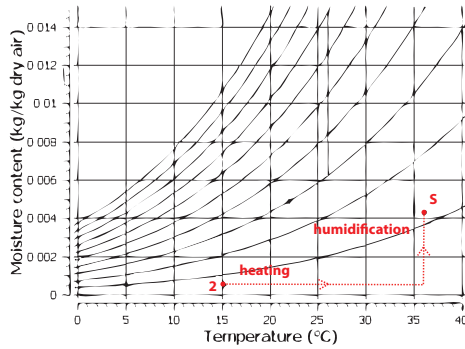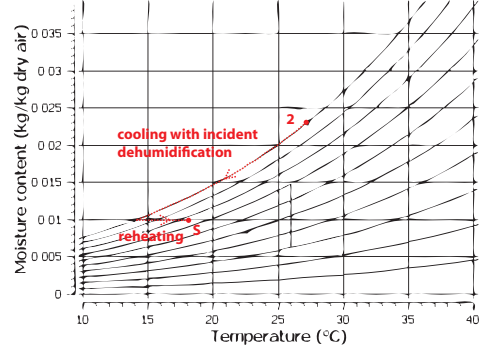
(a) Heating and humidification loads   (b) Cooling and reheat loads
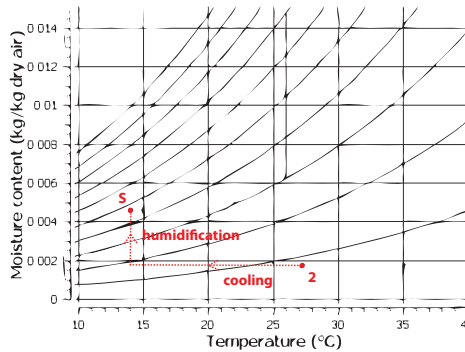
(c) Cooling and humidification loads   (d) Evaporation and cooling loads
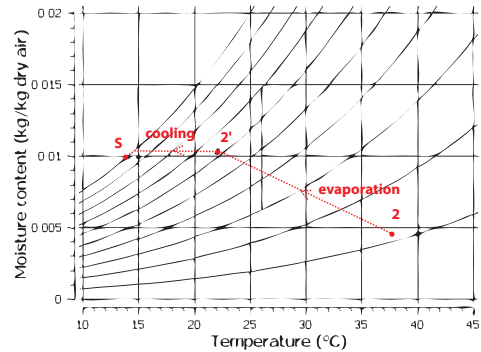
Figure 4.14: Four cases of loads to be provided to the HVAC system, shown in Carrier's psychrometric chart[3]

define 5 enthalpy demands: heating, humidification, evaporation, cooling and reheating. These enthalpy demands must be multiplied by the mass flow rate in order to obtain the heating/cooling power to be provided by machines, in watts.

Available cooling and heating loads

In order to calculate the available heating or cooling loads in the thermal zone when the HVAC demands are not fully satisfied by our machines, we reverse the order of our procedure: we start with point (T_2, ω_2) and add the available heating, cooling, humidification, reheat and evaporation loads to achieve the final (corrected) point (T_S, ω_S). In this latter operation, we

---

[3]By this we are simply referring to the form of the psychrometric chart and not to the original equations to produce it.

divide the machine capacity by the available mass flow rate to obtain the available enthalpy demands. Then from T_S we can find T_3 using Equation 4.33 and using Equation 4.31 with the available mass flow rate and the target room temperature (T_5') we can obtain the sensible heat provided to the room (Q_S).

Modelling scope

In this HVAC model, we are dealing exclusively with psychrometric processes on air handling plant and not resolving for fan power demands; likewise for heating systems when water is the working fluid, we do not resolve for pump power demands.

4.2.4 Examples

An interface for testing the HVAC model was implemented using the Open-Source library Qt and the plotting library Qwt.
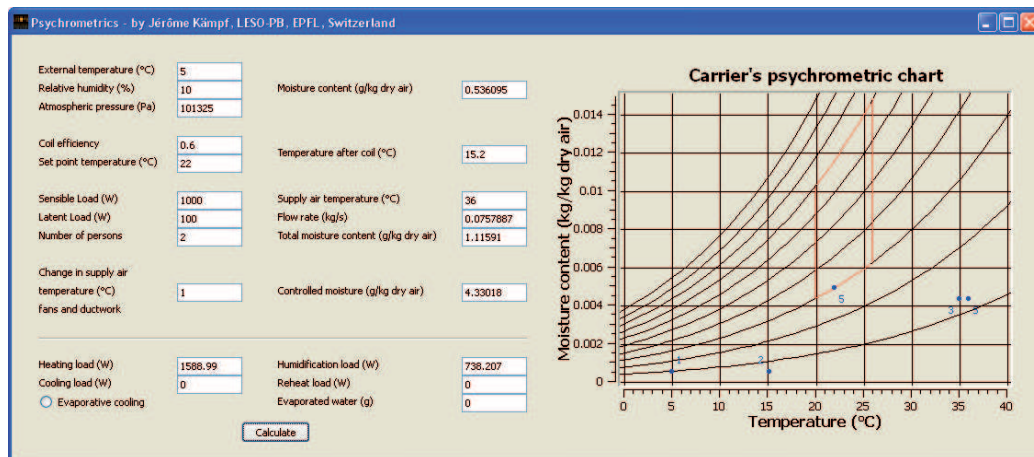
Figure 4.15: Heating and humidification

Figure 4.15 shows a heating and humidification case, in which the external air temperature is 5°C with a very low relative humidity of 10%. The supply air temperature is 36°C with a mass flow rate of 0.076 kg/s. Considering a loss in temperature due to the fans and ducts of 1°C, it gives the requested 1000 W in sensible heat. Absorbing the 100 W of latent heat in the room, the HVAC system has to provide the remaining moisture in order to come to 22°C at a relative humidity of 30% (comfort zone). Figure 4.16 shows a
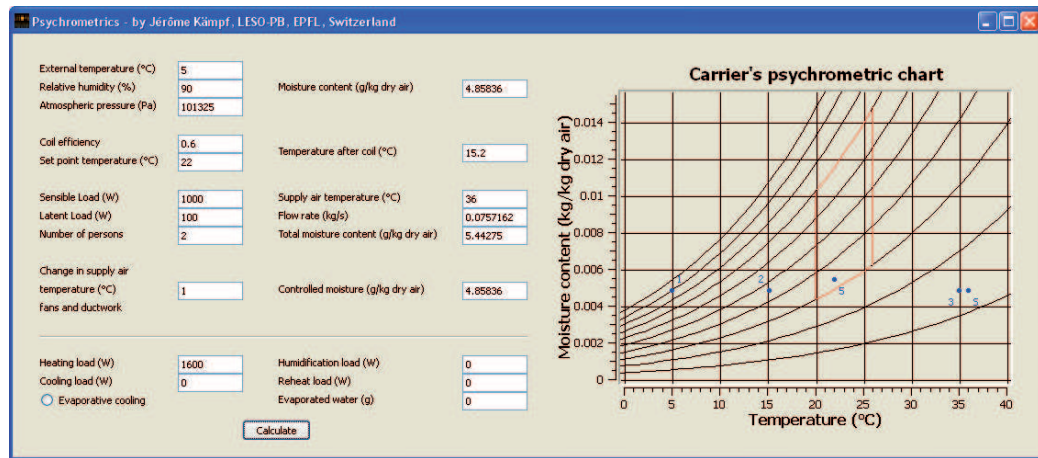
Figure 4.16: Heating

heating only case, in which the external air temperature is 5°C with a relative humidity of 90%. Due to the high moisture content of the external air, the HVAC system does not provide additional moisture to the air.
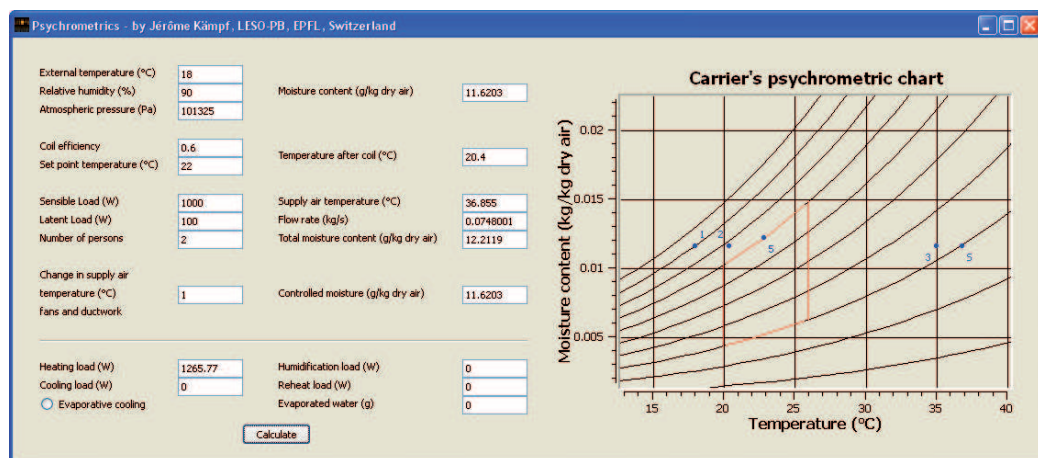
Figure 4.17: Overheating to avoid dehumidification

Figure 4.17 shows a case of overheating to avoid dehumidification. The external air temperature is 18°C with a relative humidity of 90%. The moisture content of that air exceeds the 70% of relative humidity at 22°C. In order to avoid dehumidification of the air, the set point temperature was increased to 23°C at which the moisture content represents 70% of relative humidity. Figure 4.18 shows a case of evaporative cooling. The outside air temperature
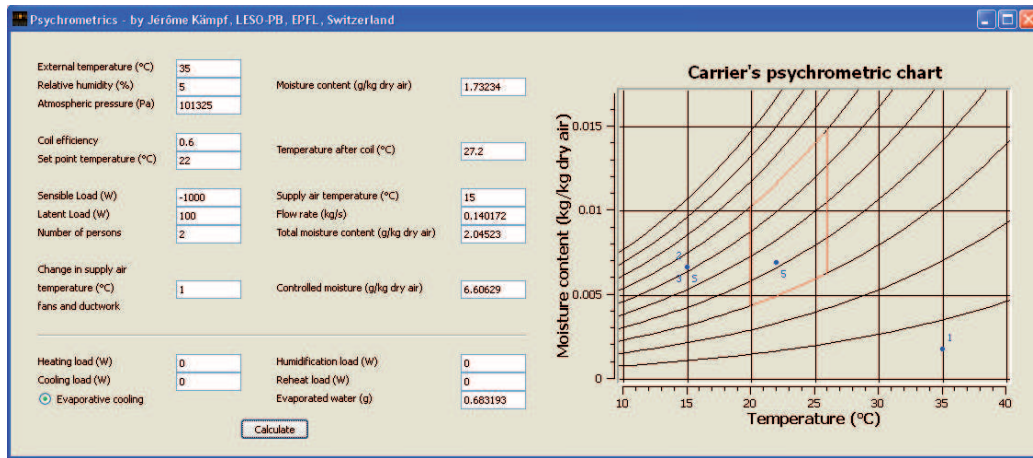
Figure 4.18: Evaporation cooling

is 35°C with a very low relative humidity of 5%. After the heat exchanger, spraying water in that air cools it down to 15°C, which is suitable for cooling the room.
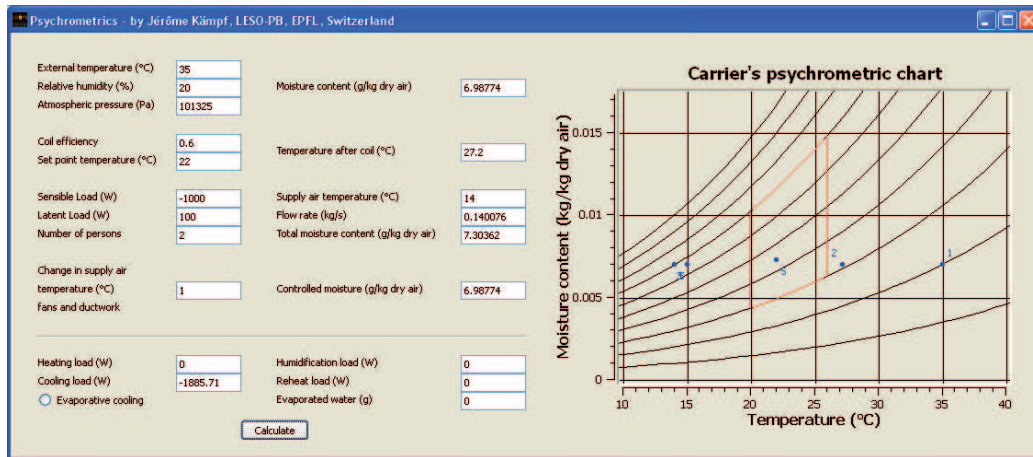
Figure 4.19: Cooling

Figure 4.19 shows a cooling case. The external air temperature is 35°C with a relative humidity of 20%. Its moisture content is suitable for the final temperature of 22°C to be in the comfort zone between 30% and 70% of relative humidity, provided some cooling. Figure 4.20 shows a cooling with incident
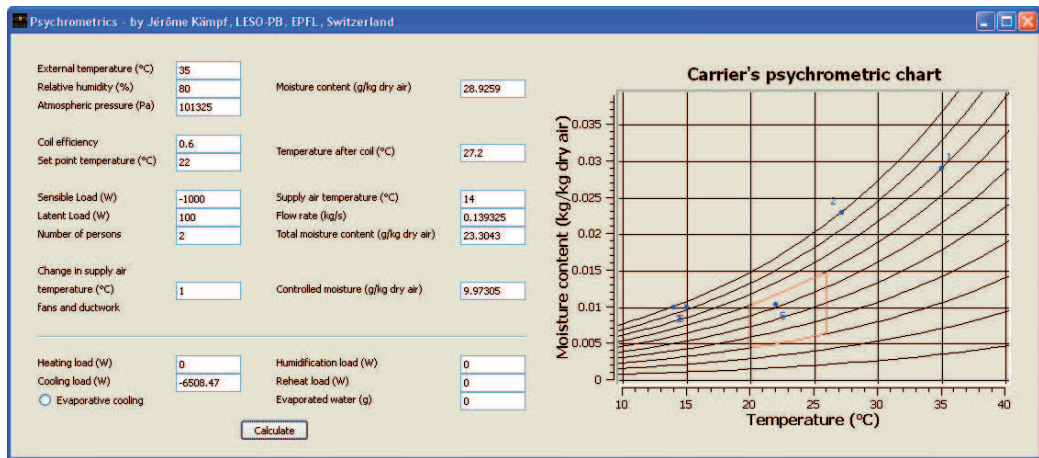
Figure 4.20: Cooling with incident dehumidification

dehumidification case. The external air temperature is 35°C with a very high relative humidity of 80%. When cooling the air condensation happens in the cooling coil, bringing dehumidification of the air.

4.3 Energy Conversion Systems

The Energy Conversion System (ECS) models implemented thus far have been chosen to represent the current most widely used devices to supply buildings' energy needs. In particular the work in this thesis has contributed models of the following:

Solar panels: Photovoltaic and Air/Water Heater

Wind Turbines

Boilers with different fuels

Heat Pumps

Cogeneration systems

Cogeneration systems combined with Heat Pumps

Once again our approach has been to develop models of the appropriate degree of complexity. They should be accurate enough for the task in hand without requiring excessive data input or computational resources.

4.3.1 Solar panel

Photovoltaic cells

The power output (in W) of a PV array with maximum power point tracking is given as:

$$P = A_C \cdot I_g \cdot \eta_{mp} \cdot \eta_e, \qquad (4.35)$$

where A_C is the array area (m^2), I_g is the global irradiance incident on the array (W/m^2), η_{mp} is the efficiency at maximum power point and η_e is the efficiency of power conditioning equipment. From [Duffie and Beckman, 1991, p.777] we have an efficiency drop of the PV panel due to a difference between the actual collector temperature T_c (°C) and the reference temperature at which the maximum power output was measured T_{ref} (°C):

$$\eta_{mp} = \eta_{mp,ref} + \mu_{P,mp} \cdot (T_c - T_{ref}), \qquad (4.36)$$

where $\eta_{mp,ref}$ is the reference efficiency and $\mu_{P,mp}$ is the maximum power point efficiency temperature coefficient. This latter can be approximated [Duffie and Beckman, 1991, p778] as:

$$\mu_{P,mp} = \eta_{mp,ref} \cdot \frac{\mu_{V_{oc}}}{V_{mp}}, \qquad (4.37)$$

where $\mu_{V_{oc}}$ is the temperature coefficient of voltage at open-circuit conditions (V/K) and V_{mp} the voltage at maximum power point (V).

The collector temperature T_c (°C) is deduced from the ambient air temperature T_a (°C) and the global irradiance incident on the panel I_g (W/m²):

$$T_c = T_a + \left(I_g \cdot \frac{\tau\alpha}{U_L} \right) \left(1 - \frac{\eta_{mp}}{\tau\alpha} \right), \tag{4.38}$$

with τ being the transmittance of any cover over the cells, α the fraction of the incident irradiance that is absorbed and U_L the total loss coefficient to the environment at ambient temperature T_a. Furthermore, Equation 4.38 can be further simplified by approximating $\frac{\eta_{mp}}{\tau\alpha}$ by $\frac{\eta_{mp}}{0.9}$.

Also in Equation 4.38, measurements of the cell temperature, ambient temperature and solar radiation can be used to determine $\frac{\tau\alpha}{U_L}$, which is assumed to be constant. Starting from standard operating conditions (SOC), one can use a measurement of the nominal operating cell temperature ($T_{c,NOCT}$) to compute:

$$\frac{\tau\alpha}{U_L} = \frac{T_{c,NOCT} - T_{a,SOC}}{I_{g,SOC}} \tag{4.39}$$

The SOC are defined as a solar irradiance of $I_{g,SOC}$=800 W/m², a wind speed of 1 m/s parallel to the array, an ambient temperature $T_{a,SOC}$ of 20°C and no load operation (open circuit).

Finally, substituting Equation 4.39 into 4.38 and reorganising the terms, we have the following expression for the efficiency at maximum power point:

$$\eta_{mp} = \eta_{mp,ref} \cdot \frac{1 + \frac{\mu_{V_{oc}}}{V_{mp}} \cdot \left(T_a + I_g \cdot \frac{T_{c,NOCT} - 20°C}{800\ W/m^2} - T_{ref} \right)}{1 + \eta_{mp,ref} \cdot I_g \cdot \frac{T_{c,NOCT} - 20°C}{800\ W/m^2} \cdot \frac{1}{0.9} \cdot \frac{\mu_{V_{oc}}}{V_{mp}}} \tag{4.40}$$

The reference maximum power point efficiency can be calculated from the maximum power point power (P_{mp}) and the panel area (A_c), taking into account the standard test conditions of a PV panel: a solar irradiance of 1000 W/m²:

$$\eta_{mp,ref} = \frac{P_{mp}}{A_c \cdot 1000\ W/m^2}. \tag{4.41}$$

Example The BP Solar SX-120S gives the following characteristics in the datasheet:

$P_{mp} = 120\ W$ $V_{mp} = 16.8\ V$ $\mu_{Voc} = $ -0.08 $V/°C$ $T_{ref} = 25\ °C$

$T_{c,NOCT} = 47\ °C$ $A_c = 1.07\ m^2$

Air/Water Thermal collectors

Most manufactures now use standard benchmarks to evaluate the performance of their thermal collectors. The European Certification (Solar Keymark www.solarkeymark.org) and American Certification (Solar Rating and Certification Corporation www.solar-rating.org) follow a similar approach, writing the heating power of a panel in the form:

$$P_{th} = A_C \cdot \left(\eta_0 \cdot I_g - a_1 \cdot (T_i - T_a) - a_2 \cdot (T_i - T_a)^2 \right), \qquad (4.42)$$

with A_C being the array area (m^2), I_g the global radiation incident on the array (W/m^2), η_0 the optical efficiency (transparent cover and absorber), a_1 the first order heat loss coefficient (W/(m^{2}K)), a_2 the second order heat loss coefficient (W/(m^{2}K^2)), T_i the mean fluid temperature (°C) and T_a the ambient temperature (°C).

Example The Conergy Aldo 240 get the following characteristics out of Keymak test:

$A_c = 2.244 \ m^2 \quad \eta_0 = 0.778 \quad a_1 = 3.59 \ \text{W/(m}^2\text{K)} \quad a_2 = 0.0096 \ \text{W/(m}^2\text{K}^2\text{)}$

4.3.2 Wind Turbine

Wind turbines manufacturers generally provide a graph of the output power as a function of the wind speed at the height of the turbine hub. This can be fitted by a polynomial function and used in conjunction with the wind speed ratio defined by Awbi [1991, p.64]. Knowing the terrain description around the meteorological station where wind speed measurements were recorded together with the height of these measurements, one can use the following relationship to establish the wind speed ν (m/s) at the wind turbine location:

$$\nu = \nu' \cdot \frac{\alpha \, (h/10)^\gamma}{\alpha' \, (h'/10)^{\gamma'}} \qquad (4.43)$$

where ν is the measured wind speed at the meteorological station (m/s), α and γ are parameters relating the terrain description around the wind turbine, α' and γ' are parameters relating the terrain description around the meteorological station, h is the height (m) of the wind turbine hub and h' is the height (m) at which the meteorological measurements were recorded. The experimentally determined parameters α and γ are given in Table 4.4. A terrain rose (sectors of approaching wind direction) can be edited for the site of interest, by supplying terrain coefficients for each wind direction sector. Moreover, the terrain coefficients are assumed to be rural for all directions

Terrain description	α	γ
Ocean or other body of water with at least 5km of unrestricted expanse	1.3	0.10
Flat terrain with some isolated obstacles (buildings or trees well separated from each other)	1.0	0.15
Rural area with low buildings, trees, etc..	0.85	0.20
Urban, industrial or forest areas	0.67	0.25
Centre of large city	0.47	0.35

Table 4.4: The parameters α and γ as a function of the terrain description

at the meteorological station. We can now calculate a corrected wind speed a the turbine height taking into consideration the local terrain conditions in any (discretised) approaching wind direction, and from this the corresponding power output of the wind turbine.

4.3.3   Boiler with different fuels

The thermal power output of a boiler is equal to:

$$P_{th} = P_{gross} \cdot \eta_{th}, \quad P_{gross} \in [0, P_{gross,max}], \qquad (4.44)$$

where P_{th} is the thermal output of the boiler (W), η_{th} is the thermal efficiency of the boiler, P_{gross} (W) the input power of the fuel and $P_{gross,max}$ (W) the maximum input power of the fuel (due to the boiler size).
In this, the boiler efficiency is considered as a constant (unless we have access to part load efficiency data, in which we may fit a polynomial function). The input power of the fuel is calculated using the Higher Heating Value (HHV), which includes the heat of condensation of water in the combustion products, as follows:

$$P_{gross} = \dot{m}_{fuel} \cdot HHV \cdot \eta_c, \qquad (4.45)$$

with $\dot{m}_{fuel}$ being the ideal mass of fuel combusted (kg/s), HHV the higher heating value of the fuel (J/kg) and η_c the combustion efficiency. Here again, the combustion efficiency is considered as a constant.

Example

A condensing boiler for a domestic house with a thermal power of 12 kW has a thermal efficiency of 0.96.

4.3.4 Heat pump

The thermal power output of a heat pump is equal to:

$$P_{th} = P_{el} \cdot \eta_{tech} \cdot \eta_{carnot}, \tag{4.46}$$

with P_{el} being the electric power consumption (W), η_{tech} the technical efficiency and η_{carnot} the carnot efficiency. The carnot efficiency is calculated as:

$$\eta_{carnot} = \frac{T_{target}}{T_{target} - T_{source}}, \tag{4.47}$$

with T_{target} being the target temperature (K) and T_{source} the source temperature (K). In the case of heating, the source temperature is lower than the target temperature (see first example), which leads to a positive carnot efficiency. In the case of cooling, the source temperature is higher than the target temperature (see second example), which leads to a negative carnot efficiency. The sign of the carnot efficiency describes how the energy is transferred in Equation 4.46.

Air source

When considering the outside ambient air as a source for the Heat Pump, we take into account its temperature given by the meteorological station as the source temperature. We further make the simplification that the source temperature is unaffected by thermal exchanges with the heat pump.

Ground source

When considering a ground temperature source, we can compute the soil temperature t_s (°C) at a certain depth z (m) using the equation [Labs, 1982]:

$$t_s = \bar{t} - \tilde{t} \cdot \exp\left(-z\sqrt{\frac{\pi}{365\alpha}}\right) \cdot \cos\left(\frac{2\pi}{365} \cdot \left(d - d' - \frac{z}{2}\sqrt{\frac{365}{\pi\alpha}}\right)\right), \tag{4.48}$$

where $\bar{t}$ is the annual mean temperature (°C), $\tilde{t}$ is the amplitude in mean daily temperature swing (°C), α is the soil diffusivity (m²/day), d is the day and d' is the day at which a minimum mean daily temperature occurred. Likewise for the air source, we make the simplification that the ground temperature is unaffected by thermal exchanges with the heat pump. Looking more closely at this equation, we can see that it is a superposition of a decaying exponential with depth and a cosine with the day phase shifted by the soil time lag at a given depth. When using fluid pipes horizontally at a defined depth, one

can use this equation without modifications. However, when the pipes are vertical, Equation 4.48 is integrated over the pipe depth in order to compute an average soil temperature $\bar{t}_s$:

$$\bar{t}_s = \frac{1}{d_{max} - d_{min}} \int_{d_{min}}^{d_{max}} t_s(z)dz \qquad (4.49)$$

The analytical form of this expression is not given here, but can be readily obtained using Mathematica for example, or found in Mazarron and Canas [2008].

Examples

The technical efficiency can be determined from manufacturers' data using the reference operating temperatures and the given COP:

$$\eta_{tech} = \frac{COP}{|\eta_{carnot}|} = COP \cdot \frac{|T_{target} - T_{source}|}{T_{target}} \qquad (4.50)$$

The technical efficiency is considered as a constant for a specific heat pump. The air heat pump Vitocal 350-A from Viessmann has a peak thermal power of 10.6 kW and a COP of 3.3 at the measurement point A2/W35 (EN 255), in which the air input temperature is 2°C and the hot water output temperature is 35°C. This leads to a technical efficiency of 0.35.
A classic inverter heat pump MSZ-HC25VA from Mitsubishi Electric, which is wall mounted, has a peak cooling power of 2.5 kW and a COP of 3.64 at nominal conditions. The nominal conditions are 35°C for the air input temperature and 19°C for the air output temperature, which leads to a technical efficiency of 0.2.

4.3.5   Cogeneration

The thermal power output P_{th} (in W) and the electric power output P_{el} (in W) of a cogeneration device are equal to:

$$P_{th} = P_{gross} \cdot \eta_{th} \qquad (4.51)$$

$$P_{el} = P_{gross} \cdot \eta_{el}, \qquad P_{gross} \in [0, P_{gross,max}], \qquad (4.52)$$

where η_{th} and η_{el} are respectively the thermal and electric efficiencies of the device, P_{gross} (W) is the input power of the fuel and $P_{gross,max}$ (W) is the maximum input power of the fuel (due to the engine size). Here again, the efficiencies are considered constant with engine load, unless performance curves are available, in which case they can be fitted with a polynomial function. When using fuel cells, the operation starts only when a fraction α of P_{th} is needed (the device is driven by heat demand).

Example

The domestic natural gas engine Dachs G 5.5 with condenser from Senertec has a peak thermal power of 14.8 kW, an electric efficiency of 0.27 and a thermal efficiency of 0.72.

4.3.6 Cogeneration combined with Heat Pump

In this configuration, the electricity produced by the cogeneration devices is used solely by a heat pump. The combination of the different efficiencies makes this configuration interesting compared to a standard boiler. The thermal power P_{th} (in W) can be written as the combination of cogeneration and heat pump equations:

$$P_{th} = P_{gross} \cdot (\eta_{th} + \eta_{el} \cdot \eta_{tech} \cdot \eta_{carnot}).$$

$$(4.53)$$

The different terms of the preceding equation can be found in the cogeneration and heat pump sub-sections. This configuration of devices is not standard in practice, but rather an idealised way of benefitting from the combined efficiencies of the cogeneration and heat pump unit.
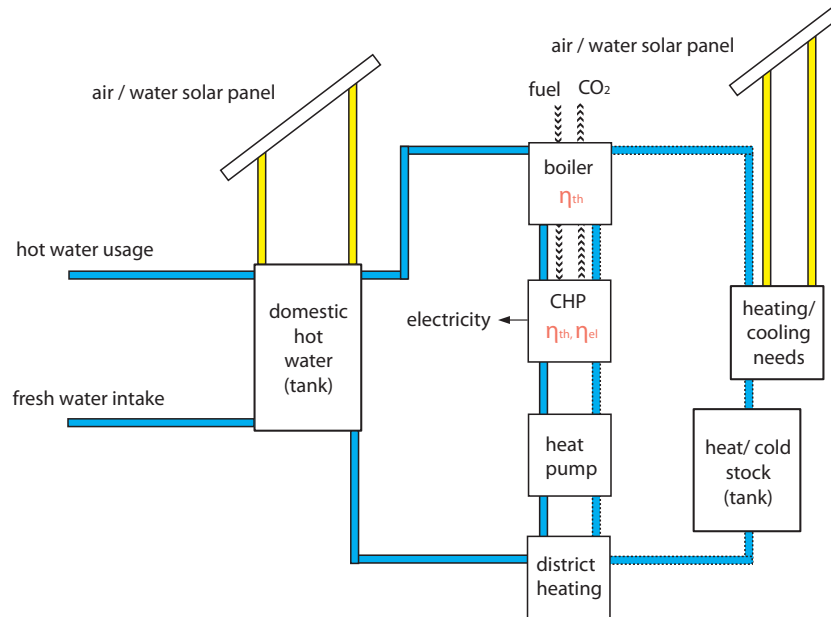
Figure 4.21: The building energy network with potential energy conversion systems

4.4   Tank Model

The first and second sections of this chapter deal principally with the evaluation of buildings' heating and cooling demands. The third section concerns the modelling of machines that can provide heating, or cooling power. Between these, we need a model that will connect the thermal producer with the thermal consumer, for this we use a tank model.

The Tank model takes into account the storage of heat for domestic hot water (DHW) and of high or low grade heat for heating or cooling purpose. Figure 4.21 shows the representation of one possible system configuration. Different energy conversion systems are represented on the diagram, but they may not all necessarily be present at the same time in a building or district energy centre.

The two types of tank can be represented in a very general way by the same equation, in which we assume the fluid to have a uniform temperature. We consider that solar thermal collectors incorporate suitable controls to prevent the tank fluid from overheating in summer and that the limiting temperature can be set. We also support the inclusion within our tanks of a phase change material (PCM) for more efficient heat storage in a constrained volume.

4.4.1 The energy conservation equation

From consideration once again of the energy conservation equation in the fluid volume of the tank, we have that:

$$
\begin{aligned}
\frac{\partial H_{pcm}}{\partial t} + \rho V Cp \frac{dT(t)}{dt} \; = \; & P_{sp} + P_p - \rho \dot{V} Cp(T(t) - T_{inlet}) - \\
& U \cdot A \cdot (T(t) - T_{amb}),
\end{aligned} \tag{4.54}
$$

with

H_{pcm} the enthalpy of phase change material in the tank (J),

ρ the fluid density (kg/m^3),

V the volume of fluid in the tank (kg),

Cp the specific heat capacity of the water in the tank (J/(kg· K)),

$T(t)$ the time dependant temperature of the fluid tank (°C),

P_{sp} the power given by the solar panel (W),

P_p the power given by the main energy conversion system (W),

$\dot{V}$ the fluid usage or loss (m^3/s),

T_{inlet} the fresh fluid intake temperature (°C),

U the conductance of the tank (W/(m^2·K)),

A the surface area of the tank (m^2) and

T_{amb} the ambient temperature outside the tank (°C).

In the heat/cold store the water leaking from the system are neglected, and therefore the term containing water usage $\dot{V}$ drops. Please note that in this approach only one temperature node is considered in the tank and therefore we assume that the water is perfectly mixed and not stratified.

Without phase change material

If phase change material is not present ($H_{pcm} = 0$), Equation 4.54 can be solved analytically with a time span comprised between two time steps of the water use model (the smallest time step among the variables). The solution is as follow:

$$
T(t) = \frac{1}{Cp \cdot \dot{V} \cdot \rho + \phi} \Big(\ P_p + P_{up} + Cp \cdot T_{inlet} \cdot \dot{V} \cdot \rho + T_{amb} \cdot \phi -
$$
$$
e^{\left(-\frac{t(Cp \cdot \dot{V} \cdot \rho + \phi)}{Cp \cdot \dot{V} \cdot \rho}\right)} \cdot \Big(P_p + P_{sp} - \tag{4.55}
$$
$$
Cp \cdot \dot{V} \cdot \rho \cdot (T0 - T_{inlet}) - \phi \cdot (T_0 - T_{amb}) \Big) \Big),
$$

with T_0 being the initial temperature (°C) and $\phi = U \cdot S$ the total conductance (W/K). Equation 4.55 may also be rewritten to estimate the energy needs P_p to reach a defined temperature T after a time t. The two ways of using this equation are represented in Figure 4.22.
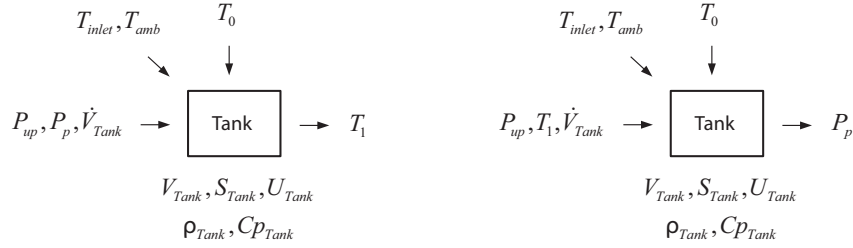
Figure 4.22: The two procedures for obtaining output of the tank model

With phase change material

If phase change material is present, its enthalpy can be written:

$$
H_{pcm}(T) = \int_0^T m_{pcm} Cp_{pcm}(x) dx, \tag{4.56}
$$

where m_{pcm} is the mass (kg) of the phase change material and $Cp_{pcm}(T)$ is its specific heat capacity (J/(kg·K)). The partial derivative of the enthalpy with respect to time, that is needed in Equation 4.54, can be written:

$$
\frac{\partial H_{pcm}}{\partial t} = \frac{\partial H_{pcm}(T)}{\partial T} \frac{\partial T}{\partial t} = m_{pcm} Cp_{pcm}(T) \frac{dT}{dt}. \tag{4.57}
$$

In the previous equation, $Cp_{pcm}(T)$ is approximated using an effective heat capacity [Neeper, 2000, Heim and Clarke, 2003, 2004, Darkwa and O'Callaghan, 2006]:

$$Cp_{pcm}(T) = C_s + \frac{L_h}{\sigma\sqrt{2\pi}} \cdot e^{\left(-\frac{1}{2}\left(\frac{T-T_m}{\sigma}\right)^2\right)}, \qquad (4.58)$$

in which C_s is the sensible heat capacity (J/(kg·K)), L_h is the latent heat capacity (J/(kg·K)), σ is the width of the phase change zone (K) and T_m is the phase change temperature (K). For this Gaussian approximation, we consider identical properties for the solid and liquid phases. Moreover, from the properties of the Gaussian function, σ represents the temperature range in which 84% of the phase change appears. This formulation has the advantage of being a continuous and differentiable function.

The phase change material characteristics (C_s, L_h, σ and T_m) can be found from previously published studies such as these due to Ibáñez et al. [2006] and Verma et al. [2008].

Using 4.58 and substituting 4.57 into 4.54 leads us to a first order differential equation with a coefficient that has a non-linear behaviour (due to Cp_{pcm}). It is solved using the explicit Euler scheme, with a time step smaller than the stability criteria (Fourier number $F \leq \frac{1}{2}$, see Kuznik et al. [2008]).

$$T^{n+1} = T^n + \Delta t \cdot \frac{P_p + P_{up} - \phi \cdot (T^n - T_a) - \rho V Cp \cdot (T^n - T_{inlet})}{\rho V Cp + m_{pcm} Cp_{pcm}(T^n)} \quad (4.59)$$

The energy demands to reach a temperature T_1 after a time t_1, which is considered to be a multiple of the time step, is evaluated at the first time step using Equation 4.59 to reach T_1, and then in order to maintain that temperature, we account for losses occurring during the following time steps. Here again, the two ways of using this equation are represented in Figure 4.22.

4.4.2 Example

Figure 4.23 shows an example of a temperature drop in a heat store of 200 litres at an initial temperature of 80°C. The water usage is equal to 86.4 litres of hot water during 4 hours, and the temperature of the fresh water inlet is 5°C. The tank's ambient temperature is 10°C. The losses are expressed in a simplified fashion, taking into account a factor ϕ equal to 20 W/K. When the PCM is present, it has a mass of 100 kg, a sensible heat capacity of 2500 J/(kg·K), a latent heat capacity of 200 kJ/(kg·K), a width of the phase change zone of 2.5°C and a phase change temperature of 58°. The illustration is provided to observe the effect of introducing a PCM into a water tank on the mean tank temperature.
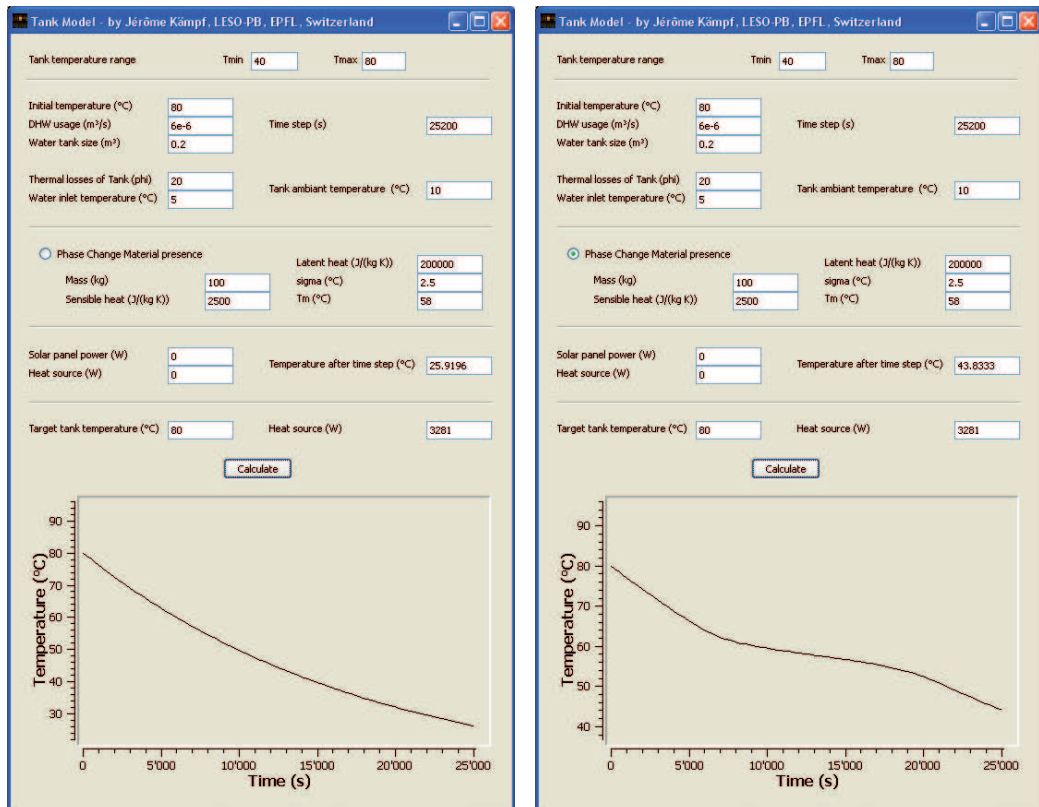
Figure 4.23: Example without (on the left) and with phase change material (on the right)

4.5 The implementation

The different models presented in the former sections were programmed using C++. This programming language has the advantage of being fast in execution and is object oriented. The structure of the different classes in the solver is very much like the structure of the potential simulated scene. Figure 4.24 shows the main classes and the links between them. Figure 4.24 can be subdivided into blocs according to to the different models that populate the solver of CitySim. At the top right corner, objects dependent on the *Scene* class are part of the simplified radiosity algorithm. At the lower right corner, classes deriving from the *EnergyConversionSystem* class are energy providers for *Building* or *District*. At the left part of the figure, the scene is decomposed into buildings that are themselves decomposed into surfaces. Each surface can be a ground, that participates in radiation exchange but does not enclose a shelter (note that other objects that shade our modelled buildings may also be represented in this way), or a Wall that is composed of different layers each having radiant and thermophysical properties, or finally a Roof, that is defined by a U-value. All Wall/Roof surfaces may have a glazing ratio and a corresponding U-value and G-value. Roofs can also be equipped with Thermal or Photovoltaic panels (this feature will be extended to other surfaces in the future). The *Model* class contains the thermal model and the HVAC model. The structure of the solver is very modular, and will be refined as further models are added.

When the solver starts, the scene to simulate, which is described in an XML file format is given as an argument to the creator of the *Xmlscene* class, which in turn creates as many objects as needed for the information it contains. The main routine then runs the *simulate()* method, which simulates on an hourly basis the energy fluxes within the scene. The next section describes this hourly simulation procedure.

4.5.1 The hourly simulation: predictor-corrector

For each hour in the year, the shortwave and longwave radiation are computed for all surfaces in the scene. The longwave radiation calculation takes the surface temperature from the previous hour (of the buildings or the ground) in order to determine the corresponding radiant exchanges. A loop on all buildings is made, in which the sensible heating or cooling demands are established using the thermal model. Depending on the presence of an HVAC system, the HVAC energy demands are then computed. A control procedure of the energy conversion systems is then invoked according to the demand, using the temperature prediction of the tank model (see next Section). The

Figure 4.24: The solver of CitySim with the different classes involved

available energy is then fed back to the HVAC model if present and the corresponding energy is supplied to the thermal model in order to predict the building's temperature. This predictor-corrector approach is shown schematically in Figure 4.25.
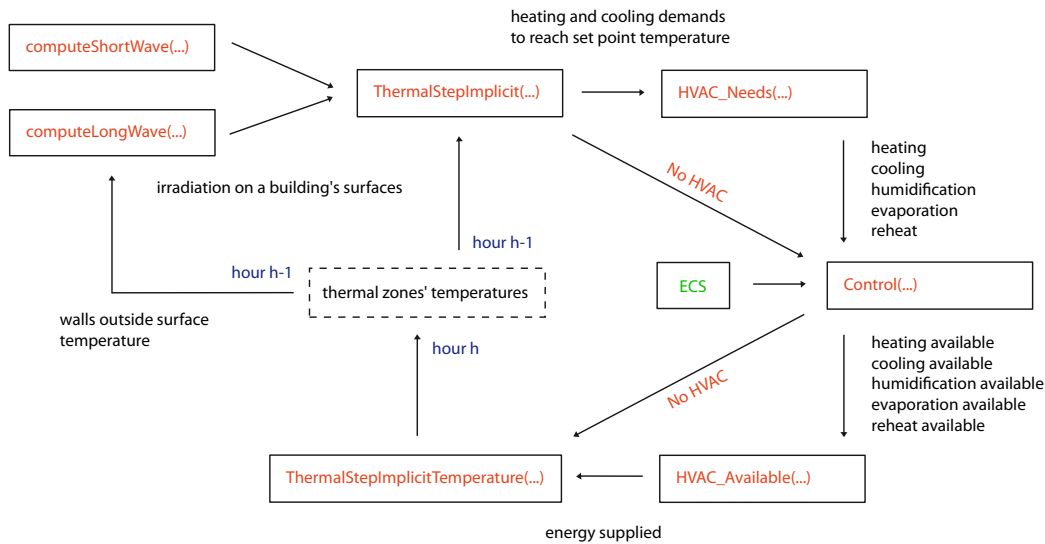
Figure 4.25: The hourly simulation, with the predictor-corrector approach for the determination of the zone's temperature.

Control strategy

The control strategy tries to satisfy the buildings' energy demands according to the energy conversion systems connected. A fluid tank is always considered present between the thermal demands and providers and the control strategy will depend on the temperature of the fluid in the tank. Indeed, the temperature of the tank must remain between an upper and lower limit. For the domestic hot water and the heating store, when the estimated temperature after a fixed time step is lower than the lower limit, it is returned to the upper limit by injecting the required amount of heat into the tank. For the cold store, the situation is reversed; when the estimated temperature after a fixed time step is higher than the upper limit, it is returned to the lower limit by extracting the required amount of heat. Figure 4.26 summarizes the procedure. Please note that this ideal control strategy is non-predictive.
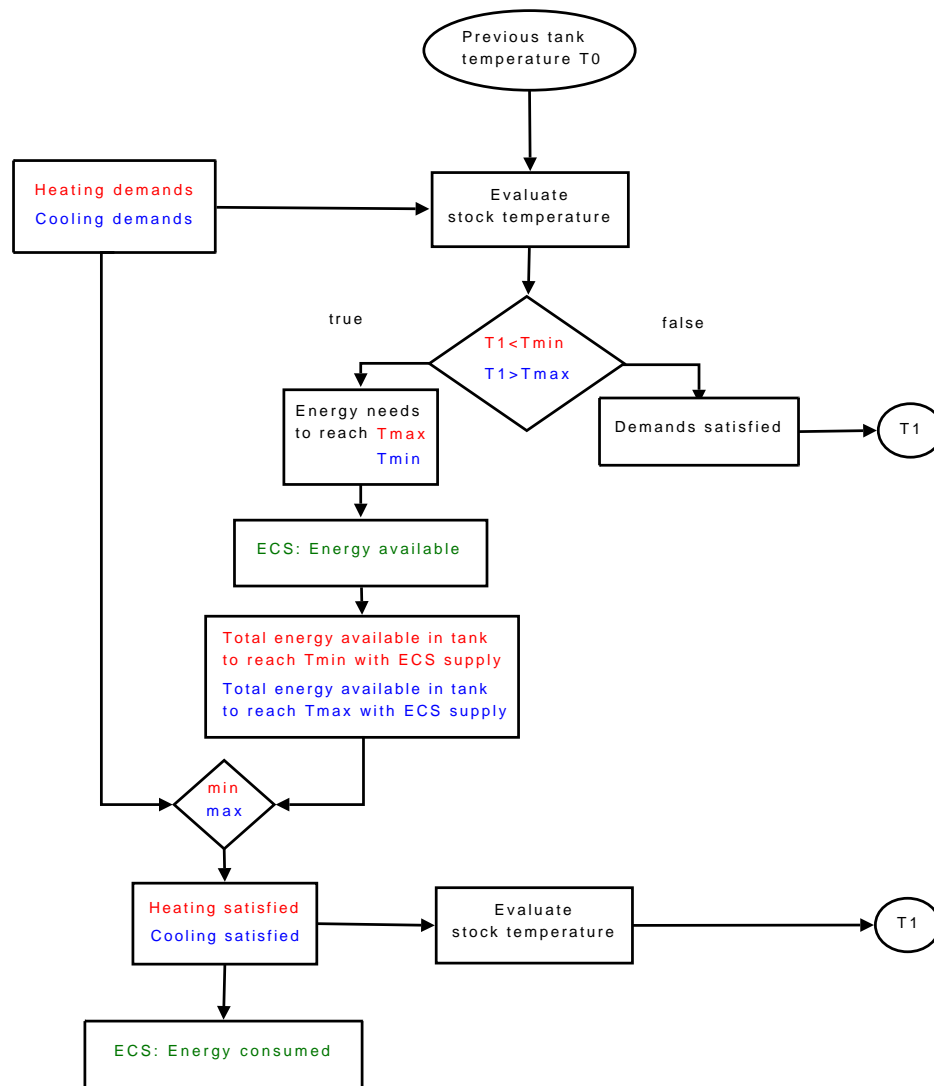
Figure 4.26: Control strategies for the heat store (in red) and cold store (in blue)

4.6 Conclusion

The work involved in this thesis combined with a previously developed radiation model represents a good start for the development of a holistic tool for simulating energy fluxes at the urban scale. Its modular structure supports the straightforward addition of future models to the existing ones. This solver can also be improved in the future by, for example:

- Parallelising the code, allowing for shortwave and longwave exchanges to be run at the same time and for the radiant scene to be subdivided and elements run in parallel. Thermally independent buildings could also be evaluated in parallel.

- Using the computer hardware resources in an efficient way by sharing tasks between CPUs and GPUs.

- Implementing an extension of the thermal model using three nodes to improve the dynamic behaviour of buildings with two heavy parts in the walls.

- Validating the thermal model using standard tests such as BESTEST [Neymark et al., 2002].

- Investigating adapted numerical methods to solve for rapidly changing phenomena, such as phase change materials integrated into walls and advective exchanges due to window openings.

- Developing a district resource (energy and matter) centre to resolve for locally centralised resource supply to buildings and potential resource exchanges between buildings.

- We have not performed any dedicated validation test on the performance regression/empirical models since the data on which they are based already describe well their bulk characteristics. There may be a case however for the validity of the Tank Model, which is assumed to be a perfectly mixed single or two phase medium.

Chapter 5

Optimisation of urban energy performance

> The part of the thesis presenting the Case Study and the Minimisation of on-site energy demand was published in the proceedings of the International Building Performance Simulation Conference held in Glasgow (UK) in July 2009 [Kämpf and Robinson, 2009c].

The work described in this thesis culminates in the modelling and optimisation of buildings' energy performance at the urban scale. For this, we have selected the district of Matthäus in Basel (Switzerland), for which the 3D information of the whole district is available to us; likewise a subset of the national census data for the year 2000 and the results from a recent visual field survey of the district. From the CENSUS 2000, we have the construction year, the last renovation date, the heating fuel used and the number of inhabitants for each building. From the district visual survey we have observations of the glazing ratio, the state of the facades backed up by photographs. With the help of renovation specialists (EPIQR Rénovation, Lausanne) we have linked the construction year / renovation date and the physical properties of the walls, roofs and windows needed by CitySim to simulate the buildings' thermal performance (see Appendix A). Finally, we have meteorological data measured at a weather station in Basel, which is available as part of the software Meteonorm. As a first application of the optimisation methodology, we decided to use only a part of the Matthäus district.

5.1 Case Study

For the application of our proposed methodolody to optimise urban energy flows, we have selected a block of buildings within Matthäus located between Matthäusstrasse, Müllheimerstrasse, Klybeckstrasse and Feldbergstrasse (see Figure 5.1). This block consists of 26 individual buildings, with construction

Figure 5.1: The part of the Matthäus district used for the case-study

years ranging from the beginning of the 19th century to the 1970's; with some buildings having been renovated between the 1970's and the 1990's. The buildings have central heating systems, but are not equipped with air-conditioning systems.

The chosen part of the district is subdivided administratively by the city authorities into three zones as shown in Figure 5.2. The Schutzzone is a historical part of the city that is protected, so that we are not allowed to change the walls, the roofs and the fire walls. The Schonzone is less restrictive: only the external appearance of the building should not be modified. The remaining Zone 5a is not historical and may be modified under the approbation of the authorities.

5.1.1 Data extrapolation

With the geometric information available to us, we are able to create an XML description file that will be used by the solver of CitySim, which is then completed by the physical properties of each building. Each building in the Census and visual survey have a unique identification number that allows us to make a link between the physical street address and the building characteristics. In Figure 5.2 we have superimposed the identification number
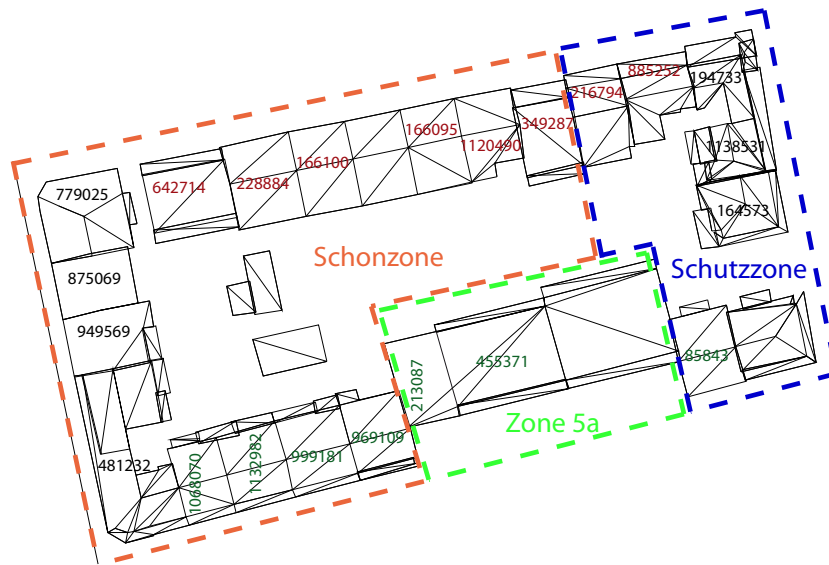
Figure 5.2: The three administrative zones in the selected group of buildings

on each of the buildings in our case study site. Unfortunately, the information set was not complete for all buildings present in the sector; indeed we had nothing more than the 3D information for 4 buildings out of the 26. For this, we examined the pictures taken during the visual survey and estimated their characteristics. However, for subsequent studies we have developed a procedure to infer the missing physical properties from the data available to us for other buildings, provided of course that their number is statistically significant. In Matthäus the Census and the visual field survey data are available for a sample in excess of 1000 buildings. Using this data we derive a probability of occurrence of each value that a given variable may take and from this define a cumulative distribution function (CDF). We then draw a random number and, from the CDF, we determine which value of our variable this corresponds to. Figure 5.3 shows an example of the procedure for the data available in the CENSUS 2000.

5.1.2   Simulation without occupants

By way of example, Figure 5.4 shows the internal building temperature and the delivered heating energy to maintain a temperature at or above 21°C for the building identified by the number 969109 (see Figure 5.2 to locate it in the group of buildings). The solver calculations take into account the obstructions and inter-reflections for the shortwave and longwave energy fluxes
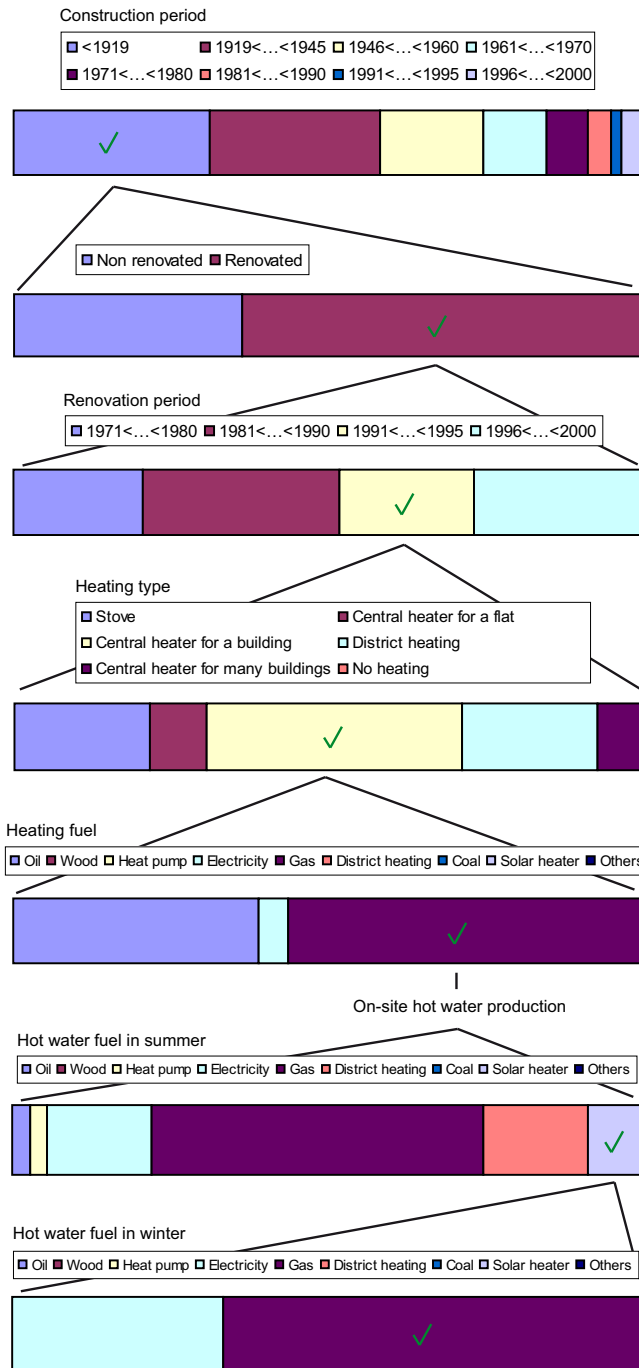
Figure 5.3: An example of the Monte-Carlo procedure of inferring missing data from a large sample
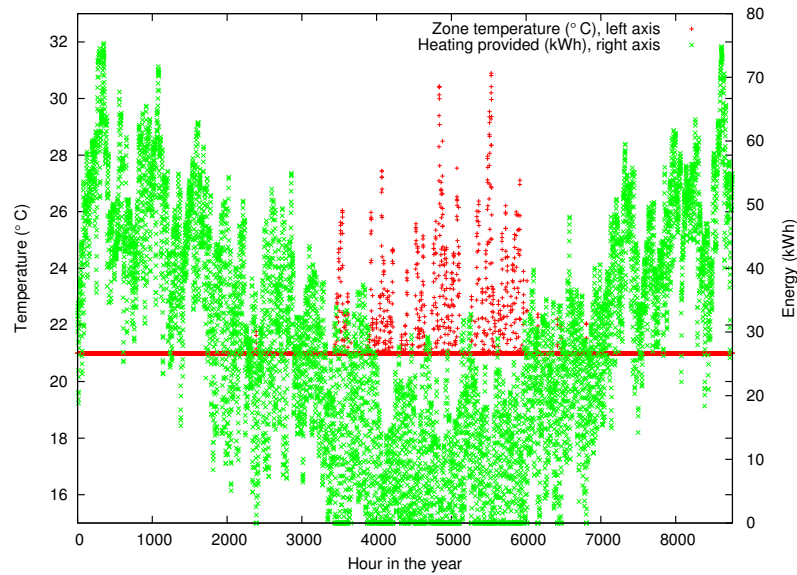
Figure 5.4: Simulation results with the solver of CitySim for building identified by number 969109 without occupants, shown for a whole year

on the adjacent buildings. However, we make the assumption that buildings in contact with each other do not exchange heat at this boundary (adiabatic boundary conditions). A further simplification is that the buildings are unoccupied so that occupants' interactions with blinds and windows to control excess heat gains are ignored. Under these assumptions building 969109 spent 68 hours above 26°C. The group of buildings was provided with 4.88 GWh for heating purposes. As an indication of the cooling load the combined cooling degree-hours, with respect to a reference of 26°C was 35971. On average over the group of buildings, (220±433) hours were spent above 26°C during the year, corresponding to (1383±4734) degree-hours.

5.1.3   Simulation with occupants and blinds control

To demonstrate the impact of occupants' presence and interactions with blinds we simulate the same group of buildings, but this time taking into account occupants' metabolic sensible heat gains (assumed to be perfectly convective) and the deterministic control of blinds. The number of occupants is available to us from the CENSUS 2000. After [Jones, 2000, p.201] we assume that, when present, each occupant emits 90 W sensible heat. For these residential buildings we furthermore assume that occupants are present

outside of standard working hours, so that on weekdays, people are at home until 7am, from 12am to 1pm, and from 6pm in the evening; on Saturdays, people are at home until 10 am, from 12 am to 2pm, and from 5 pm in the afternoon; on Sundays, people are at home until 10am, from 12am to 2pm, and from 4pm in the afternoon.

A simplistic blind control model was implemented, in which the unshaded blind fraction is a function of the irradiance incident on the facade. After Wienold [2007], the Automatic cut-off with fixed height strategy is represented as follows: the blinds are lowered completely if the facade irradiance exceeds 150 W/m^2, and are retracted if this falls below 50 W/m^2. This strategy is implemented using a logit function, in which the unshaded blind fraction f_u is given as follow:

$$f_u = \frac{1}{1 + e^{\lambda(I_f - 100)}}, \tag{5.1}$$

where I_f is the facade irradiance (W/m^2) and λ the logit scale factor, taken as 0.2. This function allows for a smooth transition between the open and closed states of the blinds.
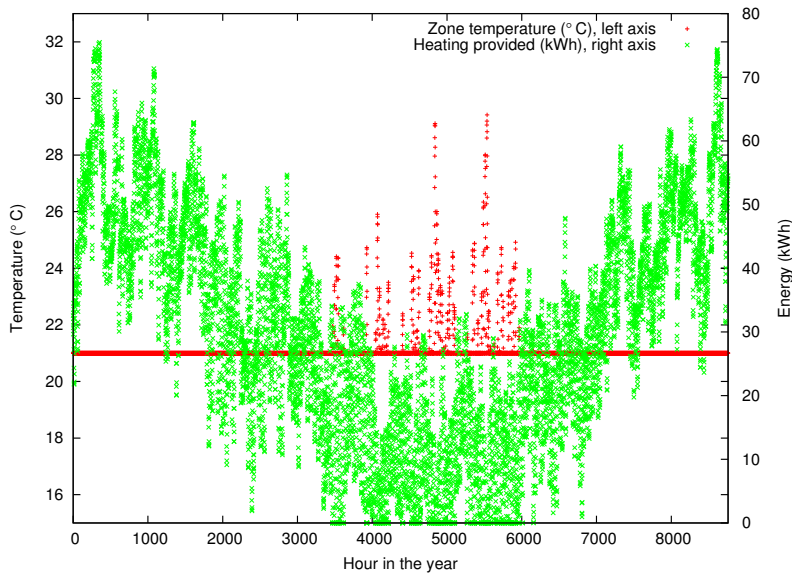
Figure 5.5: Simulation results with the solver of CitySim for building identified by number 969109 with occupants and blinds' control, shown for a whole year

As before, Figure 5.5 shows the internal temperature and heating energy

demand for building 969109 (see Figure 5.2). This building now spends only 28 hours above 26°C, although the overall heating energy demand of the group of buildings has increased to 5.07 GWh (+4%). This is because the simple blind control strategy does not differentiate between useful (to offset heating demands) and unuseful (to prevent overheating) solar gains. However, this strategy does emulate occupants' tendency to lower the blinds to avoid glare even in winter. The buildings' cooling degree-hours has reduced to 1694, which is a dramatic change compared to the test without blind control. On average the buildings in our group spent (37±61) hours above 26°C during the year, which corresponds to an average (65±130) degree-hours.

5.1.4 Simulation with occupants, blinds control and window openings

In addition to occupants' presence and blind control described above, a deterministic window opening strategy was taken from Beausoleil-Morrison [2009], in which the windows are open if $T_a > T_{min} + 1°C$ and $T_a - T_{ext} > 1°C$, where T_a is the internal air temperature (°C), T_{ext} is the outside air temperature (°C) and T_{min} is the minimum allowed air temperature (°C) for the heating calculation. When the windows are open, a ventilation rate n_{vent} (h^{-1}) (see Section 4.1.5, Equation 4.19) is considered between the outside air node and the inside air node. The ventilation rate is approximated using the following logit function [Haldi and Robinson, 2009]:

$$n_{vent} = n_{vent,max} \cdot \frac{\exp(1.459 + 0.1448 \cdot T_{ext} - 0.1814 \cdot T_a)}{1 + \exp(1.459 + 0.1448 \cdot T_{ext} - 0.1814 \cdot T_a)}, \qquad (5.2)$$

with $n_{vent,max}$ the maximum ventilation rate (h^{-1}) considered as an average over the simulation time step of one hour. From one of ESP-r's Example Models ("the office portion"), we have taken $n_{vent,max} = 2$ h^{-1}.

Figure 5.6 shows the internal temperature, the outdoor temperature, the ideal heating demand and the ventilation rate for building 349287 (see Figure 5.2), day 147, which corresponds to the 28th May. We have chosen to change the building on which we put the focus, as this additional strategy does not bring significant difference for building 969109.

During the night, some heat is provided to the zone to maintain a temperature of 21°C. In the morning, both the outdoor and zone temperature increase, but their difference remains less than 1°C, resulting in zero ventilation. In the afternoon, the zone temperature exceeds the outdoor air temperature by more than 1°C, resulting in appreciable ventilation rate to reduce overheating risk. In the evening, when the temperature is below 22°C, the ventilation
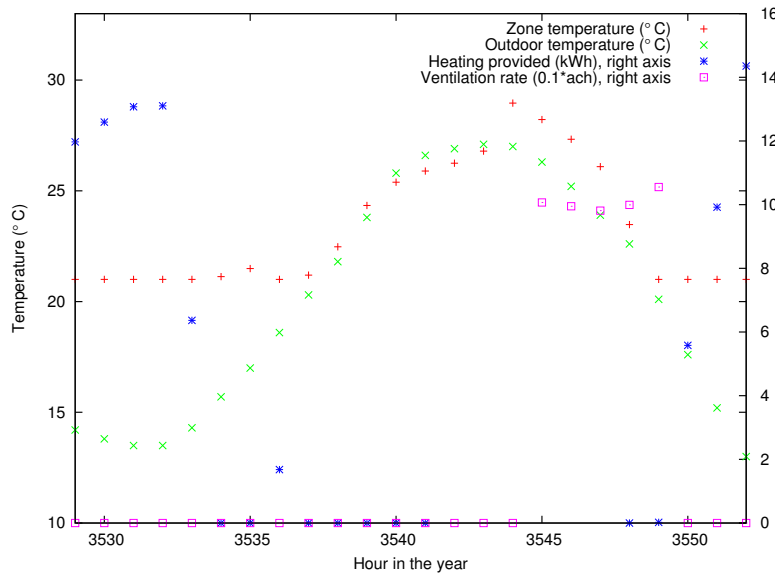
Figure 5.6: Simulation results with the solver of CitySim for building identified by number 349287 with occupants, blinds' control and window openings, shown for the 147th day of the year (28th May)

rate is zero again. Please note however that the ventilation rate is controlled using the zone temperature from the previous time step.

We have selected this building as the windows opening strategy is most effective, indeed it reduces the degree-hours above 26°C from 535 (without windows opening) to 423 (-21%). Regarding the group of buildings, the total heating energy demand is still 5.07 GWh, but the estimated cooling load is now reduced to 1512 degree-hours (11% reduction compared to the strategy without window openings). On average the group of buildings spent (34±52) hours were spent above 26°C during the year, which corresponds to an average (58±106) degree-hours.

Different values for $n_{vent,max}$ were tested, such as 5 and 10 h^{-1}, but, whilst these further reduced overheating risks, they also increase the heating load. Indeed, during spring and autumn the ventilation rate provides too much cooling, creating a necessity for heating. However this conflict may be avoided by reducing the simulation time step, say to 5 minutes.

5.1.5   Conclusion

CitySim allows us to simulate a group of buildings, in a manner that is sensitive to the urban context, taking into account the shortwave and longwave exchanges between the buildings. In this study, we have taken 26 buildings in the Matthäus district of Basel (Switzerland), and completed their physical characteristics for a simulation with CitySim. The heating energy requirements were calculated, along with the cooling degree-hours above 26°. The performance of a base case (unoccupied) model was compared with other models in which occupants' presence and behaviour is represented; in particular with respect to blind control and window opening. Using simple deterministic strategies, we showed that cooling loads in the simulated group of buildings can be dramatically reduced to the extent that with temperatures exceeding 26°C for only 34 hours a year the installation of air-conditioning units is not justified. We suspect that a more realistic windows opening model with a reduced time step (of say 5 minutes) would diminish this overheating risk.

5.2 Minimisation of on-site energy demand

The first optimisation study with CitySim is performed on the group of 26 buildings in the Matthäus district as described in the former section, considering the buildings empty from occupants and with no blind control[1].

5.2.1 Parameterisation

Of the vast parameter space that can be explored at the city scale, we have defined a sub-parameter space for this study. In this the following characteristics can be changed:

- glazing ratio (fraction of the facade that is glazed)

- window U-Value

- position of the insulation of the walls (internal or external)

- wall insulation thickness

Note that the glazing G-Value is held constant at 0.7. For this preliminary exercise we also limit ourselves to the simulation of energy demand, so that energy conversion systems are also not considered.

From the sub-parameter space of urban variables that was chosen for this study we apply constraints of the allowed changes that can be made within the three administrative zones in Matthäus (see Figure 5.2). In the Schutzzone we can improve the windows by adding a second frame inside the building. In the Schonzone, we can improve the windows and add internal wall insulation, as these modifications are not visible from outside. Finally in Zone 5a, we can change the windows and even add external wall insulation (which tends to perform better than internal insulation).

Table 5.1 shows the remaining parameters after taking into account their constraints. We have clustered the buildings by construction date (as in the dwelling classification system of Gadsden et al. [2003]), according to the physical properties of the walls, windows and roofs. Additional insulation of up to 12 cm can be placed on the inside of the walls for the Schonzone or on the outside of the walls for the Zone 5a. The windows' U-values may vary from the original single glazed units to more recent double glazing with a low emissivity coating. Buildings' glazing ratios are considered to be the same on all facades, but between buildings this may vary from a somewhat minimal ratio to being almost fully glazed.

---

[1]For this preliminary study, the behavioural models had not yet been implemented.

Table 5.1: The thirteen parameters for the group of buildings in Matthäus

Group	Parameter description	Symbol and Domain
Schonzone built <1919 (14 buildings)	Walls internal insulation (cm) Windows U-Value (W/(m²K))	$x_1 \in [0,12]$ $x_2 \in [1.5,6]$
Schonzone built '46 until '60 (1 building)	Walls internal insulation (cm) Windows U-Value (W/(m²K))	$x_3 \in [0,12]$ $x_4 \in [1.5,6]$
Schonzone built '61 until '70 (1 building)	Walls internal insulation (cm) Windows U-Value (W/(m²K))	$x_5 \in [0,12]$ $x_6 \in [1.5,6]$
Schutzzone built <1919 (7 buildings)	Windows U-Value (W/(m²K))	$x_7 \in [1.5,6]$
Zone 5a built '61 until '70 (2 buildings)	Walls external insulation (cm) Windows U-value (W/(m²K)) Glazing ratio	$x_8 \in [0,12]$ $x_9 \in [1.5,6]$ $x_{10} \in [0.1,1[$
Zone 5a built '71 until '80 (1 building)	Walls external insulation (cm) Windows U-value (W/(m²K)) Glazing ratio	$x_{11} \in [0,12]$ $x_{12} \in [1.5,6]$ $x_{13} \in [0.1,1[$

5.2.2 Objective function

The objective function used in the optimisation is the sum of the ideal heating and cooling demands (assuming that both are required, or that overheating risk - indicated by cooling energy demand - is to be minimised) for the group of simulated buildings for an average year. The heating set point is assumed to be 21°C and that for cooling to be 26°C. Each evaluation for a given combination of the available parameters takes about 5 minutes on a machine with an Opteron 2.3GHz processor and 4 GB RAM. In total we have 13 parameters, which is convenient for a number of evaluations ranging between 3000 and 6000 and we assume that the objective function's response is similar to the Ackley or Rastrigin benchmark functions.

5.2.3 Results

After about 3000 function evaluations (or runs of CitySim), we noticed a plateau in the objective function (see Figure 5.7). Moreover, after around 5000 evaluations we notice that there are less evaluations for each run of the CMA-ES. This is due to the usage of a cache that stores the evaluation of individuals and so avoids their re-evaluation. The EA seems to have found a stable optimum in the aggregate ideal heating and cooling demands of the 26 buildings. In its current state the estimated heating and cooling energy demands for this city block is 4.95 GJ. In the optimised case this is reduced to 3.96 GJ, so that even by modifying a relatively small number of constrained parameters substantial energy demand reductions (∼20%) are possible. The
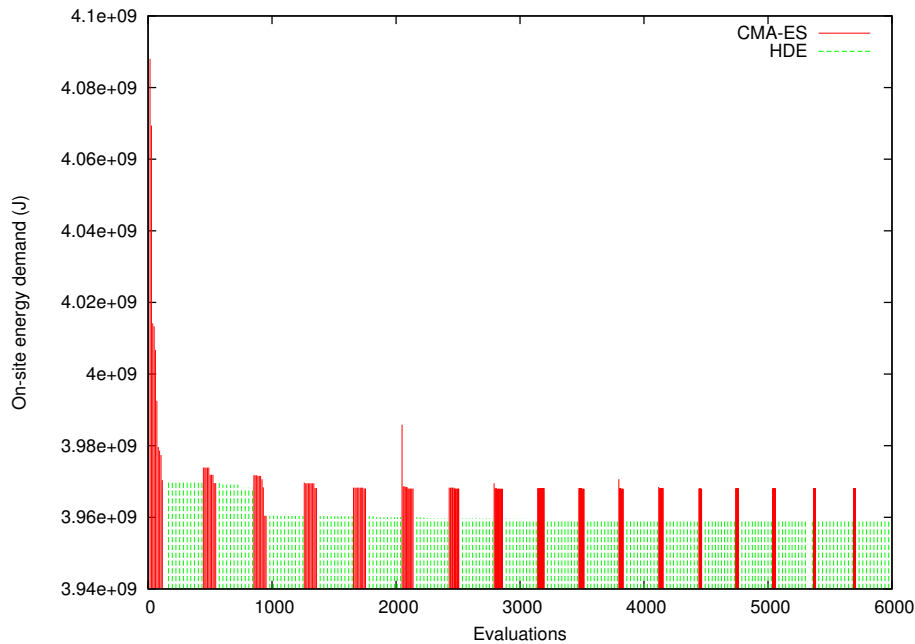
Figure 5.7: Evolution of the on-site energy demand with the number of evaluations in the hybrid CMA-ES/HDE

parameter values resulting from this optimisation process are shown in Table 2. We notice in the results that the insulation is always increased to the maximum thickness; likewise for the windows' U-value which tends to the lowest available. This result is rather encouraging as it is compatible with what we would have expected. There is only one exception the building in the Schonzone built between the 60's and the 70's, for which no insulation is proposed. In this case the wall is composed of two heavy parts (brick and concrete) separated by a layer of insulation, so that it does not require additional internal insulation, which would diminish the building's internal thermal inertia and therefore increase overheating risk and associated cooling loads. For the glazing ratio in Zone 5a, a compromise had to be found to satisfy the building's needs for the whole year. As a reminder we compute the heating needs and cooling needs taking into account the irradiation on the facades that is transmitted through the glazed surface into the building. No shading control system was implemented for this scenario. If the building is well insulated and well glazed, relatively high solar gains necessitating cooling, can be experienced even in winter. Therefore a balance between the cooling season gains and heating season losses is needed to ensure a good

Table 5.2: The thirteen parameters' value obtained after 6000 evaluations

Group	Parameter description	Value
Schonzone built <1919 (14 buildings)	Walls internal insulation (cm) Windows U-Value (W/(m^{2}K))	$x_1 = 12$ $x_2 = 1.5$
Schonzone built '46 until '60 (1 building)	Walls internal insulation (cm) Windows U-Value (W/(m^{2}K))	$x_3 = 12$ $x_4 = 1.5$
Schonzone built '61 until '70 (1 building)	Walls internal insulation (cm) Windows U-Value (W/(m^{2}K))	$x_5 = 0$ $x_6 = 1.58$
Schutzzone built <1919 (7 buildinga)	Windows U-Value (W/(m^{2}K))	$x_7 = 1.5$
Zone 5a built '61 until '70 (2 buildings)	Walls external insulation (cm) Windows U-value (W/(m^{2}K)) Glazing ratio	$x_8 = 12$ $x_9 = 1.5$ $x_{10} = 0.21$
Zone 5a built '71 until '80 (1 building)	Walls external insulation (cm) Windows U-value (W/(m^{2}K)) Glazing ratio	$x_{11} = 12$ $x_{12} = 1.5$ $x_{13} = 0.12$

performance over the whole year. For this relatively low glazing ratios (10 to 20%) are required. It is interesting to note that in contrast to the insulation position and thickness and window thermal transmittance, we would not necessarily have been able to identify these optimal glazing ratios by intuition alone.

5.2.4   Conclusion

This section presents a first application of Evolutionary Algorithms to optimise the performance of a group of buildings. For this we used CitySim (a holistic urban simulation tool) as a performance evaluator applied to a case study site in the city of Basel (Switzerland). For this first test we examined a selection of thirteen physical parameters associated with a block of 26 buildings grouped by construction date. In addition, we added as a constraint the protection status which is associated with some of these buildings. In this test we have seen that the results obtained are both reasonable and physically understandable. This first proof of concept has been somewhat limited in scope and we will now add further complexity to our problem by accounting for occupants' interactions with the envelope (albeit in a deterministic way) as well as energy conversion systems.

5.3   Minimisation of primary energy demand

The second optimisation study with CitySim is performed on the same group of 26 buildings in the Matthäus district as in former section, but this time considering occupants' presence and their control of blinds and window opening (as described in Section 5.1.4) and also accounting for energy supply systems.

5.3.1   Parameterisation

We have refined the subdivision of the three administrative zones in Matthäus (see Figure 5.2) to take into account the last renovation date. To simplify our analysis, but also to take into account realistic changes to the glazing, the windows may remain as they are or be replaced by double glazed low emissivity (U-value of 1.1 W/(m²K)) or triple glazed low emissivity units (U-value of 0.5 W/(m²K)). The energy conversion systems can be 1) a natural gas condensing boiler ($\eta_{th} = 0.96$), 2) an air heat pump ($\eta_{tech} = 0.35$, $T_{target} = 35°C$), 3) a cogeneration natural gas engine ($\eta_{th} = 0.72$, $\eta_{el} = 0.27$) or 4) a combined cogeneration natural gas engine with an air heat pump ($\eta_{th} = 0.72$, $\eta_{el} = 0.27$, $\eta_{tech} = 0.35$, $T_{target} = 35°C$). We have also increased the maximum allowable insulation size to 20 cm. The other parameters remain the same as in the former section (see Table 5.3). The parameters that belong to an ensemble of discrete values, such as the windows' U-value and energy conversion system, were coded using natural numbers starting from 0, but these are shown in a more human readable format in Table 5.3. For these discrete parameters, the absolute precisions ($\vec{\epsilon_3}$) were chosen to be 1. For the insulation thickness they were set to be 1 cm, for the glazing ratio to 0.01 and for the photovoltaic panels to 1% of the roof area.

5.3.2   Constraints

We provide as constraints the maximum capital cost p_{invest} that can be invested in our renovations, for which each renovation intervention is associated with an approximate price. Therefore, we can write:

$$
\begin{aligned}
g_1(\vec{x}) \;=\; & p_{insulation} \cdot \sum_{i \in \{1,4,7,10,13,16,19,32,37\}} x_i \cdot A_{wall,i} \\
& + \sum_{i = \{2,5,8,11,14,17,20,22,24,26,28,30,33,38\}} p_{window}(x_i) \cdot A_{window,i} \\
& + \sum_{i = \{3,6,9,12,15,18,21,23,25,27,29,31,35,40\}} p_{system}(x_i)
\end{aligned}
$$

Table 5.3: The forty-one (discrete[a] and continuous) parameters for the group of buildings in Matthäus

Group	Parameter description	Symbol and Domain
Schonzone built <1919 non-renovated (2 buildings)	Walls internal insulation (cm) Windows U-Value (W/(m^{2}K)) Energy conversion system[b]	$x_1 \in [0, 20]$ $x_2 \in \{0.5, 1.1, 6.0\}$ $x_3 \in \{1,2,3,4\}$
Schonzone built <1919 renovated '71 until '80 (1 building)	Walls internal insulation (cm) Windows U-Value (W/(m^{2}K)) Energy conversion system[b]	$x_4 \in [0, 20]$ $x_5 \in \{0.5, 1.1, 2.8\}$ $x_6 \in \{1,2,3,4\}$
Schonzone built <1919 renovated '81 until '90 (3 buildings)	Walls internal insulation (cm) Windows U-Value (W/(m^{2}K)) Energy conversion system[b]	$x_7 \in [0, 20]$ $x_8 \in \{0.5, 1.1, 2.8\}$ $x_9 \in \{1,2,3,4\}$
Schonzone built <1919 renovated '91 until '95 (6 buildings)	Walls internal insulation (cm) Windows U-Value (W/(m^{2}K)) Energy conversion system[b]	$x_{10} \in [0, 20]$ $x_{11} \in \{0.5, 1.1, 2.0\}$ $x_{12} \in \{1,2,3,4\}$
Schonzone built <1919 renovated '96 until '00 (2 buildings)	Walls internal insulation (cm) Windows U-Value (W/(m^{2}K)) Energy conversion system[b]	$x_{13} \in [0, 20]$ $x_{14} \in \{0.5, 1.1, 1.5\}$ $x_{15} \in \{1,2,3,4\}$
Schonzone built '46 until '60 renovated '81 until '90 (1 building)	Walls internal insulation (cm) Windows U-Value (W/(m^{2}K)) Energy conversion system[b]	$x_{16} \in [0, 20]$ $x_{17} \in \{0.5, 1.1, 2.8\}$ $x_{18} \in \{1,2,3,4\}$
Schonzone built '61 until '70 non-renovated (1 building)	Walls internal insulation (cm) Windows U-Value (W/(m^{2}K)) Energy conversion system[b]	$x_{19} \in [0, 20]$ $x_{20} \in \{0.5, 1.1, 5.5\}$ $x_{21} \in \{1,2,3,4\}$
Schutzzone built <1919 non-renovated (1 building)	Windows U-Value (W/(m^{2}K)) Energy conversion system[b]	$x_{22} \in \{0.5, 1.1, 6.0\}$ $x_{23} \in \{1,2,3,4\}$
Schutzzone built <1919 renovated '71 until '80 (1 building)	Windows U-Value (W/(m^{2}K)) Energy conversion system[b]	$x_{24} \in \{0.5, 1.1, 2.8\}$ $x_{25} \in \{1,2,3,4\}$
Schutzzone built <1919 renovated '81 until '90 (3 buildings)	Windows U-Value (W/(m^{2}K)) Energy conversion system[b]	$x_{26} \in \{0.5, 1.1, 2.8\}$ $x_{27} \in \{1,2,3,4\}$
Schutzzone built <1919 renovated '91 until '95 (1 building)	Windows U-Value (W/(m^{2}K)) Energy conversion system[b]	$x_{28} \in \{0.5, 1.1, 2.0\}$ $x_{29} \in \{1,2,3,4\}$
Schutzzone built <1919 renovated '96 until '00 (1 buildings)	Windows U-Value (W/(m^{2}K)) Energy conversion system[b]	$x_{30} \in \{0.5, 1.1, 1.5\}$ $x_{31} \in \{1,2,3,4\}$
Zone 5a built '61 until '70 non-renovated (2 buildings)	Walls external insulation (cm) Windows U-value (W/(m^{2}K)) Glazing ratio Energy conversion system[b] Photovoltaic panels (% roof area)	$x_{32} \in [0, 20]$ $x_{33} \in \{0.5, 1.1, 5.5\}$ $x_{34} \in [0.1, 1[$ $x_{35} \in \{1,2,3,4\}$ $x_{36} \in [0,100[$
Zone 5a built '71 until '80 non-renovated (1 building)	Walls external insulation (cm) Windows U-value (W/(m^{2}K)) Glazing ratio Energy conversion system[b] Photovoltaic panels (% roof area)	$x_{37} \in [0, 20]$ $x_{38} \in \{0.5, 1.1, 2.8\}$ $x_{39} \in [0.1, 1[$ $x_{40} \in \{1,2,3,4\}$ $x_{41} \in [0,100[$

[a]The discrete parameters are handled internally by the CMA-ES/HDE using real-values between [0,n-1[, where n is the number of discrete choices, and are rounded to the lower integer value.
[b]1=boiler, 2=heat pump, 3=cogeneration, 4=cogeneration + heat pump

$$+ \sum_{i=\{36,41\}} p_{pv} \cdot x_i \cdot A_{roof,i} - p_{invest} \leq 0, \tag{5.3}$$

where $p_{insulation}$ is the price of the insulation per m^3, $A_{wall,i}$ is the total wall area of the considered building(s) in m^2, $p_{window}(x_i)$ is a function that returns the investment for windows, $A_{window,i}$ is the total window area of the considered building(s) in m^2, $p_{system}(x_i)$ is a function that returns the investment for the energy conversion system, p_{pv} is a function that returns the price of the photovoltaic panels per m^2 and $A_{window,i}$ is the total roof area of the considered building(s) in m^2.

For the present application, approximate values in Swiss francs (CHF) for the investments were obtained by contacting the suppliers (private companies). These values were used to demonstrate the principle of an investment-based optimisation. The insulation investment is of:

$$p_{insulation} = 150 \text{ CHF/m}^3 \tag{5.4}$$

The window investment[2] is of:

$$p_{window}(x_i) = \begin{cases} 600 \text{ CHF/m}^2 & \text{if } x_i = 0.5 \\ 450 \text{ CHF/m}^2 & \text{if } x_i = 1.1 \\ 0 \text{ CHF/m}^2 & \text{otherwise} \end{cases} \tag{5.5}$$

The energy conversion system investment is of:

$$p_{system}(x_i) = \begin{cases} 4500 \text{ CHF} & \text{if } x_i = 1 \\ 18000 \text{ CHF} & \text{if } x_i = 2 \\ 31000 \text{ CHF} & \text{if } x_i = 3 \\ 49000 \text{ CHF} & \text{if } x_i = 4 \end{cases} \tag{5.6}$$

The photovoltaic investment is of:

$$p_{pv}(x_i) = 1700 \text{ CHF/m}^2 \tag{5.7}$$

The minimum investment for refurbishment corresponds to the installation of a condensing boiler in every house, which costs 63 kCHF. The maximum investment for refurbishment (the most expensive technology and insulation) costs 4198 kCHF in total, which involves 136 kCHF for insulation, 2328 kCHF for windows replacement, 686 kCHF for cogeneration with a heat pump and 1049 kCHF for photovoltaic panels. Within this range we have set an investment limit of 2 million CHF.

---

[2]Please note that in this cost approximation, we do not take into account the cost of labour involved in the dismantling and installation process.

5.3.3   Objective function

The use of blinds and window openings in the simulation reduces cooling energy demand to a negligible value, compared to heating demands (see Section 5.1.4). Therefore, the cooling loads will not be taken into account in the objective function. The objective function in this optimisation is the sum of the annual primary energy used for the group of simulated buildings, which is minimised. The calculation takes into account the efficiencies in energy transformation:

$$f(\vec{x}) = Q_{gas}(\vec{x})/\eta_{gas} + E_{el}(\vec{x})/\eta_{el}, \tag{5.8}$$

where $\vec{x}$ are the parameters, Q_{gas} is the on-site energy consumption (J) in gas form, η_{gas} is the energy conversion efficiency for gas production and transport, E_{el} is the on-site electricity consumption (positive) or production (negative) in J and η_{el} is the energy conversion efficiency for electricity production and transport. The energy conversion efficiencies are the inverse of the source energy factors (Table 5.4), which are given as the ratio of the primary energy consumption over the on-site energy consumption. For one joule of electricity

Fuel	Source energy factor
Electricity	2.057
Gas	1.007

Table 5.4: Source energy factors for Electricity and Gas (production and transport), Switzerland

consumed on-site, 2.057 joules of primary energy are needed. The calculation method for the source energy factors is taken from EPA [2007] and the data from SFOE [2007].

The heating set point is assumed to be 21°C for all buildings. Each evaluation for a given combination of the available parameters takes about 5 minutes on a machine with an Opteron 2.3 GHz processor and 4 GB RAM. The number of function evaluations was chosen to be 18000, corresponding to 5 days of optimisation.

5.3.4   Results

A plateau was found in the objective function after 15619 evaluations, as shown in Figure 5.8. The best configuration found for the buildings consumed about 6.587 TJ of primary energy per year (or 1823 MWh/year and an average of 70 MWh/year/building). The CMA-ES and HDE have both contributed to the improvement of the objective function (Figure 5.8). Table 5.5 shows the parameters resulting from this optimisation. The suggested

Table 5.5: Results of the forty-one parameters for the group of buildings in Matthäus

Group	Parameter description	Value
Schonzone built <1919 non-renovated (2 buildings)	Walls internal insulation (cm) Windows U-Value (W/(m^{2}K)) Energy conversion system[a]	$x_1 = 20$ $x_2 = 0.5$ $x_3 = 2$
Schonzone built <1919 renovated '71 until '80 (1 building)	Walls internal insulation (cm) Windows U-Value (W/(m^{2}K)) Energy conversion system[a]	$x_4 = 20$ $x_5 = 2.8$ $x_6 = 2$
Schonzone built <1919 renovated '81 until '90 (3 buildings)	Walls internal insulation (cm) Windows U-Value (W/(m^{2}K)) Energy conversion system[a]	$x_7 = 20$ $x_8 = 1.1$ $x_9 = 2$
Schonzone built <1919 renovated '91 until '95 (6 buildings)	Walls internal insulation (cm) Windows U-Value (W/(m^{2}K)) Energy conversion system[a]	$x_{10} = 20$ $x_{11} = 2.0$ $x_{12} = 2$
Schonzone built <1919 renovated '96 until '00 (2 buildings)	Walls internal insulation (cm) Windows U-Value (W/(m^{2}K)) Energy conversion system[a]	$x_{13} = 20$ $x_{14} = 1.5$ $x_{15} = 2$
Schonzone built '46 until '60 renovated '81 until '90 (1 building)	Walls internal insulation (cm) Windows U-Value (W/(m^{2}K)) Energy conversion system[a]	$x_{16} = 20$ $x_{17} = 0.5$ $x_{18} = 2$
Schonzone built '61 until '70 non-renovated (1 building)	Walls internal insulation (cm) Windows U-Value (W/(m^{2}K)) Energy conversion system[a]	$x_{19} = 20$ $x_{20} = 5.5$ $x_{21} = 2$
Schutzzone built <1919 non-renovated (1 building)	Windows U-Value (W/(m^{2}K)) Energy conversion system[a]	$x_{22} = 6.0$ $x_{23} = 2$
Schutzzone built <1919 renovated '71 until '80 (1 building)	Windows U-Value (W/(m^{2}K)) Energy conversion system[a]	$x_{24} = 0.5$ $x_{25} = 2$
Schutzzone built <1919 renovated '81 until '90 (3 buildings)	Windows U-Value (W/(m^{2}K)) Energy conversion system[a]	$x_{26} = 2.8$ $x_{27} = 2$
Schutzzone built <1919 renovated '91 until '95 (1 building)	Windows U-Value (W/(m^{2}K)) Energy conversion system[a]	$x_{28} = 0.5$ $x_{29} = 2$
Schutzzone built <1919 renovated '96 until '00 (1 buildings)	Windows U-Value (W/(m^{2}K)) Energy conversion system[a]	$x_{30} = 0.5$ $x_{31} = 2$
Zone 5a built '61 until '70 non-renovated (2 buildings)	Walls external insulation (cm) Windows U-value (W/(m^{2}K)) Glazing ratio Energy conversion system[a] Photovoltaic panels (% roof area)	$x_{32} = 20$ $x_{33} = 5.5$ $x_{34} = 0.1$ $x_{35} = 2$ $x_{36} = 100$
Zone 5a built '71 until '80 non-renovated (1 building)	Walls external insulation (cm) Windows U-value (W/(m^{2}K)) Glazing ratio Energy conversion system[a] Photovoltaic panels (% roof area)	$x_{37} = 20$ $x_{38} = 0.5$ $x_{39} = 0.1$ $x_{40} = 2$ $x_{41} = 100$

[a] 1=boiler, 2=heat pump, 3=cogeneration, 4=cogeneration + heat pump
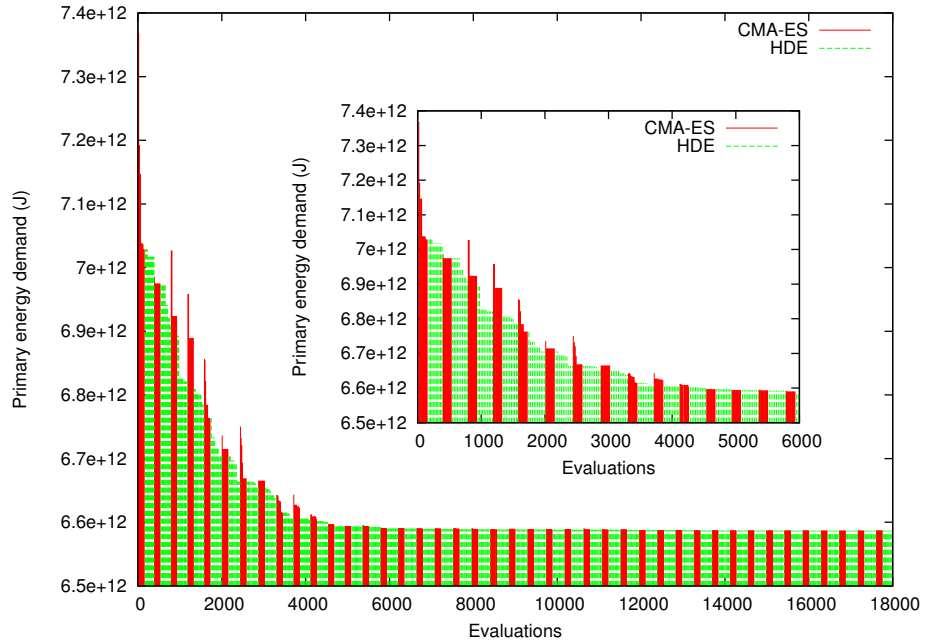
Figure 5.8: Evolution of the primary energy demand with the number of evaluations in the hybrid CMA-ES/HDE. Shown inset is the same graph but focussing on the range [0,6000] evaluations.

energy conversion system for all buildings is the heat pump, due to the combination of its efficiency and the corresponding source energy ratio. Table 5.6 shows the combined efficiency of the energy conversion system with the source energy ratio for Switzerland and a comparison with San Francisco, considering a yearly average source temperature for the heat pump of 15°C. The choice of energy conversion system for San Francisco would have been cogeneration and heat pump, as the source energy ratio for electricity is higher. This result is encouraging, suggesting that our optimiser chose the correct parameters for the energy conversion system.

The optimiser also suggests that photovoltaic panels should cover 100% of the roof area and that the thickness of insulation should be maximised (to 20 cm). However, the replacement of all windows, which is a large investment (twice the price of PV) was not proposed by the optimiser. Instead, only a proportion of windows were replaced according to our total investment threshold (the actual total cost was predicted to be 1983 kCHF, which is very close to the maximum amount allowed by the constraint). Finally the glazing ratio in the last two groups of buildings was chosen to be the smallest possi-

	Switzerland	San Francisco
Source energy ratio		
Gas	1.007	1.092
Electricity	2.057	3.095
Combined efficiency		
Boiler	0.95	0.88
Heat pump	2.63	1.74
Cogeneration	1.27	1.42
Cogeneration and heat pump	2.16	1.99

Table 5.6: Comparison of combined efficiency for the different energy conversion systems in two locations

ble (0.1). To understand this, we compared in Figure 5.9 for a typical winter day and for the last group of buildings, which contains only one building identified by number 213087, performance with parameters corresponding to a glazing ratio of 0.1 and the extreme of 0.99 assuming all windows to be replaced by triple glazing ignoring the fact that at a 99% glazing ratio the investment exceeds 2 millions CHF. With this changed in the group of buildings, the investment was of 2.191 millions CHF and the total primary energy consumption grew to 6.686 TJ (+1.5%). The increased solar gains during the day for the larger windows which do reduce daytime heating demands do not compensate for the excess thermal losses through these windows during the night. There we reach a limit in the models currently implemented in CitySim: in particular there is no daylighting model, so that photoresponsive control of artificial lighting is not considered, which may change this trend. We have also disengaged the modelling of mechanical cooling in this scenario, although this could be easily rectified.

5.3.5 Conclusion

This section proves our central hypothesis. Urban energy fluxes, as modelled by our holistic simulation tool CitySim, can and have been optimised using an Evolutionary Algorithm. In this, the objective was first to minimise the primary energy consumption of a part of a city, taking as parameters possible refurbishment options. Constraints arising from local regulations were also considered; likewise those due to limits in the maximum amount of money that can be invested in the renovations. The optimiser found a trade-off between the investment (set a-priori) and the primary energy consumption of the group of buildings.

The methodology developed in this thesis for optimising urban energy performance is very general; it has the advantages of handling analytical constraints and parallelising the function evaluations. It is also true that with
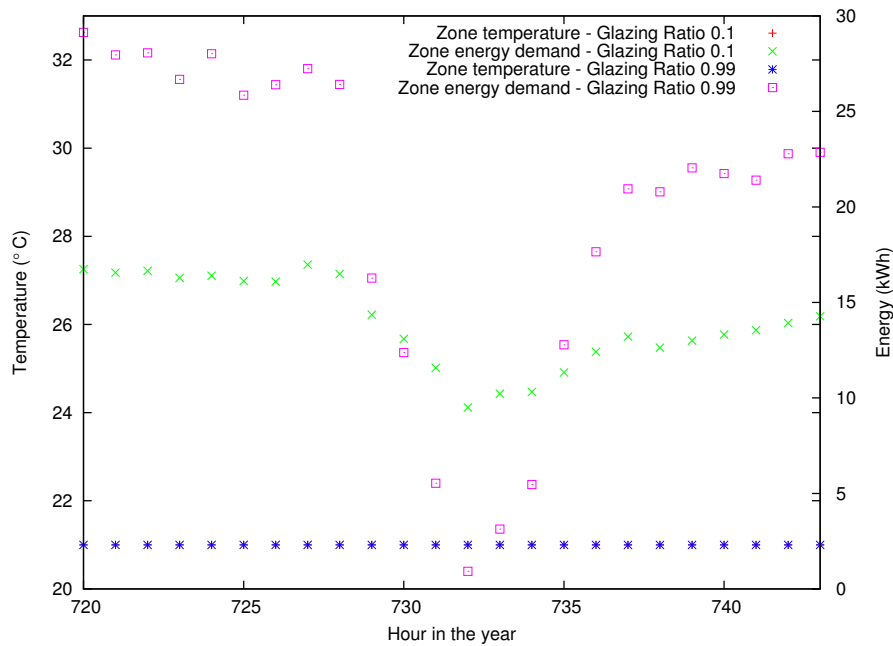
Figure 5.9: Comparison on a winter day (30th January) between a glazing ratio of 0.1 and 0.99 for building 213087

a few adaptations, any optimiser (for example MOO or GenOpt) could be used in place of our hybrid CMA-ES/HDE. However, our hybrid algorithm has proven to be particulary robust in identifying global optima with respect to highly multi-modal functions.

As future work, it would be interesting in the future to test the sensitivity of parameters resulting from the optimisation. We could get which are the most influencing on the objective function value. Moreover, analysing not only the best candidate found by the optimiser but also the following ones might give us some insights about which configuration of the parameters is the most robust. By robust we mean that the final result (for example primary energy consumption) is not too influenced by slight changes in the parameter values.

Chapter 6

Conclusion

The principle objective of the work described in this thesis was to develop and test new methods for efficiently optimising the environmental sustainability of urban planning and design proposals. To this end we have, in the first instance, tackled the problem of optimising the layout and form of buildings for the utilisation of solar radiation. In contrast to previous studies, in which trial and error has been used to search for well performing solutions, we introduced a methodology using the multi-objective evolutionary algorithm MOO. The geometric shape of the buildings was parameterised, allowing for their representation by a vector of real numbers, and the parameter space was searched in order to maximise the solar irradiation potential. In order to take the constraint of allowable volume into account, we introduced a second objective to minimise the volume of the urban shape. The methodology was applied successfully to study cases in the Matthäus district of Basel (Switzerland), producing interesting results along the corresponding Pareto fronts.

When volume constraints are known prior to optimisation, the previous methodology involves many redundant evaluations that are outside of the scope of the constraints. To resolve this, we developed a new hybrid evolutionary algorithm that avoids evaluations that violates constraints. The hybridisation of two evolutionary algorithms (CMA-ES and HDE) showed superior results in terms of robustness (100% of convergence to the global minimum) with respect to two difficult benchmark functions, compared to the methods taken separately. Moreover, the application of the hybrid to a real-world problem of solar energy potential maximisation showed good results compared to the multi-objective evolutionary algorithm MOO. The constraint handling procedure also showed satisfactory results on a constrained benchmark function on the basis that the objective function was not evaluated as well as on applications of solar irradiation maximisation. These applications also identified some highly interesting and non-intuitive optimal

building forms. Finally, the hybrid also performed well in optimising the primary energy demand of buildings simulated by EnergyPlus compared to the PSO/HJ algorithm, a combination of heuristic and direct search algorithms which is widely used in building optimisation. The CMA-ES/HDE also outperformed the PSO/HJ algorithm when applied to highly multi-modal benchmark functions.

Key contributions have also been made to the development of a new holistic urban energy modelling tool which at present focusses on prediction of energy performance of many buildings at the same time, taking into account radiant interactions between them. For this, a mono and multi-zone thermal model based on the analogy between heat and electricity was proposed and tested against the dynamic thermal simulation program ESP-r. From this it was concluded that the simplified model is able to produce good results with a minimum of information describing the buildings' geometry, materials, systems and occupational characteristics. This thermal model is linked to an HVAC model, which computes the increased energy demands due to the use of air as medium for heating, cooling and fresh air supply. A range of energy conversion systems are also modelled in a simplified way to complete the provision of heating/cooling as well as electricity. For this, a tank model provides the coupling between thermal energy consumers and producers. This contribution to CitySim was implemented in C++, in which a predictor-corrector approach is used to determine the evolution of buildings' temperature.

As a first application, CitySim was used to model a case study of 26 buildings in the Matthäus district (Basel). Different deterministic strategies were implemented to account for occupants' presence and their interactions with blinds and window openings. The results indicated that air conditioning plants should not be necessary in Switzerland if occupants behave appropriately. It was also evident that the simulation of window openings requires relatively fine time steps. The on-site heating and cooling demands were then minimised, first considering the buildings to be empty of occupants. The results from this first optimisation were found to be convincing. The problem was then made more complex by accounting for occupants' interactions with the envelope and energy conversion systems. The primary energy demand was then minimised, considering five types of energy conversion systems and a finer grouping of the buildings according to the last refurbishment date. Each refurbishment was associated with a price, and the total investment was constrained to be below a maximum amount. Results showed a preference for facade refurbishment including insulation, the installation of PV panels on roofs and the replacement of the energy conversion system by a heat pump. However, windows are only sporadically replaced. Where possible the

glazing ratio was reduced to its minimal value. There a limit of the models in CitySim was reached, indicating a need for a daylighting model to take into account the electricity demands associated with the use of artificial lighting. From the work described above it is considered that the central hypothesis set out in this document, that "Computational methods, in conjunction with an holistic urban simulation tool, can be used to identify optimal solutions for urban environmental sustainability", has been demonstrated. In achieving this, the main contributions of the present thesis to science are as follows:

- A new hybrid Evolutionary Algorithm with analytical constraints handling: CMA-ES/HDE, which is robust on Ackley and Rastrigin benchmark functions, comparable in performance with MOO on solar irradiation maximisation and comparable with PSO/HJ on building performance optimisation using EnergyPlus.

- A methodology for optimising the solar irradiation potential using Evolutionary Algorithms

- Key contributions to a new holistic urban energy flow modelling tool: CitySim

- A methodology for optimising urban scale energy flows using the new EA in combination with CitySim

6.1 Future work

The work in the modelling and optimisation of urban energy flows is far from complete. There are many avenues available for further exploration. With respect to the work described in this thesis, the following would be of value in the short term to reinforce CitySim and its coupling with the evolutionary algorithm.

- The thermal model should be tested against standard benchmark thermal tests such as BESTEST [Neymark et al., 2002].

- The code of CitySim should be optimised and parallelised for rapid simulations at the urban scale.

- Further models should be added to CitySim, such as: stochastic models for occupants' presence and interactions with the envelope, the daylight model, water and waste flows and heat derivation from waste

- The calibration of the energy predictions of CitySim according to measurements, using for example the hybrid CMA-ES/HDE for the minimisation of the difference between the measured and predicted energy use

- The CMA-ES/HDE should see its comparison operator improved for multi-objective optimisation and fitted with a ranking algorithm.

- We have thus far only considered the storage of heat (with the Tank Model). We should also consider electrical energy storage (whether direct - on-site batteries, plug-in hybrid or fully electric cars, soleniods, - or indirect, such as by compressed air storage, . . .) and the control of energy demand, storage and supply (smart grids).

- The optimisation of the control of energy demand, storage and supply and their interactions with system dimensions. One example would be the adaptation of the heat tank volume in order to downsize the energy conversion system.

Appendix A

Construction references in Switzerland

A.1 Building categories in Switzerland

With the help of renovation specialists, EPIQR Rénovation (Lausanne), we came to building categories according to the construction year and renovation date. Those should be considered as an average construction type over the period. Please note that the G-value of the windows is always considered to be 0.7.

A.1.1 Until 1946

The external walls are considered to be constructed with

- 40 cm of rubble masonry.

The U-values $(W/(m^2K))$ are considered to be

- 6 for the windows,
- 2.5 for the roofs.

The infiltration rate (h^{-1}) is taken as 2.0.

A.1.2 1946 to 1960

The external walls are considered to be constructed from inside to outside with

- 1 cm of plaster,

- 4 cm of solid brick,

- 6 cm of air gap,

- 20 cm of solid brick,

- 2 cm of render.

The U-values $(W/(m^2K))$ are considered to be

- 5.5 for the windows,

- 1.0 for the roofs.

The infiltration rate (h^{-1}) is taken as 1.8.

A.1.3   1960 to 1970

The external walls are considered to be constructed from inside to outside with

- 1 cm of plaster,

- 8 cm of hollow brick,

- 2 cm of polystyrene insulation,

- 15 cm of hollow brick,

- 2 cm of render.

The U-values $(W/(m^2K))$ are considered to be

- 5.5 for the windows,

- 0.8 for the roofs.

The infiltration rate (h^{-1}) is taken as 1.6.

A.1.4   1970 to 1980

The external walls are considered to be constructed from inside to outside with

- 1 cm of plaster,

- 8 cm hollow brick,

- 6 cm of polystyrene insulation,

- 8 cm of hollow brick,

- 1 cm of render.

The U-values (W/(m²K)) are considered to be

- 2.8 for the windows,

- 0.6 for the roofs.

The infiltration rate (h⁻¹) is taken as 1.4.

A.1.5 1980 to 1990

The external walls are considered to be constructed from inside to outside with

- 1 cm of plaster,

- 15 cm of concrete block,

- 8 cm of polystyrene insulation,

- 10 cm of concrete block.

The U-values (W/(m²K)) are considered to be

- 2.8 for the windows,

- 0.46 for the roofs.

The infiltration rate (h⁻¹) is taken as 1.2.

A.1.6 1990 to 2000

The external walls are considered to be constructed from inside to outside with

- 1 cm of plaster,

- 20 cm reinforced concrete,

- 12 cm of polystyrene insulation,

- 2 cm of render.

The U-values (W/(m²K)) are considered to be

- 1.6 for the windows,

- 0.32 for the roofs.

The infiltration rate (h⁻¹) is taken as 1.0.

Renovation year	Action	U-value (W/(m²·K))	R-value (m²·K/W)
1970-1990	Window replacement	2.8	
1990-1995	Window replacement	2.0	
	Roof insulation, 10-*12* cm of polystyrene		2.87
	Wall insulation, 6-*8* cm of polystyrene		1.90
1996-2000	Window replacement	1.5	
	Roof insulation, 12-*15* cm of polystyrene		3.57
	Wall insulation, 8-*12* cm of polystyrene		2.87

A.2 Renovations

The actions taken for the renovation of buildings are summarised in Table A.2. For each period of time, we consider the replacement of the glazing by a better performing one, given by a lower U-value. The insulation of the roofs are considered by the addition of a resistor value ($R_{th} = \Delta x / \lambda$) to the actual roof's U-value, with Δx the thickness and λ the conductivity of the insulation. The insulation of the facades are added to the walls' physical layer attribution.

The air infiltration rate is considered to be improved by the renovation as shown in Table A.2.

Renovation year	Air infiltration rate (h^{-1})
1970-1980	1.4
1980-1990	1.2
1990-2000	1.0

A.3 Physical properties of the materials

The physical properties of the construction materials were taken from the database of LESOSAI version 5.5, and shown in Table A.1.

Table A.1: Physical properties of construction materials

Material	Conductivity (W/(m·K))	Density (kg/m³)	Specific heat capacity (J/(kg·K))
Rubble masonry	1.3	2000	800
Solid brick	1	1600	1000
Hollow brick	0.47	1200	900
Reinforced concrete	1.8	2400	1100
Concrete block	0.7	1200	1100
Plaster	0.58	1200	900
Render	0.87	1800	1100
Polystyrene insulation	0.042	15	1400

A.4 Sample of the XML description file for CitySim

The following XML sample shows the description of the outside surfaces' physical characteristics and a building's infiltration rate. Please note that the wall layers are given from outside to inside.

```
<CitySim>
    <District>
        <OutsideSurface type="1900-1946">
            <Layer id="1" Thickness="0.40" Conductivity="1.3" Cp="800" Density="2000"/>
        </OutsideSurface>
        <OutsideSurface type="1946-1960">
            <Layer id="1" Thickness="0.02" Conductivity="0.87" Cp="1100" Density="1800"/>
            <Layer id="2" Thickness="0.20" Conductivity="1.00" Cp="1000" Density="1600"/>
            <Layer id="3" Thickness="0.06" Conductivity="0.3529" Cp="1000" Density="1.2"/>
            <Layer id="4" Thickness="0.04" Conductivity="1.00" Cp="1000" Density="1600"/>
            <Layer id="5" Thickness="0.01" Conductivity="0.58" Cp="900" Density="1200"/>
        </OutsideSurface>
        <OutsideSurface type="1960-1970">
            <Layer id="1" Thickness="0.02" Conductivity="0.87" Cp="1100" Density="1800"/>
            <Layer id="2" Thickness="0.15" Conductivity="0.47" Density="1200" Cp="900"/>
            <Layer id="3" Thickness="0.02" Conductivity="0.042" Density="15" Cp="1400"/>
            <Layer id="4" Thickness="0.08" Conductivity="0.47" Density="1200" Cp="900"/>
            <Layer id="5" Thickness="0.01" Conductivity="0.58" Cp="900" Density="1200"/>
        </OutsideSurface>
        <OutsideSurface type="1970-1980">
            <Layer id="1" Conductivity="0.87" Cp="1100" Density="1800" Thickness="0.01"/>
            <Layer id="2" Conductivity="0.47" Density="1200" Cp="900" Thickness="0.08"/>
            <Layer id="3" Thickness="0.06" Conductivity="0.04" Density="60" Cp="600"/>
            <Layer id="4" Thickness="0.08" Conductivity="0.47" Density="1200" Cp="900"/>
            <Layer id="5" Thickness="0.01" Conductivity="0.58" Cp="900" Density="1200"/>
        </OutsideSurface>
        <OutsideSurface type="1980-1990">
            <Layer id="1" Conductivity="0.87" Cp="1100" Density="1800" Thickness="0.01"/>
            <Layer id="2" Density="1200" Thickness="0.10" Conductivity="0.7" Cp="1100"/>
            <Layer id="3" Conductivity="0.04" Density="60" Cp="600" Thickness="0.08"/>
            <Layer id="4" Thickness="0.15" Conductivity="0.7" Density="1200" Cp="1100"/>
            <Layer id="5" Thickness="0.01" Conductivity="0.58" Cp="900" Density="1200"/>
        </OutsideSurface>
        <OutsideSurface type="1990-2000">
            <Layer id="1" Conductivity="0.87" Cp="1100" Density="1800" Thickness="0.02"/>
            <Layer id="3" Thickness="0.12" Conductivity="0.042" Density="15" Cp="1400"/>
            <Layer id="4" Thickness="0.20" Conductivity="1.8" Density="2400" Cp="1100"/>
            <Layer id="5" Thickness="0.01" Conductivity="0.58" Cp="900" Density="1200"/>
        </OutsideSurface>
        <Building ID="969109" Vi="1989.61"  Ninf="2.0" ...>
            <Wall id="0" type="1900-1946" GlazingRatio="0.2">
                <V0 x="45.780161" y="-24.200418" z="36.245598"/>
                <V1 x="45.780161" y="-24.200418" z="20.221000"/>
                <V2 x="39.846901" y="-25.746555" z="20.221000"/>
                <V3 x="39.846901" y="-25.746555" z="36.245598"/>
            </Wall>
            ...
            <Roof id="0" Uvalue="2.5" GlazingRatio="0.2">
                <V0 x="39.432192" y="-24.155120" z="35.745598"/>
                <V1 x="36.525681" y="-24.912523" z="35.745598"/>
                <V2 x="36.940390" y="-26.503958" z="36.245598"/>
                <V3 x="39.846901" y="-25.746555" z="36.245598"/>
            </Roof>
```

```
            ...
        </Building>
        ...
    </District>
</CitySim>
```

Appendix B

Code parallelisation

In order to speed up the optimisation process and using the fact that each function evaluation is independent from other function evaluations, we thought of parallelising the evaluation phase from the heuristics.

B.1 POSIX threads

We use Linux, and more precisely Ubuntu, as an operating system. In C++, we use the *pthreads* library, with which different threads doing different tasks can be created by the main program. The threads share the memory allocated to the main program, and semaphores must be used to avoid simultaneous access to the data. An Evaluation class was written to handle parallelism, which is shown in the following lines.

```cpp
1  class Evaluation {

3      private:

5          Problem *problem;

7      public:

9          static map<unsigned int, vector<double> > idAllelesMap;
           static map<unsigned int, vector<double> > idFitnessMap;
11
           Evaluation(Problem *problem):problem(problem) {};
13
           void start() {
15
               pthread_t threads[NTHREADS];
17             int iret[NTHREADS];

19             /* Create independent threads that will consume the work */
               for (unsigned int i=0;i<NTHREADS;i++) iret[i] = pthread_create(
                   &threads[i], NULL, consumer, problem);
21             /* Waiting for all threads to have completed the work */
```

```
                   for (unsigned int i=0;i<NTHREADS;i++) pthread_join(threads[i],
                        NULL);
23
                   return;
25
               }
27
           void insert(unsigned int id, vector<double> alleles) {
29
                   if ( idAllelesMap.size() < idAllelesMap.max_size() )
                       idAllelesMap.insert( pair<unsigned int,vector<double> > (id,
                            alleles) );
31                 else throw ("Cannot allocate idAllelesMap, map full.");
                   return;
33             }
35         vector<double> get(unsigned int id) {
37                 return idFitnessMap[id];
39             }
41 };
```

Each thread created accesses a pile of work to do, while blocking the access
to the other threads. It takes the first task to do in the pile and removes it
from the pile. Then does the evaluation and puts back the outcome in the
pile of work completed. When the pile of work to do is empty, the thread
exits. This procedure is shown in the following consumer method.

```
1 void* consumer(void *ptr) {

3      Problem *problem;
       problem = (Problem *) ptr;
5
       unsigned int id;
7      vector<double> allelesVector;

9      for (;;) {

11       pthread_mutex_lock( &mut1 );
         if ( Evaluation::idAllelesMap.empty() ) {
13             pthread_mutex_unlock( &mut1 );
               pthread_exit(NULL); // pile of work to do empty
15       }
         else { // work to do
17
         id            = Evaluation::idAllelesMap.begin()->first;
19       allelesVector = Evaluation::idAllelesMap.begin()->second;

21       Evaluation::idAllelesMap.erase(Evaluation::idAllelesMap.begin());
         pthread_mutex_unlock( &mut1 );
23
         // evaluation of the fitness
25       vector<double> fitnessVector = problem->evaluate(id, allelesVector);

27       // puts the result in the pile of work completed
             pthread_mutex_lock( &mut1 );
29           if ( Evaluation::idFitnessMap.size() < Evaluation::idFitnessMap.
                 max_size() ) {
```

```
             Evaluation :: idFitnessMap . insert ( pair<unsigned int , vector<double
                >> (id , fitnessVector) );
31       }
         else throw ("Cannot allocate idFitnessMap , map full.");
33       pthread_mutex_unlock( &mut1 );
       }
35   }
}
```

Glossary

BESTEST	Building Energy Simulation TEST
CMA-ES	Covariance Matrix Adaptation Evolution Strategies
CPU	Central processing unit
DE	Differential Evolution
EA	Evolutionary Algorithm
ES	Evolution Strategies
GPU	Graphics Processing Unit
HDE	Hybrid Differential Evolution
HVAC	Heating, Ventilation and Air-Conditioning
MOO	Multi-Objective Optimiser from LENI/EPFL
PV	Photovoltaic
TRY	Test Reference Year
XML	Extensible Markup Language

Bibliography

G. G. J. Achterbosch, P. P. G. de Jong, C. E. Krist-Spit, S. F. van der Meulen, and J. Verberne. Development of a convenient thermal dynamic building model. *Energy & Buildings*, 8(3):183–196, 1985.

Charles Audet and John E. Dennis, Jr. Analysis of Generalized Pattern Searches. *SIAM Journal on Optimization*, 13(3):889–903, 2003.

H. B. Awbi. *Ventilation of Buildings*. E & FN Spoon, first edition, 1991.

N. Baker and D. Hoch. A design tool which combines the energy value of daylight with the thermal value of solar gain. In *Proceedings of the 6th PLEA Conference*, 1988.

D. Bartholomew and D. Robinson. Building energy and environmental modelling. *Application Manual AM11, CIBSE*, April 1998, 1998.

Ian Beausoleil-Morrison. On Predicting The Magnitude And Temporal Variation Of Cooling Loads In Detached Residential Buildings. In *Proceedings of the 11th International Building Performance Simulation Association Conference*, pages 300–307, Glasgow, Scotland, July 2009.

Hans-Georg Beyer and Hans-Paul Schwefel. Evolution Strategies: A comprehensive introduction. *Natural Computing*, 1:3–52, 2002.

B. H. Bland. Conduction in dynamic thermal models: Analytical tests for validation. *Building Services Engineering Research and Technology*, 13(4): 197–208, 1992.

D.P. Bloomfield, K. J. Lomas, and C. J. Martin. Assessing programs which predict the thermal performance of buildings. *BRE Information Paper*, IP 7/92, 1992.

Raffaele Bolliger, Daniel Favrat, and François Maréchal. Advanced Power Plant Design Methodology using Process Integration and Multi-Objective

Thermo-Economic Optimisation. In *ECOS 2005, 18th International Conference on Efficiency, Cost, Optimization, Simulation and Environmental Impact of Energy Systems*, volume 2, pages 777–784, Trondheim, Norway, 2005.

David Bradley and Michaël Kummert. New Evolutions In TRNSYS - A Selection Of Version 16 Features. In *Ninth International IBPSA Conference*, pages 107–114, Montreal, Canada, August 12-15 2005.

Lam T. Bui, Omar Soliman, and Hussein A. Abbass. A modified strategy for the constriction factor in particle swarm optimization. In *Lecture Notes in Computer Science (including subseries Lecture Notes in Artificial Intelligence and Lecture Notes in Bioinformatics)*, volume 4828 LNAI, pages 333–344. Springer Berlin / Heidelberg, 2007.

L. G. Caldas and L. K. Norford. A design optimization tool based on a genetic algorithm. *Automation in Construction*, 11(2):173–184, 2002.

Cyril Carter. Computational methods for passive solar simulation. *Solar Energy*, 45(6):379–384, 1990.

C. F. Chang, J. J. Wong, J. P. Chiou, and C. T. Su. Robust searching hybrid differential evolution method for optimal reactive power planning in large-scale distribution systems. *Electric Power Systems Research*, 77 (5-6):430–437, 2007.

V. Cheng, K. Steemers, M. Montavon, and R. Compagnon. Urban Form, Density and Solar Potential. In *PLEA*, Geneva, Switzerland, 2006.

J. A. Clarke. *Environmental Systems Performance*. PhD thesis, Glasgow: University of Strathclyde, 1977.

J.A. Clarke. *Energy Simulation in Building Design*. Butterworth-Heinemann, Oxford, 2001.

R. Compagnon and D. Raydan. Irradiance and illuminance distributions in urban areas. In *Proceedings of PLEA 2000*, pages 436–441, Cambridge UK, July 2000.

Raphaël Compagnon. PRECis: Assessing the Potential for Renewable Energy in Cities, Annexe3: Solar and daylight availability in urban areas. Technical report, University of Applied Sciences, July 2000.

Raphaël Compagnon. Solar and daylight availability in the urban fabric. *Energy & Buildings*, 36(4):pp. 321–328, 2004.

J. A. Crabb, N. Murdoch, and J. M. Penman. Simplified thermal response model. *Building Services Engineering Research and Technology*, 8(1):13–19, 1987.

K. Darkwa and P.W. O'Callaghan. Simulation of phase change drywalls in a passive solar building. *Applied Thermal Engineering*, 26(8-9):853 – 858, 2006. ISSN 1359-4311. doi: 10.1016/j.applthermaleng.2005.10.007.

M. Deru and P. Torcellini. Source Energy and Emission Factors for Energy Use in Buildings. Nrel/tp-550-38617, National Renewable Energy Laboratory, U.S. Department of Energy, June 2007.

V. Arnold Dirk and MacLeod Alexander. Hierarchically organised evolution strategies on the parabolic ridge. In *GECCO'06*, Seattle, Washington, USA, 2006.

F. Déqué, F. Ollivier, and A. Poblador. Grey boxes used to represent buildings with a minimum number of geometric and thermal parameters. *Energy & Buildings*, 31(1):29–35, 2000.

J. A. Duffie and W. A. Beckman. *Solar Engineering of Solar Processes*. Wiley - Interscience, second edition, 1991.

R. C. Eberhart and J. Kennedy. A new optimizer using particle swarm theory. In *Sixth International Symposium on Micro Machine and Human Science*, pages 39–43, Nagoya, Japan, Oct 1995. IEEE.

EPA. Energy star performance ratings methodology for incorporating source energy use. Technical report, U.S. Environment Protection Agency, 2007.

Vitaliy Feoktistov. *Differential Evolution: In Search of Solutions*. Springer, 2006.

David B. Fogel. *Evolutionary Computation: Toward a New Philosophy of Machine Intelligence*. Wiley, 2006.

L. J. Fogel, A. J. Owens, and Walsh M. J. *Artificial Intelligence through Simulated Evolution*. John Wiley and Sons, New York, 1966.

G. Fraisse, C. Viardot, O. Lafabrie, and G. Achard. Development of a simplified and accurate building model based on electrical analogy. *Energy & Buildings*, 34(10):1017–1031, 2002.

S. Gadsden, M. Rylatt, K. Lomas, and D. Robinson. Predicting the urban solar fraction: A methodology for energy advisers and planners based on GIS. *Energy & Buildings*, 35(1):37–48, 2003.

Martin Gassner and François Maréchal. Methodology for the optimal thermo-economic, multi-objective design of thermochemical fuel production from biomass. *Computers & Chemical Engineering*, 33(3):769–781, 2009. ISSN 0098-1354. doi: 10.1016/j.compchemeng.2008.09.017. Selected Papers from the 17th European Symposium on Computer Aided Process Engineering held in Bucharest, Romania, May 2007.

H. Girardet. *Creating sustainable cities*. Schumacher Briefing 2. Green Books, 1999.

David E. Goldberg. *Genetic Algorithms in Search, Optimization and Machine Learning*. Addison-Wesley, 1992.

M. Gough. *Modelling Heat Flow in Buildings: An Eigenfunction Approach*. PhD thesis, University of Cambridge, 1982.

Frédéric Haldi and Darren Robinson. Interactions with window openings by office occupants. *Building and Environment*, In Press, Corrected Proof, 2009. ISSN 0360-1323. doi: 10.1016/j.buildenv.2009.03.025.

N. Hansen and A. Ostermeier. Completely Derandomized Self-Adaptation in Evolution Strategies. *Evolutionary Computation*, 9(2):pp. 159–195, 2001.

Nilokaus Hansen and Stefan Kern. Evaluating the CMA Evolution Strategy on Multimodal Test Functions. In *Parallel Problem Solving from Nature, PPSN 2004*. Springer-Verlag, 2004.

Dariusz Heim and Joe A. Clarke. Numerical Modelling And Thermal Simulation Of Phase Change Materials With ESP-r. In *Proceedings of the 8th International Building Performance Simulation Association Conference*, Eindhoven, Netherlands, 2003.

Dariusz Heim and Joe A. Clarke. Numerical modelling and thermal simulation of PCM-gypsum composites with ESP-r. *Energy & Buildings*, 36 (8):795 – 805, 2004. ISSN 0378-7788. doi: 10.1016/j.enbuild.2004.01.004. Performance Simulation for Better Building Design.

J. H. Holland. *Adaptation in Natural and Artificial Systems*. The University of Michigan Press, Ann Arbor, Michigan, 1975.

Manuel Ibáñez, Luisa F. Cabeza, Cristian Solé, Joan Roca, and Miquel Nogués. Modelization of a water tank including a PCM module. *Applied Thermal Engineering*, 26(11-12):1328 – 1333, 2006. ISSN 1359-4311. doi: 10.1016/j.applthermaleng.2005.10.022.

E. Jochem. *Steps towards a sustainable development*. Novatlantis, white book edition, 2004.

P. J. Jones, J. Williams, and S. Lannon. An energy and environmental prediction tool for planning sustainability in cities. In *Rebuild*, Florence, Italy, 1998.

W. P. Jones. *Air Conditioning Engineering*. Butterworth-Heinemann, fifth edition, 2000.

R. Judkoff and J.A. Neymark. A testing and diagnostic procedure for building energy simulation programs. In *Building Environmental Performance*, Warwick, 1994.

Jérôme Henri Kämpf and Darren Robinson. A simplified thermal model to support analysis of urban resource flows. *Energy & Buildings*, 39(4): 445–453, 2007. doi: 10.1016/j.enbuild.2006.09.002.

Jérôme Henri Kämpf and Darren Robinson. A hybrid CMA-ES and HDE optimisation algorithm with application to solar energy potential. *Applied Soft Computing*, 9:738–745, 2009a. doi: 10.1016/j.asoc.2008.09.009.

Jérôme Henri Kämpf and Darren Robinson. Optimisation of building form for solar energy utilisation using constrained evolutionary algorithms. *Energy & Buildings*, 2009b. Accepted.

Jérôme Henri Kämpf and Darren Robinson. Optimisation of Urban Energy Demand using an Evolutionary Algorithm. In *Proceedings of the 11th International Building Performance Simulation Association Conference*, pages 668–673, Glasgow, Scotland, July 2009c.

Jérôme Henri Kämpf, Michael Wetter, and Darren Robinson. A comparison of global optimisation algorithms with standard benchmark functions and real-world applications using EnergyPlus. *Journal of Building Performance Simulation*, 2009. Accepted.

Jérôme Henri Kämpf, Marylène Montavon, Josep Bunyesc, Raffaele Bolliger, and Darren Robinson. Optimisation of buildings daylight availability. In *CISBAT*, pages 469–473, Lausanne, Switzerland, 2007.

Jérôme Henri Kämpf, Marylène Montavon, Josep Bunyesc, Raffaele Bolliger, and Darren Robinson. Optimisation of buildings' solar irradiation availability. *Solar Energy*, 2009. Article In Press.

Tamara G. Kolda, Robert Michael Lewis, and Virginia Torczon. Optimization by direct search: New perspectives on some classical and modern methods. *SIAM Review*, 45:385–482, 2003.

J. R. Koza. *Genetic Programming*. The MIT Press, Cambridge, Massachusetts, 1992.

Frédéric Kuznik, Joseph Virgone, and Jean-Jacques Roux. Energetic efficiency of room wall containing PCM wallboard: A full-scale experimental investigation. *Energy & Buildings*, 40(2):148 – 156, 2008. ISSN 0378-7788. doi: 10.1016/j.enbuild.2007.01.022.

K. Labs. Regional analysis of ground and above-ground climate conclusion. *Underground Space*, 7(1):37–65, 1982.

P. Lagonotte, Y. Bertin, and J. B. Saulnier. Qualitative analysis of reduced nodal models using the two-port (transfer function) method [analyse de la qualité de modèles nodaux réduits à l'aide de la méthode des quadripôles]. *International Journal of Thermal Sciences*, 38(1):51–65, 1999.

G. W. Larson and R. Shakespeare. *Rendering with Radiance: The Art and Science of Lighting Visualization*. Morgan-Kaufmann, San Francisco, 1998.

Greg Ward Larson. RADIANCE File Formats. http://radsite.lbl.gov/radiance/refer/filefmts.pdf, 1992.

G. Lefebvre, J. Bransier, and A. Neveu. Simulation of the thermal behaviour of a room by reduced order numerical methods [simulation du comportement thermique d'un local par des methodes numeriques d'ordre reduit]. *Revue générale de thermique*, 26(302):106–114, 1987.

R. M. Lewis and V. Torczon. Pattern search algorithms for bound constrained minimization. *SIAM Journal on Optimization*, 9(4):1082–1099, 1999.

Geoffrey Basil Leyland. *Multi-Objective Optimisation Applied to Industrial Energy Problems*. PhD thesis, École Polytechnique Fédérale de Lausanne, 2002.

P. J. Littlefair, M. Santamouris, S. Alvarez, A. Dupagne, D. Hall, J. Teller, J. F. Coronel, and N. Papanikolaou. *Environmental site layout planning:*

solar access, microclimate and passive cooling in urban areas. Construction Research Communications Ltd, 2000.

K. J. Lomas, H. Eppel, C. J. Martin, and D.P. Bloomfield. Empirical validation of building energy simulation programs. *Energy & Buildings*, 26(3): 253–276, 1997.

F. Lorenz and G. Masy. Méthode d'évaluation de l'économie d'énergie apportée par l'intermittance de chauffage dans les bâtiments. traitement par différences finies d'un modèle à deux constantes de temps. Technical report, Laboratoire de Physique du Bâtiment, Université de Liège, Janvier 1982.

H. B. Mann and D. R. Whitney. On a test of whether one of two random variables is stochastically larger than the other. *Annals of Mathematical Statistics*, 18:50–60, 1947.

J. Mardaljevic and M. Rylatt. An image-based analysis of solar radiation for urban settings. In *PLEA 2000*, pages 442–447, Cambridge, UK, 2000.

François Maréchal, Daniel Favrat, Francesca Palazzi, and Julien Godat. Thermo-economic modelling and optimisation of fuel cell systems. *fuel cells*, 5(1):5–24, 2005. doi: 10.1002/fuce.200400055.

George Marsaglia and Wai Wan Tsang. The Ziggurat Method for Generating Random Variables. *Journal of Statistical Software*, 5(8):1–7, 10 2000.

L. Martin and L. March. *Urban Space and Structures*. Cambridge University Press, UK, 1972.

Fernando R. Mazarron and Ignacio Canas. Exponential sinusoidal model for predicting temperature inside underground wine cellars from a Spanish region. *Energy & Buildings*, 40(10):1931 – 1940, 2008. ISSN 0378-7788. doi: 10.1016/j.enbuild.2008.04.007.

Z. Michalewicz and M. Schoenauer. Evolutionary Algorithms for Constrained Parameter Optimization Problems. *Evolutionary Computation*, 4(1):1–32, 1996.

N. O. Milbank and J. Harrington Lynn. Thermal response and the admittance procedure. *Build Serv Eng*, 42:38–50, 1974.

Melanie Mitchell. *An Introduction to Genetic Algorithms*. The MIT Press, 1998.

Adam Molyneaux. *A Practical Evolutionary Method for the Multi-Objective Optimisation of Complex Energy Systems, including Vehicle Drivetrains.* PhD thesis, École Polytechnique Fédérale de Lausanne, 2002.

Marylène Montavon, Jean-Louis Scartezzini, and Raphaël Compagnon. Comparison of the solar energy utilisation potential of different urban environments. In *PLEA2004*, Eindhoven, The Netherlands, 2004.

D. M. Murphy and T. Koop. Review of the vapour pressures of ice and supercooled water for atmospheric applications. *Quarterly Journal of the Royal Meteorological Society*, 131(608):1539–1565, 2005. 10.1256/qj.04.94.

D. A. Neeper. Thermal dynamics of wallboard with latent heat storage. *Solar Energy*, 68(5):393 – 403, 2000. ISSN 0038-092X. doi: 10.1016/S0038-092X(00)00012-8.

J. Neymark, R. Judkoff, G. Knabe, H.-T. Le, M. Dürig, A. Glass, and G. Zweifel. Applying the building energy simulation test (BESTEST) diagnostic method to verification of space conditioning equipment models used in whole-building energy simulation programs. *Energy & Buildings*, 34(9):917–931, 2002.

T. R. Nielsen. Simple tool to evaluate energy demand and indoor environment in the early stages of building design. *Solar Energy*, 78(1):73–83, 2005.

A. Nobakhti and H. Wang. A simple self-adaptive Differential Evolution algorithm with application on the ALSTOM gasifier. *Applied Soft Computing Journal*, 8(1):350–370, 2008.

J. Page, N. Morel, D. Robinson, and J.-L. Scartezzini. Simulating stochastic demand of resources within an urban neighbourhood. In *Proceedings of CISBAT*, pages 509–513, Lausanne, Switzerland, September 2005.

J. Page, D. Robinson, and J.-L. Scartezzini. Stochastic Simulation of Occupant Presence and Behaviour in Buildings. In *Building Simulation 2007*, Beijing, 2007.

J. Page, D. Robinson, N. Morel, and J.-L. Scartezzini. A generalised stochastic model for the simulation of occupant presence. *Energy & Buildings*, 40 (2):83–98, 2008.

Jessen Page. *Simulating occupant presence and behaviour in buildings.* PhD thesis, Ecole Polytechnique Fédérale de Lausanne, 2007.

K. E. Parsopoulos and M. N. Vrahatis. Recent approaches to global optimization problems through particle swarm optimization. *Natural Computing*, 1:235–306, 2002.

William H. Press, Saul A. Teukolsky, William T. Vetterling, and Brian P. Flannery. *Numerical Recipes in C++: The Art of Scientific Computing*. Cambridge University Press, February 2002. ISBN 0521750334.

D. Quagliarella, J. Périaux, C. Poloni, and G. Winter. *Genetic Algorithms and Evolution Strategies in Engineering and Computer Science*. Recent Advances and Industrial Applications. John Wiley and Sons, 1998.

Ingo Rechenberg. *Evolutionsstrategie: Optimierung technischer Systeme nach Principen der biologischen Evolution*. Fromman-Holzboog Verlag, Stuttgart, 1973.

D. Robinson. Urban Morphology and indicators of radiation availability. *International Journal of Solar Energy*, 80(12):1643–1648, 2006.

D. Robinson and N. Baker. Simplified modelling - recent developments in the LT Method. *Building Performance*, 3:pp. 14–19, 2000.

D. Robinson and A. Stone. Solar radiation modelling in the urban context. *Solar Energy*, 77(3):295–309, 2004a.

D. Robinson and A. Stone. Irradiation modelling made simple: the cumulative sky approach and its applications. In *Plea2004*, Eindhoven, The Netherlands, 2004b.

D. Robinson and A. Stone. A simplified radiosity algorithm for general urban radiation exchange. *Building Services Engineering Research and Technology*, 26(4):271–284, 2005.

D. Robinson and A. Stone. Internal illumination prediction based on a simplified radiosity algorithm. *Solar Energy*, 80(3):260–267, 2006.

D. Robinson, N. Campbell, W. Gaiser, K. Kabel, A. Le-Mouele, N. Morel, J. Page, S. Stankovic, and A. Stone. On the simulation and optimisation of urban neighbourhood resource flows. *Energy & Buildings*, 2006.

D. Robinson, N. Campbell, W. Gaiser, K. Kabel, A. Le-Mouel, N. Morel, J. Page, S. Stankovic, and A. Stone. SUNtool - A new modelling paradigm for simulating and optimising urban sustainability. *Solar Energy*, 81(9): 1198–1211, 2007. doi: 10.1016/j.solener.2007.06.002.

T. Runarsson and X. Yao. Stochastic ranking for constrained evolutionary optimization. *IEEE Transactions on Evolutionary Computation*, 4:284–294, 2000.

Jean-Louis Scartezzini, Marylène Montavon, and Raphaël Compagnon. Computer evaluation of the solar energy potential in an urban environment. In *EuroSun*, Bologna, 2002.

Hans-Paul Schwefel. *Evolution and Optimum Seeking*. Wiley-Interscience, 1995.

SFOE. Statistique globale suisse de l'énergie. Technical report, Swiss Federal Office of Energy, 2007.

Yun-Wei Shang and Yu-Huang Qiu. A Note on the Extended Rosenbrock Function. *Evolutionary Computation*, 14(1):119–126, 2006. doi: 10.1162/ evco.2006.14.1.119.

L. D. Shorrock and J. E. Dunster. The physically-based model BREHOMES and its use in deriving scenarios for the energy use and carbon dioxide emissions of the UK housing stock. *Energy Policy*, 25(12):1027–1037, 1997.

K. Steemers, N. Baker, D. Crowther, J. Dubiel, M.H. Nikolopoulou, and C. Ratti. City texture and microclimate. *Urban Design Studies*, 3:25–50, 1997.

Rainer Storn and Kenneth Price. Minimizing the real functions of the ICEC'96 contest by differential evolution. In *Proceedings of the IEEE Conference on Evolutionary Computation*, pages 842–844, 1996.

A. Tindale. Third-order lumped-parameter simulation method. *Building Services Engineering Research and Technology*, 14(3):87–97, 1993.

H. Titheridge and G. Boyle. The development and application of an urban energy model. In G. MacKerron and P. Pearson, editors, *The UK energy experience: A Model or A Warning?*, pages 281–293. Proceedings of the British Institute of Energy Economics Conference, 1995.

Marco Tomassini. *Spatially Structured Evolutionary Algorithms: Artificial Evolution in Space and Time*. Natural Computing. Springer-Verlag New York, Inc., 2005. 1051297.

V. Torczon. On the convergence of pattern search algorithms. *SIAM Journal on Optimization*, 7(1):1–25, 1997.

United Nations. World Urbanization Prospects: The 2007 Revision, 2007.

U.S. Department of Energy. *EnergyPlus Engineering Reference: The Reference to EnergyPlus Calculations*, April 2009.

Prashant Verma, Varun, and S.K. Singal. Review of mathematical modeling on latent heat thermal energy storage systems using phase-change material. *Renewable and Sustainable Energy Reviews*, 12(4):999 – 1031, 2008. ISSN 1364-0321. doi: 10.1016/j.rser.2006.11.002.

Donald Watson and Michael J. Crosbie. *Time-saver standards for Architectural Design*. McGraw-Hill, eighth edition edition, 2004.

M. Wetter and J. Wright. A comparison of deterministic and probabilistic optimization algorithms for nonsmooth simulation-based optimization. *Building and Environment*, 39(8 SPEC. ISS.):989–999, 2004.

Michael Wetter. GenOpt, generic optimization program, user manual, version 2.0.0. Technical Report LBNL-54199, Lawrence Berkeley National Laboratory, Berkeley, CA, USA, January 2004.

Michael Wetter and Elijah Polak. A convergent optimization method using pattern search algorithms with adaptive precision simulation. *Building Services Engineering Research and Technology*, 25(4):327–338, 2004.

Jan Wienold. Dynamic Simulation Of Blind Control Strategies For Visual Comfort And Energy Balance Analysis. In *Proceedings of the 10th International Building Performance Simulation Association Conference*, pages 1197–1204, Beijing, China, September 2007.

J. A. Wright, H. A. Loosemore, and R. Farmani. Optimization of building thermal design and control by multi-criterion genetic algorithm. *Energy & Buildings*, 34(9):959–972, 2002.

Jérôme Henri KÄMPF

Date and place of birth	April 26, 1978 in Neuchâtel (CH)
Origin	Sigriswil / BE (CH)
	jerome.kaempf@epfl.ch

Education, awards

Postgraduate Certificate in Education (Master), Pedagogic School, Lausanne, Switzerland **July 2005**

Degree in Physics and Computer Science (Master), University of Lausanne, Switzerland **August 2003**
Thesis work on Cellular Evolutionary Algorithms

Degree in Physics (Bachelor & Master), University of Lausanne, Switzerland **Mars 2001**
Thesis work on Monte-Carlo simulation of γ-rays in a Positron Emission Tomography camera

Diploma in Physics with Merit, University of Kent at Canterbury, UK **September 1999**

Cyril Isenberg prize for performance, University of Kent at Canterbury, UK **August 1999**

Work experience

PhD Student **September 2005 → present**
Solar Energy and Building Physics Laboratory, Swiss Institute of Technology Lausanne
Teaching assistantship leader for Building Physics I and II
Reviewer for an international journal (Journal of Building Performance Simulation)
Key developments to an urban energy modelling and optimisation tool "CitySim"

Visiting Scientist in Simulation Research Group **June 2008 (one month) and May 2009 (two weeks)**
Environmental Energy Technologies Division, Lawrence Berkeley National Laboratory, USA
Comparison of performance of two hybrid optimisation algorithms with application to primary building energy consumption using EnergyPlus

Math, Science and Information Technology Teacher **August 2004 → July 2006**
Secondary school De Félice, Yverdon-les-Bains, Switzerland
Form tutor of a class, leader for the robotics projects at school

Teaching and Research Assistant **October 2001 → June 2003**
Solar Energy and Building Physics Laboratory, Swiss Institute of Technology Lausanne
Daylighting simulations with Radiance, integration of BTDFs using Radiance primitives
Teaching assistantship for Building Physics I and II

Languages

French	Native language
English	Fluent oral and written
German	Basic skills

Computing skills

System administrator of a multi-processor Linux machine
Database management (Access, mySQL) and PHP programming
Expert in C++: responsible for the development of an integrated energy solver
Good knowledge of Java, FORTRAN and Pascal
ESP-r user for thermal simulations of buildings
Mathematica user for the modelling and analysis of results of physical systems
Parallel computing with POSIX threads, Qthreads and MPI-2
Knowledge of CUDA, using GPUs for scientific purposes

Publications

6 publications in international journals
7 peer-reviewed conference papers